January 2012

Tiered Networks: Modeling, Resource and Interference Management

Mustafa Cenk Erturk
University of South Florida, merturk@mail.usf.edu

Tiered Networks: Modeling, Resource and Interference Management

by

Mustafa Cenk Ertürk

A dissertation submitted in partial fulfillment
of the requirements for the degree of
Doctor of Philosophy
Department of Electrical Engineering
College of Engineering
University of South Florida

Major Professor: Hüseyin Arslan, Ph.D.
Richard D. Gitlin, Sc.D.
Wilfrido Moreno, Ph.D.
Kenneth Christensen, Ph.D.
Özgür Oyman, Ph.D.

Date of Approval:
October 30, 2012

Keywords: Aeronautical Communication Networks, Device-to-device Networks, Doppler Mitigation, Femtocell Networks, Heterogeneous Networks

DEDICATION

To my parents Hatice Ertürk, and M. Fikri Ertürk

ACKNOWLEDGMENTS

First, I would like to thank my advisor Dr. Hüseyin Arslan for his guidance, encouragement, and support throughout my Ph.D. studies. It has been a privilege to have the opportunity to do research as a member of the Wireless Communications and Signal Processing (WCSP) research group. I would like to thank to all of my colleagues in the WCSP group and the Electrical Engineering Department for their sincere friendship.

I would like to thank Dr. Richard D. Gitlin, Dr. Wilfrido Moreno, Dr. Kenneth Christensen, and Dr. Özgür Oyman for serving in my committee and for offering their valuable feedback, and Dr. Muhammad Rahman for chairing my defense. I hope to be able to benefit from their profound knowledge and experience in the future, as well.

I am grateful to Dr. İsmail Güvenç for his valuable collaboration and sincere friendship. It is an honor for me to work with such an outstanding researcher. I also would like to thank to my colleagues Hiroyuki Ishii, Dr. Sayandev Mukherjee, and Dr. Jamal Haque for their support and contribution to my studies.

I owe much to my family in Tampa: Can Us and Çigdem Us. We shared so many things over the years and I am grateful to them for being with me on the way.

I would like to thank Luz Marina Hernandez for all of her love, patience, and encouragement. She is the one who supported me every day and every step in my studies. I also would like to thank the Hernandez family.

Last, but by no means least, my deepest gratitude goes to my parents Hatice Ertürk, and M. Fikri Ertürk, and my brothers Berk Ertürk and Candaş Aksoy for bringing me up, leading me to the right direction, and always encouraging me for pursuing higher degrees. It is not possible to thank them enough, but I want them to know that I will be grateful to them throughout my life. I could not even try to obtain this degree without them.

TABLE OF CONTENTS

LIST OF TABLES

LIST OF FIGURES

ABSTRACT

The wireless networks of the future are likely to be tiered, i.e., a heterogeneous mixture of overlaid networks that have different power, spectrum, hardware, coverage, mobility, complexity, and technology requirements. The focus of this dissertation is to improve the performance and increase the throughput of tiered networks with resource/interference management methods, node densification schemes, and transceiver designs; with their applications to advanced tiered network structures such as heterogeneous networks (i.e., picocells, femtocells, relay nodes, and distributed antenna systems), device-to-device (D2D) networks, and aeronautical communication networks (ACN).

Over the last few decades, there has been an incredible increase in the demand for wireless services in various applications in the entire world. This increase leads to the emergence of a number of advanced wireless systems and networks whose common goal is to provide a very high data rate to countless users and applications. With the traditional macrocellular network architectures, it will be extremely challenging to meet such demand for high data rates in the upcoming years. Therefore, a mixture of different capability networks has started being built in a tiered manner. While the number and capabilities of networks are increasing to satisfy higher requirements; Modeling, managing, and maintaining the entire structure has become more challenging.

The capacity of wireless networks has increased with various different advanced technologies/methodologies between 1950-2000 which can be summarized under three main titles: spectrum increase (x25), spectrum efficiency increase (x25), and network density (spectrum reuse) increase (x1600). It is vital to note that among different schemes, the most important gain is explored with increasing the reuse and adding more nodes/cells into the

system, which will be the focus of this dissertation. Increasing the reuse by adding nodes into the network in an uncoordinated (irregular in terms of power, spectrum, hardware, coverage, mobility, complexity, and technology) manner brought up heterogeneity to the traditional wireless networks: multi-tier resource management problems in uncoordinated interference environments.

In this study, we present novel resource/interference management methods, node densification schemes, and transceiver designs to improve the performance of tiered networks; and apply our methodologies to heterogeneous networks, D2D networks, and ACN.

The focus and the contributions of this research involve the following perspectives:

1. Resource Management in Tiered Networks: Providing a fairness metric for tiered networks and developing spectrum allocation models for heterogeneous network structures.

2. Network Densification in Tiered Networks: Providing the signal to interference plus noise ratio (SINR) and transmit power distributions of D2D networks for network density selection criteria, and developing gateway scheduling algorithms for dense tiered networks.

3. Mobility in Tiered Networks: Investigation of mobility in a two-tier ACN, and providing novel transceiver structures for high data rate, high mobility ACN to mitigate the effect of Doppler.

CHAPTER 1 :

INTRODUCTION

The wireless networks of the future are likely to be tiered, i.e., a heterogeneous mixture of overlaid networks that have different power, spectrum, hardware, coverage, mobility, complexity, and technology requirements. The focus of this dissertation is to improve the performance and increase the throughput of tiered networks with novel resource/interference management methods, node densification schemes, and transceiver designs; with their applications to advanced tiered network structures such as heterogeneous networks (i.e., picocells, femtocells, relay nodes, and distributed antenna systems), device-to-device (D2D) networks, and aeronautical communication networks (ACN).

1.1 Growth in Wireless Communications

The demand for wireless broadband data has been growing dramatically over the recent years, which introduces an important challenge for the next-generation radio access networks. Recent predictions show that due to the increasing range of throughput-demanding applications on mobile devices, a global data growth as large as $1000\times$ is forecasted by most of the analysts between $2010 - 2020$ [1]- [4]. Moreover, the data consumed by applications of mobile devices such as smartphones and Google glasses will provide extreme burdens to the network providers since users will demand high data rates for their devices anytime and anywhere.

Over the last few decades, there has been an incredible increase in the demand for wireless services in various applications in the entire world. This increase leads to the emergence of a number of advanced wireless systems and networks whose common goal is to provide a very high data rate to countless users and applications, which requires an

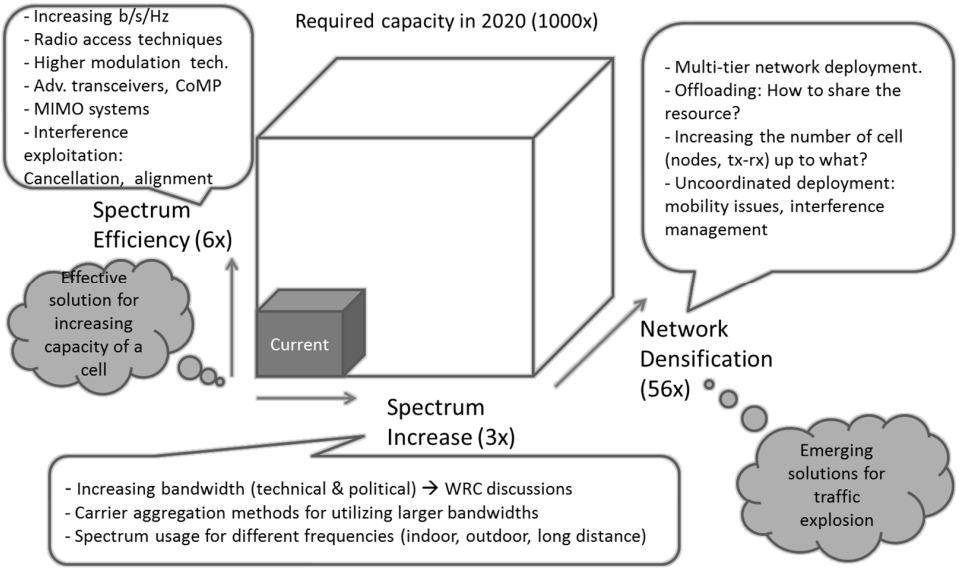

Figure 1.1 Growth in Wireless Communications

enormous capacity everywhere and anytime. The approaches to address this growth in wireless communications are presented in Fig. 1.1.

The main three approaches to enhance the capacity of wireless networks to satisfy this exponential growth in data traffic can be summarized as: increasing the spectrum, increasing the spectrum efficiency, and increasing the density of the network (spectrum reuse).

The capacity of a wireless communication network can be expressed as:

$$\underbrace{\text{Capacity}}_{\text{bits/s}} = \underbrace{\text{Quantity of spectrum}}_{\text{Hz}} \times \underbrace{\text{Efficiency of spectrum}}_{\text{bits/s/Hz}} \times \underbrace{\text{Reuse of spectrum}}_{\text{No units}}. \quad (1.1)$$

It is vital to note that, between 1950-2000, among different schemes the most important gain was explored with spectrum reuse: 1)Spectrum increase (x25), 2) Spectrum efficiency (x25), and 3) Network density (Spectrum reuse) (x1600) [5]. Although the focus of this dissertation will be on network densification, we will summarize these methodologies to present the importance of tiered networks in wireless communications:

1.1.1 Spectrum Increase

The resource in a wireless communication system can be defined by the multi-dimensional electrospace: time, frequency, space, polarization, and orthogonal signalization [6]. The overlapping of different wireless signals in *all* dimensions of electrospace causes interference. If a perfect orthogonality in one of the dimensions in electrospace is satisfied, then the interference will not be an issue. However, intentional overlapping in order to utilize the electrospace is allowed, and unintentional overlapping due to imperfectness of the devices exists. Therefore, the various overlapping scenarios in orthogonal domains (thus interference) are always an issue in wireless communications.

Shannon's capacity equation for a point-to-point wireless link in the presence of interference can be given as

$$C = B \times \log_2 (1 + \text{SINR}), \tag{1.2}$$

where C is the capacity of the link in bit/s, B is the bandwidth in Hz, and SINR is the signal to interference and noise ratio (SINR). (1.2) shows that the basic way of address growth in wireless communication systems is to increase the bandwidth. Traditionally; all new emerging wireless technologies have been demanding wider bands than the existing ones [7]. However, with current technology, only a part of the spectrum could be used for wireless communication purposes due to propagation characteristics of electromagnetic waves especially for outdoor environment, and due to the lack of low cost high performance RF-sections [8]. Additionally, aggregating different carriers to use the underutilized bandwidth chunks in different parts of the spectrum, and aggregating the new carriers for backward compatibility of the devices are also important studies toward addressing the growth of wireless communications [9].

1.1.2 Spectrum Efficiency

Spectral efficiency of a communication system is the data rate that can be transmitted over a given bandwidth in a link and it is measured by bit/s/Hz. It is a measure

of how efficiently a limited frequency spectrum is utilized. The capacity of the wireless communication systems can be enhanced by increasing the spectrum efficiency.

To address the growth in wireless communication with spectrum efficiency, there has been studies to provide new radio access techniques, higher-order modulation techniques, and coordinated multi-point processing (CoMP) transmission techniques. Usage of massive antenna multiple input multiple output (MIMO) techniques for spatial multiplexing and beamforming, and development of advanced transceivers to exploit the interference (i.e., interference avoidance, cancellation, coordination, and alignment) are all topics studied within the title of spectrum efficiency to increase the capacity of wireless communications [10].

1.1.3 Network Densification

Emerging solutions for the traffic explosion consider extreme network densification and the reuse of resources as priority [1]- [2]. Although the traditional (regular, coordinated) macrocellular network architectures have a successful history in wireless communications, it will be extremely challenging to meet the growth in the upcoming years as different capability networks will be required.

Benefits of building different capability networks in a multi-tiered manner can be summarized as increased data rates for users, reduced overall power transmission, enhanced network capacity, better load balancing, and extended coverage area. Therefore, in recent years, a mixture of different capability networks has started being built in a tiered manner to increase the capacity. On the other hand, while the number and capabilities of networks are increasing to satisfy higher requirements; Modeling, managing and maintaining the entire structure has become more challenging.

Increasing the reuse by adding nodes into the network in an uncoordinated (irregular in terms of power, spectrum, hardware, coverage, mobility, complexity, and technology) manner brought up heterogeneity to the traditional wireless networks: multi-tiered resource management problems in uncoordinated interference environments [11], [12]. Therefore

there has been studies in cellular/heterogeneous domains, *ad hoc* wireless communications domain, as well as multi-tiered future aeronautical radio communications domain towards addressing issues related to network densification for the growth of wireless communications [13] - [15].

1.1.4 The Scope of the Dissertation

The scope of this dissertation is to improve the performance and increase the throughput of tiered networks with novel resource/interference management methods, node densification schemes, and transceiver designs; with their applications to advanced tiered network structures such as heterogeneous networks (i.e., picocells, femtocells, relay nodes, and distributed antenna systems), D2D networks, and ACN.

The focus and the contributions of this research involve the following perspectives:

1. Resource Management in Tiered Networks: Providing a fairness metric for tiered networks and developing spectrum allocation models for heterogeneous network structures.

2. Network Densification in Tiered Networks: Providing the signal to interference plus noise ratio (SINR) and transmit power distributions of D2D networks for network density selection criteria, and developing gateway scheduling algorithms for dense tiered networks.

3. Mobility in Tiered Networks: Investigation of mobility in a two-tier ACN, and providing novel transceiver structures for high data rate, high mobility ACN to mitigate the effect of Doppler.

1.2 Impact Statement and Contributions

The impact of tiered network structures (see Fig. 1.2) which uses different power, spectrum, hardware, coverage, mobility, and technology requirements on the future of wireless communication networks is evident. Today, networks *already* have heterogeneity. A

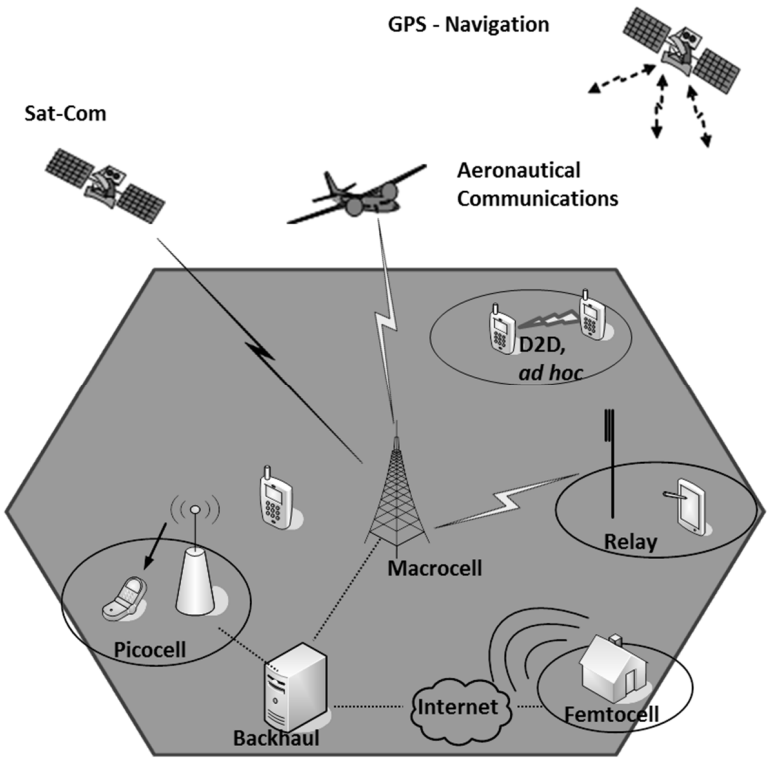

Figure 1.2 Tiered Network Structure

typical 3G/4G cellular provider's network has macrocellular base stations (mBSs) which are deployed coordinated, have high powers, and are aimed to provide almost universal coverage. Picocells, relays, and distributed antenna systems are also introduced within the macrocellular network which are relatively less coordinated, have lower power, and are aimed to provide an increase in the capacity and a decrease in the deadzones. Femtocells, which are user (arbitrarily) deployed very low power nodes, are also small BSs that are designed for both open access (OA) and closed subscriber groups (CSG) with co-channel and dedicated channel options. The major difference of femtocells compared to other heterogeneous networks is that they are connected to the core network through the Internet. D2D and other *ad hoc* network strategies are also bringing additional complementary tiers to the network. Most of the current user equipment and base stations are also taking advantage of the global positioning systems (GPS) and satellite radios to provide a better capacity and variety of applications [16, 17].

The wireless connectivity has become an integral part of our society. However, high data rate aeronautical communications are still under research to be an additional tier in the multi-tiered network structure. The objective of aeronautical communication networks is to provide low latency and low cost services for in-flight multimedia access [18], as well as to use AC systems as a backbone for terrestrial communication networks [19]. Being a new type of tier in the network, high speed, high coverage ACN increases the heterogeneity of the networks and opens up new research directions with new technology requirements and transceiver architectures.

1.2.1 Resource Management in Tiered Networks

In order to address the growth in the wireless communications, cellular providers have an increasing interest in deploying low-power nodes within the coverage areas of macro-cellular networks, such as picocells, femtocells, relay nodes, device-device networks, and distributed antenna systems. These networks, which are commonly referred as heterogeneous networks [20], can efficiently reuse the wireless resources (power, spectrum, hardware, available nodes, and networks) due to low-power operation, and at the same time maintain good link qualities with the end users due to the relatively shorter communication distances.

In heterogeneous networks, frequency[1] resources can be allocated to different tiers in a co-channel (shared-spectrum) or dedicated-channel (split-spectrum) manner, or through a hybrid technique which is a combination of the two approaches. In the co-channel approach, while the spectrum resources are fully reused in different tiers, cross-tier interference may cause crucial setbacks to the system. The split spectrum approach partitions the allocated spectrum between multiple tiers. Each tier can use its own segment of resource and therefore there is no cross-tier interference [21]. However, the amount of bandwidth available to each tier is reduced. Hybrid methods use a mixture of co-channel and dedicated channel methods, and aim to reuse the spectrum resources whenever feasible.

[1] Although resource management schemes in frequency dimension of the electrospace is discussed in this dissertation, the methods can be easily applied for other dimensions of electrospace.

1.2.1.1 Contributions on Resource Management in Tiered Networks

1. A novel metric to measure the fairness of resource management in tiered networks is proposed. Properties of the metric are investigated and examples of usage scenarios are shown.

2. Spectrum splitting models for dedicated channel and hybrid channel heterogeneous networks are proposed and optimization (in terms of overall capacity, tier capacity, fairness) of the spectrum splitting ratio between the macrocell network and the femtocell network is performed. We show that a well-designed spectrum split ratio enjoys the best cell-edge user performance, with minimal degradation in the sum-throughput of macrocell users when compared with that of the co-channel approach.

1.2.2 Network Densification in Tiered Networks

Increasing the number of nodes/BSs/links increases the capacity of the wireless communication systems for a well-designed network. However, the uncoordinated increase in the number of cells may cause severe interference and failure in the system. Therefore the number of cells (links) in a certain area (the density of the network) should be selected carefully so as not to cause a failure in the system. Particularly, with the concepts of self organizing networks (SON), and increased densities of smaller cells, ideal (closed-loop) power control in the networks becomes important to manage uncoordinated interference scenarios. In most of the traditional macrocellular networks, fixed high power is used for the downlink (DL) to provide a universal coverage and path loss compensation-based (open-loop) power control is used for the uplink (UL). However, as the number of the cells are increasing with an uncoordinated deployment manner, the overlapping power footprints of the regions are increasing and the interference level of the environment without power control becomes severe. Therefore, most of the studies consider using power control for dense deployment of small cells [22, 23].

One promising method for enhanced data rates is to employ one transmitter for each receiver (device-to-device (D2D) based communication). When the number of such supported pairs increases, the spectrum reuse of a D2D network increases. The benefits of D2D-based networks include increased data rates, reduced power transmission, enhanced network capacity, better load balancing, and extended coverage [24].

The capacity of a dense network is directly related to the signal to interference plus noise ratio (SINR) at the receiver, and therefore, we shall focus on the statistical properties of the SINR and scheduling. The main focus of this study is to determine the density limit of the network for a given target SINR for links employing power control with a set of network-assisted parameters (i.e., bandwidth, noise power, path loss formula), and to identify the scheduling for a set of dense small cells.

1.2.2.1 Contributions on Network Densification in Tiered Networks

1. Since the dense network simulations are time consuming, slow, expensive, and in some cases impractical, we propose a set of analytical derivations as a tool for investigation of dense network structures using power control.

2. We study the relationship between the network density, transmit power distribution, and target SINR in both simulations and analytical derivations; and find the limits of network densification in a power controlled D2D-based network scenario.

3. Scheduling and cell selection algorithms for dense network gateways are proposed which optimizes the network operation point, and shows the trade-off between cell selection, capacity and fairness.

1.2.3 Mobility in Tiered Networks

Mobility causes the Doppler effect and therefore is an important issue that limits the performance of wireless communication networks. In mobile terrestrial wireless communication systems, the channel model is generally based on the assumption that directions of arrival (DOA) of the signal at the receiver are uniformly distributed which yields to a

Doppler spectrum of the classical Jakes model. As opposed to the Jakes Doppler spectrum in mobile terrestrial communications, ACN channels are modeled with a dual Doppler shift [25]. Therefore, it is possible to estimate and mitigate the effect of Doppler in ACN. In this dissertation, we study the mobility issues in a two-tiered ACN to increase the throughput.

ACN is an emerging concept in which aeronautical platforms are considered to be a part of the multi-tier network for future wireless communication systems. Programs led by the National Aeronautics and Space Administration (NASA), the Federal Aviation Administration (FAA), and EUROCONTROL all include the aeronautical platforms as part of the multi-tier network [15, 26, 27]. The driving reasons for development of high data rate AC systems are: 1) The increase in data demand for Air Traffic Control and Air Traffic Management due to the growth in air transportation [28], 2) The need for low latency and low cost services to provide in-flight multimedia access [18], and 3) The potential to use AC systems as a backbone for terrestrial communication networks [19]. AC systems can provide service for ground networks, public safety, military communications, and improved cockpit data communications. To date, most ground/aircraft cockpit communications are done through voice only, and they are prone to language differences, accents, stress, and cultural barriers [29]. High data rate AC systems can augment the cockpit verbal communication with video and text to reduce cockpit errors. Furthermore, there is a growing demand for high speed data to meet commercial in-flight Internet activities [30].

1.2.3.1 Contributions on Mobility in Tiered Networks

Wireless communication takes place over noisy multipath fading channels. A multipath fading channel is generally characterized as a linear, time-varying system model. Multipath propagation causes delay spread, and time variation of multipath components cause Doppler spread [31]. As opposed to the Jakes Doppler spectrum in terrestrial communications, aeronautical channels are modeled with dual Doppler shift [25]. In aeronautical channels, as the received signal has a dual path with corresponding Doppler shifts, the

Doppler spectrum can be interpreted as a combination of two frequency offsets with corresponding gains. Therefore, it is possible to estimate and mitigate the effect of Doppler shifts by separating and compensating the shifts individually.

1. We changed the traditional receiver structure for the aeronautical channel since the Doppler spectrum model is not the classical Jakes model.

2. We used parametric based estimation algorithms and beamforming techniques for development of novel aeronautical receivers to remove the effect of Doppler and showed that by using these methods, aeronautical receivers can achieve high data rates and the performance of the no Doppler scenario in terms of error rates.

1.3 Dissertation Outline

This dissertation is organized as follows (Fig. 1.3): Chapter 2 investigates the resource management in heterogeneous networks. In this chapter, fairness metric for tiered

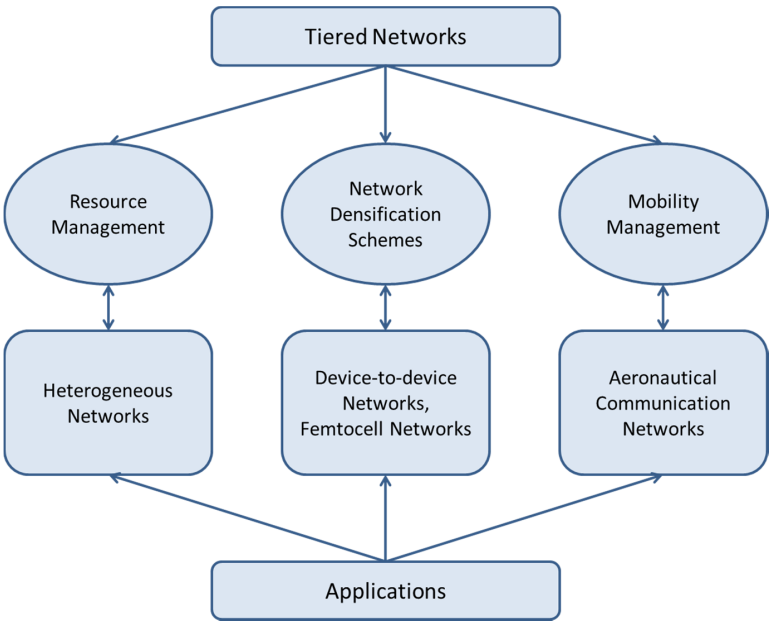

Figure 1.3 Dissertation Organization

networks is proposed, and spectrum allocation optimization is done. In chapter 3, scheduling algorithms for dense networks gateways are proposed and the trade-off between cell-selection, throughput and fairness is presented for different optimizations. For a given target SINR for links employing power control with a set of network-assisted parameters, what would be the density of the network and the distribution of the transmit power is the focus of this chapter. In chapter 4, aeronautical communication networks are studied to investigate the effect of mobility on the tiered networks. Novel transceiver algorithms for high data rate, high mobility aeronautical communication networks are proposed and studied, followed by the conclusions in chapter 5.

1.3.1 Chapter 2: Resource Management in Tiered Networks

In heterogeneous networks, frequency resources can be allocated to different tiers in a co-channel (shared-spectrum) or dedicated-channel (split-spectrum) manner, or through a hybrid technique which is a combination of the two approaches. In the co-channel approach, while the spectrum resources are fully reused in different tiers, cross-tier interference may cause crucial setbacks to the system. The split spectrum approach, on the other hand, partitions the allocated spectrum between multiple tiers. Each tier can use its own segment of resource and therefore there is no cross-tier interference [21]. However, the amount of bandwidth available to each tier is reduced. Hybrid methods use a mixture of co-channel and dedicated channel methods, and aim to reuse the spectrum resources whenever feasible (e.g., when a femtocell is far away from the macrocell base station).

Performance of dedicated-channel and co-channel femtocell/macrocell networks have been investigated and compared through computer simulations in [32, 33]. Both papers show that co-channel deployment increases the total system throughput at the expense of some degradation in the throughput of macrocell users that are close to the femtocells. However, the impact of different spectrum splitting ratios (SSRs) on the overall network has not been studied in these works. Capacity cumulative distribution functions (CDFs) of indoor and outdoor users for different SSRs have been compared through computer

simulations in [34], which shows that for certain scenarios, performance close to the co-channel deployment can be obtained by appropriately setting the SSR value in a dedicated-channel setting. Bharucha et. al. investigate the impact of dynamic resource partitioning for downlink femto-to-macrocell interference avoidance for co-channel femtocell deployments in [35]. The simulation results show that co-channel deployment with dynamic resource partitioning can benefit from the frequency reuse property to achieve high throughputs, and femtocells can switch to orthogonal resource utilization when a close-by macrocell user is detected. However, so called X2-interface between the macrocell base station (mBS) and the femtocell base station (fBS) is assumed to be available in order to exchange the interference coordination information.

One of the key aspects of spectrum allocation in heterogeneous networks is to define a metric to measure and evaluate the degree of fairness and quality of service (QoS) in the overall system [36]. The fundamental work in the area was done by Jain [37], which analyzes all the properties of the fairness metric. Bandwidth assignment and scheduling related optimization problems using fairness criteria were investigated in the literature and utility based fairness indices have been widely recognized due to their flexibility for various application types [38].

The goal of this research is to provide a fairness metric for heterogeneous network architectures and to optimize the SSR in the dedicated-channel approach and in the hybrid-channel approach, considering the fairness and QoS constraints. The steps/methodology in this study can be provided as follows:

1. Sum-capacities of different tiers in a heterogeneous network are expressed in closed form for all approaches by using homogeneous Poisson processes (HPPs).

2. The capacity-maximizing spectrum splitting is investigated by using these expressions.

3. To fairly allocate the resources to different tiers, a modified QoS-oriented fairness metric is introduced.

4. A spectrum splitting strategy that simultaneously considers capacity maximization, fairness constraints, and QoS constraints is proposed.

5. For different SSR values, sum capacities of macrocells and femtocells are obtained through analytical derivations and computer simulations, and are compared for various scenarios.

6. In the hybrid approach, resource management with max-min scheduling is investigated.

1.3.2 Chapter 3: Network Densification in Tiered Networks

The explosion of wireless data has led to the emergence of a number of advanced wireless systems and networks whose common goal is to provide a very high data rate to a large number of users. One promising method for enhanced data rates is to employ one transmitter for each receiver (device-to-device (D2D) based communication). When the number of such supported pairs increases, the spectrum reuse of a D2D network increases. The benefits of D2D networks include increased data rates, reduced power transmission, enhanced network capacity, better load balancing, and extended coverage [24].

In 3.1, we assume that the cellular and D2D network operate on different bands, so that there is no cross-tier interference. The capacity of a D2D network is directly related to the signal to interference plus noise ratio (SINR) at the receiver, and therefore:

1. Power control is one of the key methods discussed in the literature of D2D to achieve a target SINR at the receiver [22, 23]. Therefore, we study the statistical properties of the SINR using HPP for power-controlled networks [39, 40].

2. We study the relationship between the network density, transmit power distribution, and target SINR in both simulations and analytical derivations. For a given set of network-assisted parameters (i.e., bandwidth, noise power, path loss formula), we find the limits of network densification in a power controlled D2D-based network scenario.

In 3.2, we analyze various user assignment and scheduling policies for dense networks. The trade-off between capacity maximization and fairness is investigated and a combined user assignment and proportional fair (PF) scheduling procedure for a dense network gateway is proposed. The flexibility of the proposed architecture in terms of capacity and fairness is studied via various simulation scenarios. It is shown that by changing parameters in the proposed method, one can play-out between fairness and capacity in a femtocell dense network scenario. In order to decrease the number of the handovers between femtocells, we propose that a femtocell user should be scheduled with the same femtocell base station for a duration of superframe, i.e, cell re-selection should be done in every superframe. The performance of the combined user assignment and PF scheduling scheme is investigated under different superframe considerations and it is shown that a wide range of performance results (in terms of capacity, fairness, handover frequency) could be achieved.

1. We consider the assignment of the users to neighboring femtocells through sum-capacity maximizing and SINR-based approaches, and investigate the fairness versus capacity trade-offs.

2. Then, once an initial assignment has been achieved, we investigate how the PF scheduling method can be used to find a good compromise between capacity maximization and fairness in a dense network structure.

1.3.3 Chapter 4: Mobility in Tiered Networks

ACN is an emerging concept in which aeronautical platforms are considered as a part of the multi-tier network for future wireless communication systems. Orthogonal frequency division multiplexing (OFDM) based schemes have been adopted for several current communication systems all over the world [31]. In OFDM-based systems, a serial symbol stream is converted into parallel streams and each symbol is modulated with different orthogonal subcarriers. Orthogonal subcarriers and cyclic prefix (CP) usage provide robustness to OFDM-based systems against the frequency selectivity of wireless channel. However, OFDM-based systems have relatively longer symbol durations compared to single carrier

systems. Longer symbol duration leads to weakness against the time variation of the channel, i.e., Doppler spread, which causes loss of orthogonality between subcarriers. If the orthogonality is not preserved within an OFDM symbol duration, there will be inter-carrier interference (ICI).

ICI degrades channel estimation and symbol detection performances of OFDM-based systems [41], [42]. If not compensated, ICI will cause an error floor for the symbol detection. For example, in the terrestrial OFDM systems, the channel model is generally based on the assumption that directions of arrival (DOA) of the signal at the receiver are uniformly distributed which yields to a Doppler spectrum of the classical Jakes model. The estimation of the channel and the compensation of the channel effect on the received signal are computationally complex in the Jakes Doppler spectrum scenario. Therefore, ICI is generally overcome by increasing the subcarrier spacing (decreasing the length of the OFDM symbol) and bounding the normalized Doppler frequency (NDF)[2] which causes an error floor for symbol detection in terrestrial communications [43].

As opposed to the Jakes Doppler spectrum in terrestrial communications, aeronautical channels are modeled with dual Doppler shift [25]. The result of the dual Doppler shift is also ICI in OFDM-based AC system. However, in aeronautical channels, as the received signal has a dual path with corresponding Doppler shifts, the Doppler spectrum can be interpreted as a combination of two frequency offset with corresponding gains. Therefore, it is possible to estimate and mitigate the effect of Doppler shifts by separating and compensating the shifts individually.

In the literature, OFDM channel estimation and ICI compensation for the dual Doppler shift are investigated in [44–47]. In [44], a Kalman filter-based estimation method with zero-forcing equalization is provided to cancel the effect of ICI. In [45], a digital phase lock loop is proposed to be used in order to track parameters of LOS path, and a maximum-likelihood estimator is suggested to resolve the reflected path. Then, the authors propose a Kalman-based approach to provide more accurate estimation, and to utilize an iterative

[2]Note that this method also decreases the efficiency of OFDM-based systems and will be discussed in this chapter.

cancellation method for the ICI compensation. In [46], Doppler shift compensation is suggested only for the line of sight (LOS) path, and demodulation is performed in the presence of ICI. A different version of OFDM, Non-Contiguous Orthogonal Signal Division Multiplex (NCOSDM), is considered in [47] where the number of subcarriers are decreased depending on the channel to decrease the ICI and maintain the system performance.

In this study, OFDM system will be evaluated for the aeronautical channel[3]. The usage of parametric based estimation algorithms and beamforming techniques for development of novel aeronautical receivers will be investigated as follows:

1. ICI effect on the received signal is derived and the ICI power is shown.

2. Parametric spectrum estimation methods are investigated to extract Doppler shifts since the number of paths are already very limited and predictable (i.e., two or three).

3. We investigate the modeling errors and their effects on the estimation error.

4. The beamforming based approach is examined to separate the multi-Doppler signals, based on Direction Of Arrival (DOA).

5. Once the signals are separated, conventional methods are used to correct the Doppler.

6. The results for different modeling errors and estimation errors are investigated according to the delay and complexity of the parametric spectrum estimation approaches.

7. We show that beamforming with a different number of antenna elements can create beams with resolutions that are capable of separating these Doppler affected paths and the effect on aeronautical channel can be resolved. Therefore higher

[3]In this study, we focus on multi-carrier systems i.e., OFDM. However, the methods to estimate and resolve the aeronautical channel effect on the received signal investigated in this paper can also be applied for single-carrier systems. Reader is referred to [48] for investigation of interference mitigation schemes with single-carrier systems in aeronautical environment.

data rates can be achieved in aeronautical communication networks with this novel receiver structure.

CHAPTER 2 :

RESOURCE MANAGEMENT IN TIERED NETWORKS

The demand for wireless broadband data has been growing dramatically over the recent years, which introduces an important challenge for next-generation radio access networks. Recent predictions show that due to the increasing range of throughput-demanding applications on mobile devices, a global data growth as large as $1000\times$ is forecasted by most of the analysts between $2010-2020$ [1]- [4]. Moreover, the data consumed by applications of mobile devices such as smartphones and Google glasses will provide extreme burdens to the network providers since users will demand high data rates for their devices at anytime and anywhere. With the traditional macrocellular networks, it will be extremely challenging to meet such demand for high data rates in the upcoming years.

In order to address these challenges, there has been an increasing interest to deploy low-power nodes within the coverage areas of macrocellular networks, such as picocells [49], femtocells [21], relay nodes [50], and distributed antenna systems [51]. These networks, which are commonly referred as heterogeneous networks [20], can efficiently reuse the wireless resources (power, spectrum, hardware, available nodes and networks, etc.) due to low-power operation, and at the same time maintain good link qualities with the end users due to the relatively shorter communication distances[1].

2.1 Introduction

Efficient assignment of communication resources to different tiers in a heterogeneous network carries critical importance; it should meet the quality-of-service (QoS) requirements

[1]While the present study will be mostly focusing on femtocell/picocell networks coexisting with a macrocell network, proposed framework can be easily extended when other heterogeneous network entities are present in the system.

of different tiers, and at the same time maximize the total system capacity. In this chapter, a modified QoS-oriented fairness metric is proposed, which captures important characteristics of tiered network architectures that are not captured by the Jain's fairness index. A heterogeneous network composed of femtocells deployed within a macrocell network is considered, and optimization of the resource splitting ratio is investigated by using the proposed metric for co-channel, dedicated-channel and hybrid scenarios. First, using homogeneous Poisson processes (HPP), sum-capacities in such a network are expressed in closed-form for co-channel, dedicated-channel, and hybrid resource allocation methods. Then, a resource splitting strategy that simultaneously considers capacity maximization, fairness constraints, and QoS constraints is proposed. Detailed computer simulations utilizing 3GPP simulation assumptions show that a hybrid allocation strategy with a well-designed resource split ratio enjoys the best cell-edge user performance, with minimal degradation in the sum-throughput of macrocell users when compared with that of co-channel operation.

2.1.1 Frequency Allocation for Heterogeneous Networks

In heterogeneous networks, frequency resources[2] can be allocated to different tiers in a co-channel (shared-spectrum) or dedicated-channel (split-spectrum)[3] manner, or through a hybrid technique which is a combination of the two approaches. In the co-channel approach shown in Fig. 2.1(a), while the spectrum resources are fully reused in different tiers, cross-tier interference may cause crucial setbacks to the system. For example, macrocell users in the vicinity of closed subscriber group (CSG) femtocells are not allowed to connect to the femtocells, even if their link quality is good with these femtocells. Therefore, such macrocell users receive strong downlink interference from CSG femtocells and may fall into outage [52].

[2]Although resource management schemes in frequency dimension of the electrospace is discussed in this dissertation, the methods can be easily applied for other dimensions such as time, code, and orthogonal signalization dimensions.

[3]Throughout the chapter, the terms shared-spectrum and split-spectrum will be used interchangeably with co-channel and dedicated-channel, respectively.

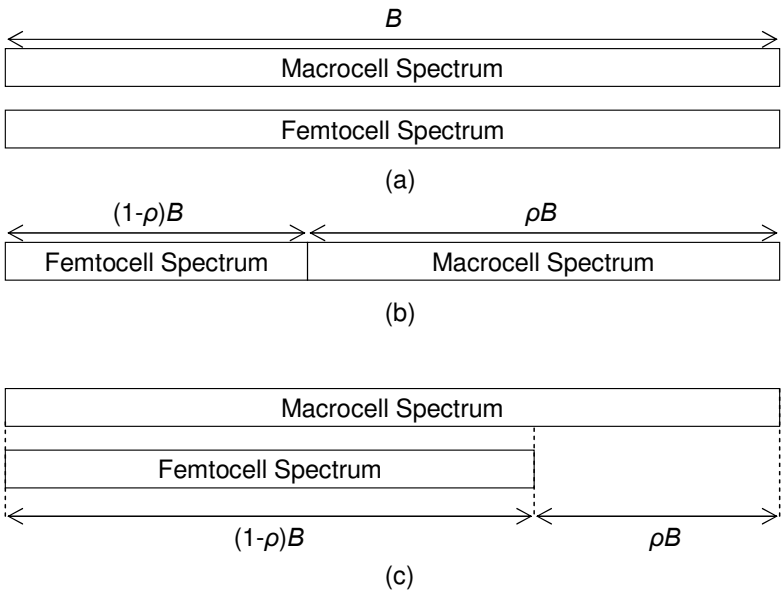

Figure 2.1 Resource Allocation Approaches: (a) Co-channel Approach, (b) Dedicated-channel Approach, and (c) Hybrid Approach

The split spectrum approach shown in Fig. 2.1(b), on the other hand, partitions the allocated spectrum between multiple tiers. Each tier can use its own segment of resource and therefore there is no cross-tier interference [21]. However, the amount of bandwidth available to each tier is reduced. Hybrid methods as shown in Fig. 2.1(c) use a mixture of co-channel and dedicated channel methods, and aim to reuse the spectrum resources whenever feasible. For example, in [53], the macrocell users are dedicated a component carrier (CC), referred as the "escape carrier", which is not used by the femtocell network. Any mMS which is close by to a femtocell is scheduled within this escape carrier, if the interference observed from the femtocell network is above a threshold. Hence, user outages are prevented by scheduling victim users in dedicated resources, while the spectrum is still reused in co-channel CCs. The resources within a certain CC may also be partitioned into smaller chunks for similar interference mitigation purposes [35].

Performance of dedicated-channel and co-channel femtocell/macrocell networks have been investigated and compared through computer simulations in [32, 33]. Both papers show that co-channel deployment increases the total system throughput at the expense of some degradation in the throughput of macrocell users that are close to the femtocells. However, impact of different spectrum splitting ratios (SSRs) on the overall network has not been studied in these works. Capacity cumulative distribution functions (CDFs) of indoor and outdoor users for different SSRs have been compared through computer simulations in [34], which shows that for certain scenarios, performance close to the co-channel deployment can be obtained by appropriately setting the SSR value in a dedicated-channel setting. Bharucha *et. al.* investigate the impact of dynamic resource partitioning for downlink femto-to-macrocell interference avoidance for co-channel femtocell deployments in [35]. The simulation results show that co-channel deployment with dynamic resource partitioning can benefit from the frequency reuse property to achieve high throughputs, and femtocells can switch to orthogonal resource utilization when a close-by macrocell user is detected. However, so called X2-interface between the macrocell base station (mBS) and the femtocell base station (fBS) is assumed to be available in order to exchange the interference coordination information.

2.1.2 Time-Domain Resource Coordination

Similar to frequency-domain resource partitioning and sharing, time domain resources may also be partitioned and shared among femtocells and macrocells. For example, as shown in Fig. 2.2, 3GPP utilizes almost blank subframes[4] (ABSs) for mitigating interference to victim macrocell users [54]- [56], such as mMS-2 and mMS-3 in Fig. 2.2. The femtocells fBS-1 and fBS-2 are configured not to schedule any transmission (other than the reference signals) in the ABSs for allowing protection of victim macrocell users. For example, in Fig. 2.2, subframes 5, 6, 9 are left blank in fBS-1, while subframes 2, 4, 8, 9 are left blank in fBS-2. Then, victim macrocell users may be scheduled in macrocell resources

[4]The subframes are named as *almost* blank, since the reference signals are still transmitted in these subframes.

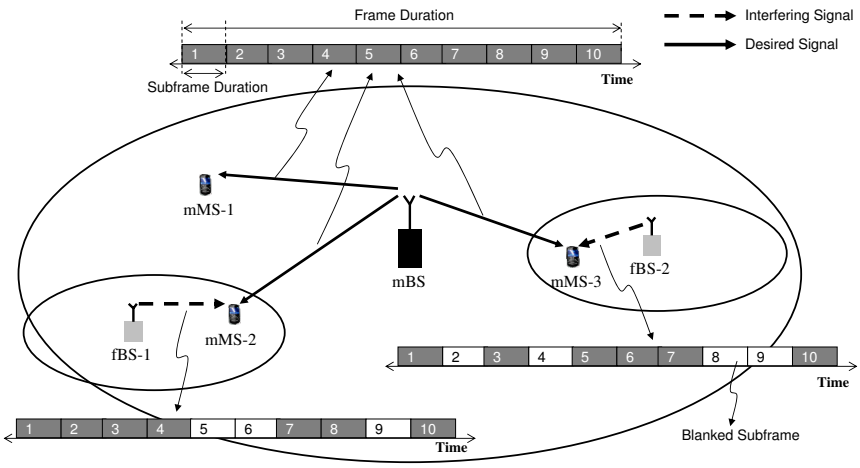

Figure 2.2 Use of Blank Subframes at Femtocells for Interference Coordination in 3GPP

overlapping with the blank subframes; i.e., mMS-2 may be scheduled in subframes 5, 6, 9, while mMS-3 may be scheduled in subframes 2, 4, 8, 9 of macrocell, while there is no scheduling restriction for mMS-1.

Even though the ABS pattern may be dynamically changed (as fast as every 40 ms [57]) for picocells through the X2 interface in LTE, for femtocells, the solutions are less dynamic due to the absence of X2 interface between femtocells and macrocell. For example, through operation and management (OAM), different blank subframe patterns (known both to the femtocells and macrocell) may be used at different times of the day [57]. In [58], three alternative solutions are proposed in order for the mBS to know the blank subframe pattern in femtocells: 1) a single ABS pattern is configured for all femtocells in the macrocell coverage area (prevents adaptation of the femtocell to the traffic variations in its coverage), 2) Configured blank subframe pattern can be signalled in the system information of femtocells (not very desirable), and 3) Macrocell users may identify the blank subframe pattern through measurements, and report the identified pattern to the macrocell (increased complexity of mMS). Nevertheless, regardless of whether a static or a dynamic approach is used, number of blank subframes should be optimized in order to accommodate different number of users and their QoS requirements [55, 56], and the framework covered in this chapter can also be readily applied for time-domain resource configuration.

2.1.3 Fairness Criteria for Resource Allocation

In order to maximize the capacity of a macrocell-femtocell network, adaptive access operation of femtocells [59], hybrid resource allocation [60], and adaptive transmit powers [61, 62] have formerly been proposed in the literature. In [63], a QoS parameter that captures the average capacities in femtocell and macrocell tiers have been defined, and spectrum allocation to different tiers is carried out based on this parameter. However, *fairness* of the overall system is not directly accounted while allocating the spectrum among the tiers.

One of the key aspects of spectrum allocation in heterogeneous networks is to define a metric to measure and evaluate the degree of fairness and quality of service (QoS) in the overall system [36]. The fundamental work in the area was done by Jain [37], which analyzes all the properties of the fairness metric. Variance (σ^2), coefficient of variation (CoV), min-max ratio, and normalized distance are some of the other traditional fairness metrics which have been used for resource allocation problems in the literature [64]. Bandwidth assignment and scheduling related optimization problems using fairness criteria were investigated in [65]. Utility based fairness indices [38] have been widely recognized due to their flexibility for various application types.

Fair resource allocation and associated criteria have also been investigated by standardization bodies. For example, normalized capacity CDFs of users are used as a fairness metric by 3GPP2. In this definition of fairness, a CDF of normalized user capacity (with respect to average capacity or maximum user capacity) is considered. Then, a fair scheduler's CDF plot of normalized throughput should lie to the right of a pre-prescribed line of reference. In order words, it ensures that the percentage of the users having very low data rate compared to average data rate does not go above a threshold value, and cell edge users are not penalized [66].

2.1.4 Chapter Outline

The goal of this chapter is to provide a fairness metric for heterogeneous network architectures and to optimize the SSR (ρ) in dedicated-channel approach as in Fig. 2.1(b) and in hybrid-channel approach as in Fig. 2.1(c), considering the fairness and QoS constraints[5]. First, sum-capacities of different tiers in a heterogeneous network are expressed in closed form for all approaches, and capacity-maximizing spectrum splitting is investigated. To fairly allocate the resources to different tiers, a modified QoS-oriented fairness metric is introduced. This metric captures important characteristics of tiered network architectures such as the number of networks in each tier, the number of users in each network, and the QoS requirements of different tiers. Therefore, fairness in the tiered system is effectively captured when compared with the Jain's fairness index (JFI) [37]. Then, a spectrum splitting strategy that simultaneously considers capacity maximization, fairness constraints, and QoS constraints is proposed. For different SSR values, sum capacities of macrocells and femtocells are obtained through analytical derivations and computer simulations, and compared for various scenarios. In hybrid approach, resource management with max-min scheduling is investigated.

The remaining part of this chapter is organized as follows. In section 2.2, the system model to provide total capacity of a macrocell-femtocell network is provided, and QoS-oriented fairness metric for tiered network structures is proposed. In section 2.3, capacities of co-channel, dedicated channel and hybrid channel approaches are derived using HPPs and a max-min fair scheduler is introduced for hybrid channel approach. Numerical results for various scenarios are presented in section 2.4, followed by concluding remarks in the last section 2.5.

2.2 Fairness Metric and System Model for Tiered Networks

Consider a two-tier macrocell-femtocell scenario (i.e., $T = 2$), where macrocell-tier network is the tier-1 network and femtocell-tier network is the tier-2 network. We follow the

[5] As mentioned in section 2.1.2, discussions in the chapter also apply to time-domain resource allocation. However, rest of the chapter will be written from the perspective of spectrum allocation.

Table 2.1 Description of Parameters and Notation

Parameter	Description
ρ	Let B_{M} and B_{F} be the total bandwidth of a macrocell-tier and femtocell-tier network, respectively. Then, ρ is the portion of the accessed bandwidth for macrocell-tier network, i.e., 1-ρ is the portion for femtocell-tier network.
i, j, k	Indices for the tiers, networks in each tier and users in each network, respectively.
$N_{\mathrm{N},i}$	Number of networks in i^{th} tier, $(i = 1, .., T)$, i.e., $N_{\mathrm{N},1} = 1$ for macrocell-tier, $N_{\mathrm{N},2}$ is the number of femtocell networks in femtocell-tier.
$N_{\mathrm{U},i,j}$	Number of users in i^{th} tier and j^{th} network, i.e., $N_{\mathrm{U},1,1}$ is the number of macrocell-tier users, $N_{\mathrm{U},2,j}$ is the number of users in the j^{th} femtocell.
N_{Tot}	Total number of users in the system. i.e., $N_{\mathrm{Tot}} = \sum_{i=1}^{T} \sum_{j=1}^{N_{\mathrm{N},i}} N_{\mathrm{U},i,j}$.
$C_{i,j,k}$	Capacity of the k^{th} user in the i^{th} tier and j^{th} network. Note that, there is only one macrocell ($j = 1$, for $i = 1$) and several femtocells ($j = 1, .., N_{\mathrm{N},2}$, for $i = 2$).
$B_{i,j,k}$	Bandwidth of the k^{th} user in the i^{th} tier and j^{th} network.
$SINR_{i,j,k}$	Signal to interference plus noise ratio (SINR) of the k^{th} user in the i^{th} tier and j^{th} network.
$P_{i,j,k}$	Received power of the k^{th} user in the i^{th} tier and j^{th} network.
$f_{\mathrm{QTFI}}(\mathbf{C})$	QoS-oriented fairness metric. Note that $\mathbf{C}$ is the 3-dimensional capacity matrix which consists of $C_{i,j,k}$, $\forall i, j, k$.

notation defined in Table 2.1 and evaluate the capacity within the coverage area of a given macrocell of interest (i.e., $j = 1$ for $i = 1$), surrounded by interfering macrocells. Moreover, $N_{\mathrm{N},2}$ femtocells ($j = 1, ..., N_{\mathrm{N},2}$ for $i = 2$) are assumed to be randomly distributed within the coverage area of the given macrocell, and our goal is to maximize

$$C_{\mathrm{Tot}} = \sum_{i=1}^{T} \sum_{j=1}^{N_{\mathrm{N},i}} \sum_{k=1}^{N_{\mathrm{U},i,j}} C_{i,j,k} \quad , \tag{2.1}$$

while considering fairness metric and QoS parameter.

2.2.1 Capacity of Macrocell and Femtocell

Using the notation given in Table 2.1, the total capacity for the femtocell-tier (tier-2) can be expressed as

$$C_{\text{Fem}} = C_2 = \sum_{j=1}^{N_{\text{N},2}} \sum_{k=1}^{N_{\text{U},2,j}} \underbrace{B_{2,j,k} \log_2 \left(1 + \frac{P_{2,j,k}}{I_{2,j,k} + B_{2,j,k} N_0}\right)}_{C_{2,j,k}} \quad , \tag{2.2}$$

where $I_{2,j,k}$ denotes interference power observed by the k^{th} user with the j^{th} femtocell, N_0 is the spectral density of noise, and $C_{2,j,k}$ is the capacity of femtocell user-k with the j^{th} femtocell.

Similarly, using the notation given in Table 2.1, the total capacity of macrocell-tier can be written as

$$C_{\text{Mac}} = C_1 = \sum_{j=1}^{N_{\text{N},1}} \sum_{k=1}^{N_{\text{U},1,j}} \underbrace{B_{1,j,k} \log_2 \left(1 + \frac{P_{1,j,k}}{I_{1,j,k} + B_{1,j,k} N_0}\right)}_{C_{1,j,k}} \quad , \tag{2.3}$$

where $I_{1,j,k}$, and $C_{1,j,k}$ denotes interference level and capacity for the k^{th} macrocell user in the j^{th} macrocell. For the sake of analytical tractability, we consider that the number of users in each femtocell is assumed to be fixed, i.e., $N_{\text{U},2,j} = N_{\text{U,F}}, \forall j$. Moreover, both macrocell users (mMS) and femtocell users (fMS) are assumed to be distributed uniformly within each circular macrocell and femtocell area.

2.2.2 QoS-orientation and Fairness Metric for Tiered Networks

We first define a fairness index and propose that a fair spectrum allocation can be achieved by considering the heterogeneous architecture of tiered networks [67]. Then a QoS parameter is also added in the fairness metric to provide QoS orientation for the spectrum allocation.

Fairness Index: Jain's fairness index (JFI) [37] has been a widely used fairness criterion in the literature for resource allocation and can be written as

$$f(x) = \frac{\left(\sum_{i=1}^{N} x_i\right)^2}{N \sum_{i=1}^{N} x_i^2} \quad , \tag{2.4}$$

where N denotes the total number of users and x_i denotes the received allocation for the i^{th} user. Some of the important properties of (2.4) are as follows: 1) Population size independence, 2) Scale and metric independence, 3) Boundedness ($f(x) \in [1/N, 1], \forall x$), 4) Direct relationship, and 5) Continuity (non-discrete).

Tiered network structures, such as those including femtocells, picocells, and relay networks overlaid with a macrocell network, introduce a multi-dimensional resource allocation problem. In tiered networks, where users are distributed among tiers and the networks within each tier, providing a global fairness index for the entire system requires a modified fairness criteria. Consider a T-tiered architecture where each tier has several networks, similar to the one defined in section 2.2.1 with the same notation defined in Table 2.1. We propose that a tiered fairness index (TFI) in such a system should be as follows

$$f_{\text{TFI}}(\mathbf{C}) = \frac{\left(\sum_{i=1}^{T} \sum_{j=1}^{N_{\text{N},i}} \sum_{k=1}^{N_{\text{U},i,j}} N_{\text{U},i,j} C_{i,j,k}\right)^2}{N_{\text{Tot}} \sum_{i=1}^{T} \sum_{j=1}^{N_{\text{N},i}} \sum_{k=1}^{N_{\text{U},i,j}} N_{\text{U},i,j}^2 C_{i,j,k}^2} \quad , \tag{2.5}$$

where $\mathbf{C}$ denotes the set of capacities of all the users in all tiers, and N_{Tot} is the total number of users in the entire system:

$$N_{\text{Tot}} = \sum_{i=1}^{T} \sum_{j=1}^{N_{\text{N},i}} N_{\text{U},i,j} \quad . \tag{2.6}$$

The difference of (2.5) from the JFI is that it is a global fairness index for a tiered network and it weighs the tiers and networks according to their number of users[6].

[6]Note that the number of users in each femtocell is assumed to be known.

Table 2.2 Bounds for Fairness Indices

FI	Lower bound	Upper bound
$f_{\text{JFI}}(\mathbf{C})$	$1/N_{\text{tot}}$	No explicit solution.[7]
$f_{\text{TFI}}(\mathbf{C})$	$1/N_{\text{tot}}$	1
$f_{\text{WJFI}}(\mathbf{C})$	$\frac{\sum_{i=1}^{T}\sum_{j=1}^{N_{\text{N},i}} 1/N_{\text{U},i,j}}{\sum_{i=1}^{T} N_{\text{N},i}}$	1
$f_{\text{QTFI}}(\mathbf{C})$	$1/N_{\text{tot}}$	1

Using the notation given in Table 2.1, (2.4) may be re-written by changing N with N_{Tot} as follows:

$$f_{\text{JFI}}(\mathbf{C}) = \frac{\left(\sum_{i=1}^{T}\sum_{j=1}^{N_{\text{N},i}}\sum_{k=1}^{N_{\text{U},i,j}} C_{i,j,k}\right)^2}{N_{\text{Tot}}\sum_{i=1}^{T}\sum_{j=1}^{N_{\text{N},i}}\sum_{k=1}^{N_{\text{U},i,j}} C_{i,j,k}^2} \quad . \tag{2.7}$$

Since the JFI in (2.7) does not consider the number of users in each network for tiered scenarios, it does not satisfy the boundedness property (see Table 2.2). In other words, $f_{\text{JFI}}(\mathbf{C})$ is no longer tightly bounded within $[1/N_{\text{Tot}}, 1]$. While the number of users in each network varies, the upper bound of JFI changes. This property will be discussed in an example case study later in section 2.4 (see Fig. 2.3).

Finding the JFI for each network in each tier and obtaining a weighted summation of them could be another approach for a modified fairness index for tiered networks which has an upper bound of 1 as opposed to JFI (see Table 2.2). The weighted sum JFI (WJFI) could be written as

$$f_{\text{WJFI}}(\mathbf{C}) = \frac{1}{\sum_{i=1}^{T} N_{\text{N},i}} \times \sum_{i=1}^{T}\sum_{j=1}^{N_{\text{N},i}} \frac{(\sum_{k=1}^{N_{\text{U},i,j}} C_{i,j,k})^2}{N_{\text{U},i,j}\sum_{k=1}^{N_{\text{U},i,j}} C_{i,j,k}^2}. \tag{2.8}$$

However, WJFI does not consider the number of users in each network and weighs the fairness with the total number of networks in the system ($\sum_{i=1}^{T} N_{\text{N},i}$). For instance, if one network (i.e., macrocell network or each one of the femtocell networks) has twice the number of users compared to another network, (2.8) does not consider this and provides

[7] Can not be expressed independent of $\mathbf{C}$

equal weights for each network. While this metric has an upper bound of 1, it does not have a lower bound of $1/N_{\text{Tot}}$. Table 2.2 shows that lower bound of the equation is increasing with the decrease in the number of users in each network, which is a very common case for a femtocell scenario.

QoS-oriented TFI: In tiered networks, it is typically expected that the tiers will have different QoS requirements. For example, in a macrocell-femtocell two-tier network, femtocell users are expected to have significantly better throughput compared to macrocell users due to better link qualities and larger spectrum resources. Therefore, the QoS characteristics of each tier should also be considered within the fairness index in order to have a better representation of fairness within the whole system. Let β_i $(i = 2, ..., T)$ denote the QoS parameter defined as the ratio of the sum capacity in the first tier (e.g., macrocell tier) to the sum capacity in a different tier (e.g., femtocell tier)

$$\beta_i = \frac{1/N_{\text{N},1} \sum_{j=1}^{N_{\text{N},1}} \sum_{k=1}^{N_{\text{U},1,j}} C_{1,j,k}}{1/N_{\text{N},i} \sum_{j=1}^{N_{\text{N},i}} \sum_{k=1}^{N_{\text{U},i,j}} C_{i,j,k}} \quad , \tag{2.9}$$

where $\beta_1 = 1$. Using this QoS parameter, a modified version of the proposed fairness index in (2.5) can be written as

$$f_{\text{QTFI}}(\mathbf{C}) = \frac{\left(\sum_{i=1}^{T} \sum_{j=1}^{N_{\text{N},i}} \sum_{k=1}^{N_{\text{U},i,j}} \beta_i N_{\text{U},i,j} C_{i,j,k}\right)^2}{N_{\text{Tot}} \sum_{i=1}^{T} \sum_{j=1}^{N_{\text{N},i}} \sum_{k=1}^{N_{\text{U},i,j}} \beta_i^2 N_{\text{U},i,j}^2 C_{i,j,k}^2}. \tag{2.10}$$

Note that (2.10) converges to (2.5) while $\beta_i \to 1$ $(i = 2, ..., T)$. Moreover, if macrocell is the only tier in the system (i.e., $T = 1$, $N_{\text{N},1} = 1$), then (2.5) converges to the Jain's fairness index given in (2.7). This proves that the provided equations are the modified versions of the JFI in order to satisfy the boundedness property within $[1/N_{\text{Tot}}, 1]$. Table 2.2 summarizes the lower and upper bounds of the above mentioned fairness indices.

It is important to note that the proposed fairness indices $f_{\text{TFI}}(\mathbf{C})$ and $f_{\text{QTFI}}(\mathbf{C})$ are bounded and independent of the number of networks in the tiered-network structure. JFI upper bound is not independent from the allocated resources, and therefore, the upper

bound can not be expressed in closed form. Similarly, lower bound of the WJFI depends on the number of networks and the number of users within the networks in each tier. As opposed to JFI and WJFI, proposed fairness indices TFI and QTFI provide a controlled metric for resource allocation problems in tiered networks.

2.3 Resource Partitioning in Macrocell-Femtocell Networks

We consider a two-tier macrocell-femtocell scenario (i.e., $T = 2$), where macrocell-tier network is the tier-1 network and femtocell-tier network is the tier-2 network. The goal is to split the total bandwidth B among tiers such that:

1. The capacity of the overall system is maximized.
2. A level of global fairness is ensured between users in different tiers.
3. QoS requirements of users in different tiers in terms of relative data rates are satisfied.

As shown in Fig. 2.1(b) for the split-spectrum approach, the portion of the accessed bandwidth for macrocell-tier is $\rho = \frac{B_{\mathrm{M}}}{B}$, where $B_{\mathrm{M}} = \sum_{k=1}^{N_{\mathrm{U},1,1}} B_{1,1,k}$. Therefore, we have $B_{\mathrm{F}} = (1-\rho)B = \sum_{k=1}^{N_{\mathrm{U},2,j}} B_{2,j,k},\ \forall j$. For the hybrid approach as in Fig. 2.1(c), the portion of the accessed bandwidth for macrocell-tier is the total bandwidth $B_{\mathrm{M}} = B$, and we have $B_{\mathrm{F}} = (1-\rho)B$ where $B_{\mathrm{M}} = \sum_{k=1}^{N_{\mathrm{U},1,1}} B_{1,1,k}$ and $B_{\mathrm{F}} = \sum_{k=1}^{N_{\mathrm{U},2,j}} B_{2,j,k},\ \forall j$. In both approaches, our goal when splitting the spectrum is to maximize

$$C_{\mathrm{Tot}}(\rho) = \sum_{i=1}^{T} \sum_{j=1}^{N_{\mathrm{N},i}} \sum_{k=1}^{N_{\mathrm{U},i,j}} C_{i,j,k}(\rho)\ , \tag{2.11}$$

while considering fairness metric and QoS parameter.

2.3.1 Macrocell and Femtocell Deployment using HPP

In this section, we focus on a general analytical formulation of the macrocell-femtocell capacities by employing statistical models for mBS and fBS locations. We fo-

cus on an arbitrary MS (called a UE in 3GPP terminology) in this region and calculate the downlink capacity for macrocell and femtocell users for dedicated channel, co-channel and hybrid channel scenarios. These results (which are functions only of the macro and femto relative densities, transmit powers, the parameters of the wireless channel, and the SSR) provide valuable insights for the architecture planning process for joint femto-macro deployments under different fairness and QoS criteria.

The mBS locations are assumed to be points of a homogeneous Poisson point process (HPP) on the plane with intensity λ, and have the following properties:

1. The number of mBSs $N(\mathbb{B})$ in any finite region $\mathbb{B}$ is Poisson($\lambda \times \text{area}(\mathbb{B})$), i.e.

$$\mathbb{P}\{N(\mathbb{B}) = n\} = \mathrm{e}^{-\lambda \times \text{area}(\mathbb{B})} \frac{[\lambda \times \text{area}(\mathbb{B})]^n}{n!} \quad \text{for } n = 0, 1, \ldots \tag{2.12}$$

   with mean $\mathbb{E}N(\mathbb{B}) = \lambda \times \text{area}(\mathbb{B})$.

2. $\forall \mathbb{B}, \mathbb{B}' : \mathbb{B} \cap \mathbb{B}' = \varnothing \Rightarrow N(\mathbb{B}), N(\mathbb{B}')$ are independent.

3. $\forall \mathbb{B}$, given $N(\mathbb{B}) = n$, these n mBS are i.i.d and uniformly distributed over $\mathbb{B}$.

Note that λ is in units of points per meter-square. We model the locations of fBS by points of an independent HPP with intensity λ' and all the fBSs are operating in CSG mode.

The wireless channel model we use in this study can be defined by the following assumptions:

1. Path loss exponent is δ.

2. Fading in all macrocellular downlinks are i.i.d. Rayleigh[8] with mean 1.

3. All mBSs (fBSs) transmit with the same reference symbol power P_{RS} (P'_{RS}).

[8]The analysis in this study can be applied to general models however the expressions are more complex, therefore we restrict ourselves for this case for brevity.

4. An MS at distance r from an mBS has reference symbol received power (RSRP in LTE terminology)

$$\text{RSRP}(r) = \frac{H}{r^{\delta}},\ H \sim \exp(P),\ P \equiv KP_{\text{RS}} \tag{2.13}$$

where the exponential distribution of H arises from the Rayleigh fading assumption, and K is a quantity that takes into account the relative heights of the transmitter and receiver on the link, etc., and is considered the same for all links from any MS location to any mBS. We are interested in MS locations whose distance from the nearest mBS exceeds some $r_{\min}$.

5. Similarly, an MS at distance r' from an fBS has RSRP given by

$$\text{RSRP}'(r') = \frac{H'}{r'^{\delta}},\ H' \sim \exp(P'),\ P' \equiv K'P'_{\text{RS}}. \tag{2.14}$$

2.3.2 Results from the Theory of Poisson Point Processes

In this section, we will review the fundamental results from theory of HPP that are applicable for the capacity analysis in this study.

Theorem: *Suppose that there are transmitters located at points of M independent HPPs $1, \cdots, M$, with intensities $\nu_1, \cdots, \nu_M$ respectively and that the MS must be a minimum distance of $d_{min,k}$ from the nearest transmitter of HPP k, $k = 1, \cdots, M$. The fading coefficients on all transmitter-MS links are independent, and those on the links between the UE and the transmitters belonging to HPP k are i.i.d. Exp(μ_k), $k = 1, \cdots, M$. Suppose the MS is at a distance of r from the nearest transmitter of HPP1. Then the cumulative CDF (CCDF) of SIR(r), the SIR at the MS when served by the nearest transmitter of HPP1, is given by*

$$\mathbb{P}\{\Gamma_1 > \gamma | R_1 = r_1\} = \exp\left(-u\gamma^{\frac{2}{\delta}}\left[G\left(\frac{1}{\gamma^{\frac{2}{\delta}}}\right) + \sum_{k=2}^{M} \Theta_k G\left(\frac{m_k}{u\gamma^{\frac{2}{\delta}}\Theta_k}\right)\right]\right). \tag{2.15}$$

where $u = \nu_1 \pi r_1^2$ *and for* $k = 1, \ldots, M$,

$$m_k = \nu_k \pi d_{\min,k}^2, \qquad \Theta_k = \frac{\nu_k}{\nu_1} \left(\frac{\mu_k}{\mu_1} \right)^{2/\delta} , \tag{2.16}$$

$$G(y) = \int_y^\infty \frac{\mathrm{d}x}{1 + x^{\frac{\delta}{2}}} = \begin{cases} \pi/2 - \tan^{-1} y & \delta = 4 \\ {}_2F_1(1, \frac{\delta}{2}; 1 + \frac{\delta}{2}; -x^{\frac{\delta}{2}}) x|_y^\infty & \delta \neq 4 \end{cases} . , \tag{2.17}$$

and ${}_2F_1(a, b; c; z)$ *is the hypergeometric function*

$${}_2F_1(a, b; c; z) = 1 + \sum_{n=1}^{\infty} \frac{z^n}{n!} \prod_{l=0}^{n-1} \frac{(a + l)(b + l)}{c + l}. \tag{2.18}$$

Proof. See [68].

To provide the mean capacity, we use the SINR (Γ) distribution[9] (2.15) in macrocell and femtocell tier capacities provided in (2.2), (2.3). Mean rate of a UE at distance $R_1 = r_1$ from nearest BS of HPP1 can be written as

$$C_1(r_1) \;\; = \;\; \mathbb{E}_{\Gamma_1} \Big[\log_2 \big(1 + \Gamma_1(r_1) \big) \Big] = \int_0^\infty \mathbb{P}\{ \Gamma_1(r_1) > 2^x - 1 | R_1 = r_1 \} \mathrm{d}x \; . \tag{2.19}$$

Let $\lambda_{\mathrm{MS},1}$ be the density of the MSs for the HPP1. Then, the aggregate rate over the region served by a single BS of HPP1 can be written as

$$C_{1,\mathrm{BS}} = \int_{d_{\min,1}}^{d_{\max,1}} 2\pi r_1 \lambda_{\mathrm{MS},1} C_1(r_1) \mathrm{d}r_1 \tag{2.20}$$

which, after a change of variable $t = r_1^2$, can be written as

$$C_{1,\mathrm{BS}} = \int_{d_{\min,1}^2}^{d_{\max,1}^2} \pi \lambda_{\mathrm{MS},1} \tilde{C}_1(t) \mathrm{d}t \; . \tag{2.21}$$

[9] Although (2.15) provides the SIR distribution, we can assume that the network is interference limited (SINR $\simeq$ SIR) .

From (2.15), $\tilde{C}(t)$ in (2.21) is given by

$$\tilde{C}(t) = \int_0^\infty \exp\left(-\nu_1 \pi t (2^x - 1)^{\frac{2}{\delta}} \left[G\left(\frac{1}{(2^x-1)^{\frac{2}{\delta}}}\right) + \sum_{k=2}^{M} \Theta_k G\left(\frac{m_k}{\nu_k \pi t (2^x-1)^{\frac{2}{\delta}} \Theta_k}\right)\right]\right) \mathrm{d}x. \tag{2.22}$$

Then, the capacity for a given tier can be written in a generalized form as follows

$$\begin{aligned} C_i &= \frac{B N_{\mathrm{N},i}}{\pi \lambda_{\mathrm{MS},1} (d^2_{\max,1} - d^2_{\min,1})} \int_{d^2_{\min,1}}^{d^2_{\max,1}} \pi \lambda_{\mathrm{MS},1} \tilde{C}(t) \mathrm{d}t \\ &= \mathbb{C}\left(B, N_{\mathrm{N},i}, M, \boldsymbol{\nu}, \boldsymbol{\mu}, \boldsymbol{m}, \boldsymbol{\Theta}, d_{\max,1}, d_{\min,1}\right) \end{aligned} \tag{2.23}$$

where the total bandwidth is assumed to be distributed in a round robin fashion in each mBS and fBS. Note that $\boldsymbol{\nu} = [\nu_1, ..., \nu_M]$, $\boldsymbol{\mu} = [\mu_1, ..., \mu_M]$, $\boldsymbol{m} = [m_1, ..., m_M]$, and $\boldsymbol{\Theta} = [\Theta_1, ..., \Theta_M]$ are vectors of $1 \times M$, with m_k and Θ_k as in (2.16). For a given area with radius R, the number of macrocells and femtocells can be calculated as $N_{\mathrm{N},1} = \lambda \pi R^2$ and $N_{\mathrm{N},2} = \lambda' \pi R^2$, respectively.

2.3.3 Co-Channel Macrocell/Femtocell Networks

Using (2.2) and the notation given in Table 2.1, the capacity of femtocell tier can be written as

$$C_{\mathrm{Fem}} = \frac{B}{N_{\mathrm{U,F}}} \mathbb{E}\left[\sum_{j=1}^{N_{\mathrm{N},2}} \sum_{k=1}^{N_{\mathrm{U,F}}} \log_2\left(1 + \Gamma_{j,k}\right)\right]. \tag{2.24}$$

where $B_{2,j,k} = \frac{B_{\mathrm{F}}}{N_{\mathrm{U},2,j}} = \frac{B}{N_{\mathrm{U,F}}}, \forall j, k$. Then using (2.23) we can re-write (2.24) as

$$C_{\mathrm{Fem}} = \mathbb{C}\left(B, N_{\mathrm{N},2}, M, \boldsymbol{\nu}, \boldsymbol{\mu}, \boldsymbol{m}, \boldsymbol{\Theta}, d_{\max,1}, d_{\min,1}\right), \tag{2.25}$$

where $M = 2$, HPP1 is fBS locations, HPP2 is mBS locations, $(\nu_1, \nu_2) = (\lambda', \lambda)$, $(\mu_1, \mu_2) = (P', P)$, $(m_1, m_2) = (\lambda' \pi r^2_{\min,\mathrm{f}}, \lambda \pi r^2_{\min,\mathrm{m}})$, $\Theta_2 = \frac{\lambda}{\lambda'}(\frac{P}{P'})^{2/\delta}$, and $(d_{\max,1}, d_{\min,1}) = (r_{\max,\mathrm{f}}, r_{\min,\mathrm{f}})$. Note that $r_{\min,\mathrm{m}}$ and $r_{\max,\mathrm{m}}$ (or $r_{\min,\mathrm{f}}$, $r_{\max,\mathrm{f}}$) are the minimum and maximum possible dis-

tances between an MS and an mBS (or an fBS), respectively. Similarly, using (2.3), we have

$$C_{\text{Mac}} = \frac{B}{N_{\text{U,M}}}\mathbb{E}\left[\sum_{j=1}^{N_{\text{N},1}}\sum_{k=1}^{N_{\text{U,M}}}\log_2\left(1+\Gamma_{j,k}\right)\right]. \tag{2.26}$$

where $B_{2,j,k} = \frac{B_{\text{F}}}{N_{\text{U},2,j}} = \frac{B}{N_{\text{U,F}}}, \forall j,k$. Then using (2.23) we can re-write (2.26) as

$$C_{\text{Mac}} = \mathbb{C}\left(B, N_{\text{N},1}, M, \boldsymbol{\nu}, \boldsymbol{\mu}, \boldsymbol{m}, \boldsymbol{\Theta}, d_{\text{max},1}, d_{\text{min},1}\right) \tag{2.27}$$

where $M = 2$, HPP1 is mBS locations, HPP2 is fBS locations, $(\nu_1, \nu_2) = (\lambda, \lambda')$, $(\mu_1, \mu_2) = (P, P')$, $(m_1, m_2) = (\lambda\pi r^2_{\text{min,m}}, \lambda'\pi r^2_{\text{min,f}})$, $\Theta_2 = \frac{\lambda'}{\lambda}(\frac{P'}{P})^{2/\delta}$, and $(d_{\text{max},1}, d_{\text{min},1}) = (r_{\text{max,m}}, r_{\text{min,m}})$.

2.3.4 Dedicated Channel Macrocell/Femtocell Networks

Using (2.2) and the notation given in Table 2.1, the capacity of femtocell tier can be written as

$$C_{\text{Fem}}(\rho) = \frac{B(1-\rho)}{N_{\text{U,F}}}\mathbb{E}\left[\sum_{j=1}^{N_{\text{N},2}}\sum_{k=1}^{N_{\text{U,F}}}\log_2\left(1+\Gamma_{j,k}\right)\right]. \tag{2.28}$$

Then using (2.23) we can re-write (2.28) as

$$C_{\text{Fem}}(\rho) = \mathbb{C}\left(B(1-\rho), N_{\text{N},2}, M, \boldsymbol{\nu}, \boldsymbol{\mu}, \boldsymbol{m}, \mathbf{0}, d_{\text{max},1}, d_{\text{min},1}\right) \tag{2.29}$$

where $M = 1$, HPP1 is fBS locations, $\nu_1 = \lambda'$, $\mu_1 = P'$, $m_1 = \lambda'\pi r^2_{\text{min,f}}$, and $(d_{\text{max},1}, d_{\text{min},1}) = (r_{\text{max,f}}, r_{\text{min,f}})$. Similarly, using (2.3)

$$C_{\text{Mac}}(\rho) = \frac{B\rho}{N_{\text{U,M}}}\mathbb{E}\left[\sum_{j=1}^{N_{\text{N},1}}\sum_{k=1}^{N_{\text{U,M}}}\log_2\left(1+\Gamma_{j,k}\right)\right]. \tag{2.30}$$

Then using (2.23) we can re-write (2.30) as

$$C_{\text{Mac}}(\rho) = \mathbb{C}\left(B\rho, N_{\text{N},1}, M, \nu, \mu, m, 0, d_{\text{max},1}, d_{\text{min},1}\right) \tag{2.31}$$

where $M = 1$, HPP1 is mBS locations, $\nu_1 = \lambda$, $\mu_1 = P$, $m_1 = \lambda\pi r_{\text{min,m}}^2$, and $(d_{\text{max},1}, d_{\text{min},1}) = (r_{\text{max,m}}, r_{\text{min,m}})$.

Therefore the total capacity for the dedicated-channel scenario using (2.29) and (2.31) can be given as $C_{\text{Tot}}(\rho) = C_{\text{Mac}}(\rho) + C_{\text{Fem}}(\rho)$. Then, spectrum splitting ρ value that maximizes the $C_{\text{Tot}}(\rho)$ can be expressed as follows:

$$\rho_{\max} = \arg \max_{0 \le \rho \le 1} C_{\text{Tot}}(\rho) \quad . \tag{2.32}$$

Note that the objective function in (2.32) is a linear combination of (2.29) and (2.31). Since each femtocell reuses the spectrum more frequently, the capacity equation given in (2.29) includes a larger multiplying term $N_{\text{N},2} > N_{\text{N},1}$. Therefore, if the SINR levels of users in each tier are similar, objective function (2.32) will be maximized at $\rho = 0$. This issue is also investigated by calculating per-tier area spectral efficiencies (ASEs) in [69] and it is shown that capacity is maximized at extreme points without a fairness or QoS parameter. Such a partitioning is obviously unfair since it results in a greedy allocation to one of the tiers which will be discussed in more detail in Section 2.4.2.

2.3.5 Hybrid Approach for Resource Allocation

In this section, we investigate the hybrid approach scenario as it is shown in Fig. 2.1(c). Using (2.2) and the notation given in Table 2.1, the total capacity of femtocell network can be calculated with a slight modification of (2.25), where the bandwidth of femtocell is ρB and femtocell users are always co-channel with macrocell, that is,

$$C_{\text{Fem}}(\rho) = \mathbb{C}\left(B(1-\rho), N_{\text{N},2}, M, \boldsymbol{\nu}, \boldsymbol{\mu}, \boldsymbol{m}, \boldsymbol{\Theta}, d_{\text{max},1}, d_{\text{min},1}\right) \tag{2.33}$$

where $M = 2$, HPP1 is fBS locations, HPP2 is mBS locations, $(\nu_1, \nu_2) = (\lambda', \lambda)$, $(\mu_1, \mu_2) = (P', P)$, $(m_1, m_2) = (\lambda' \pi r_{\text{min,f}}^2, \lambda \pi r_{\text{min,m}}^2)$, $\Theta_2 = \frac{\lambda}{\lambda'}(\frac{P}{P'})^{2/\delta}$, and $(d_{\text{max},1}, d_{\text{min},1}) = (r_{\text{max,f}}, r_{\text{min,f}})$. Note that $r_{\text{min,m}}$ and $r_{\text{min,f}}$ are the minimum distances between an MS-mBS and an MS-fBS, respectively, and $r_{\text{max,m}}$ and $r_{\text{max,f}}$ are the maximum distances between an MS-mBS, and an MS-fBS, respectively. On the other hand, to calculate the macrocell capacity, following steps should be followed:

1. Consider a macrocell MS at distance r_1 from its nearest mBS. Let γ_c be the minimum rate for scheduling an mMS to dedicated channel portion of hybrid channel. Then the instantaneous rate of this MS from the MBS can be given as

$$C_{\text{macro}}(r_1) = (1-\rho) C_{\text{co}}(r_1) 1\{C_{\text{co}}(r_1) > \gamma_c\} + \rho C_{\text{ded}}(r_1) 1\{C_{\text{co}}(r_1) \leq \gamma_c\} \ . \quad (2.34)$$

   Note that $C_{\text{co}}(r_1)$, $C_{\text{ded}}(r_1)$ are instantaneous (includes effects of fading) rates derived in (2.19) for co-channel and dedicated channel scenarios[10], respectively.

2. Therefore mean rate for that MS can be written as

$$\begin{aligned} \bar{C}_{\text{macro}}(r_1) &= (1-\rho)\mathbb{E}\big[C_{\text{co}}(r_1) 1\{C_{\text{co}}(r_1) > \gamma_c\}\big] \\ &+ \rho \mathbb{E}\big[C_{\text{ded}}(r_1) 1\{C_{\text{co}}(r_1) \leq \gamma_c\}\big] \ . \end{aligned} \quad (2.35)$$

3. And finally, aggregate rate for an mBS can be written as

$$C_{\text{Mac}}(\rho) = \frac{B N_{\text{N},1}}{\pi \lambda_{\text{MS},1} (d_{\text{max},1}^2 - d_{\text{min},1}^2)} \int_{d_{\text{min},1}}^{d_{\text{max},1}} 2\pi \lambda_{\text{MS},1} r_1 \bar{C}_{\text{macro}}(r_1) \text{d}r_1 \ . \quad (2.36)$$

[10] As it is described in sections 2.3.3 and 2.3.4, for co-channel scenario, we have $M = 2$, HPP1 is mBS locations, HPP2 is fBS locations, $(\nu_1, \nu_2) = (\lambda, \lambda')$, $(\mu_1, \mu_2) = (P, P')$, $(m_1, m_2) = (\lambda \pi r_{\text{min,m}}^2, \lambda' \pi r_{\text{min,f}}^2)$, $\Theta_2 = \frac{\lambda'}{\lambda}(\frac{P'}{P})^{2/\delta}$, and $(d_{\text{max},1}, d_{\text{min},1}) = (r_{\text{max,m}}, r_{\text{min,m}})$. On the other hand, for dedicated-channnel scenario, we have $M = 1$, HPP1 is mBS locations, $\nu_1 = \lambda$, $\mu_1 = P$, $m_1 = \lambda \pi r_{\text{min,m}}^2$, and $(d_{\text{max},1}, d_{\text{min},1}) = (r_{\text{max,m}}, r_{\text{min,m}})$.

Therefore the macro-tier capacity can be provided as in (2.36), by solving for (2.35). Let $X = C_{\text{co}}(r_1)1\{C_{\text{co}}(r_1) > \gamma_c\}$. Then,

$$\mathbb{P}\{X > x\} = \begin{cases} \mathbb{P}\{\Gamma_{\text{Co}}(r_1) > 2^{\gamma_c} - 1\} & 0 < x \leq \gamma_c \\ \mathbb{P}\{\Gamma_{\text{Co}}(r_1) > 2^{x} - 1\} & x > \gamma_c \end{cases} , \tag{2.37}$$

from which we can write

$$\begin{aligned} \mathbb{E}[X] &= \int_0^\infty \mathbb{P}\{X > x\}\mathrm{d}x \\ &= \gamma_c \underbrace{\mathbb{P}\{\Gamma_{\text{Co}}(r_1) > 2^{\gamma_c} - 1\}}_{\text{substitute } \gamma = 2^{\gamma_c} - 1 \text{ in (2.15)}} + \underbrace{\int_{\gamma_c}^\infty \mathbb{P}\{\Gamma_{\text{Co}}(r_1) > 2^{x} - 1\}\mathrm{d}x}_{\text{integral in (2.19) with } \gamma_c} . \end{aligned} \tag{2.38}$$

To calculate (2.35), we assume that interference from indoor femtocells to outdoor macrocell MSs is negligible due to low power of femtocells and wall loss, therefore $C_{\text{ded}}(r_1) \simeq C_{\text{co}}(r_1)$. Then

$$\begin{aligned} \mathbb{E}\big[C_{\text{ded}}(r_1)1\{C_{\text{co}}(r_1) \leq \gamma_c\}\big] &\simeq \mathbb{E}\big[C_{\text{co}}(r_1)\left(1 - 1\{C_{\text{co}}(r_1) > \gamma_c\}\right)\big] \\ &= \mathbb{E}\left[C_{\text{co}}(r_1)\right] - \underbrace{\mathbb{E}\Big[C_{\text{co}}(r_1)\left(1\{C_{\text{co}}(r_1) > \gamma_c\}\right)\Big]}_{\mathbb{E}[X]} . \end{aligned} \tag{2.39}$$

Therefore (2.36) can be calculated using

$$\begin{aligned} \bar{C}_{\text{macro}}(r_1) &= (1-\rho)\mathbb{E}\Big[C_{\text{co}}(r_1)1\{C_{\text{co}}(r_1) > \gamma_c\}\Big] + \rho\mathbb{E}\Big[C_{\text{ded}}(r_1)1\{C_{\text{co}}(r_1) \leq \gamma_c\}\Big] \\ &= (1-2\rho)\mathbb{E}[X] + \rho\mathbb{E}\big[C_{\text{co}}(r_1)\big] , \end{aligned} \tag{2.40}$$

and the total capacity for the hybrid-channel scenario using (2.33) and (2.36) can be given as $C_{\text{Tot}}(\rho) = C_{\text{Mac}}(\rho) + C_{\text{Fem}}(\rho)$. Then, similar to (2.32), spectrum splitting ρ value that maximizes the $C_{\text{Tot}}(\rho)$ can be expressed as

$$\rho_{\max} = \arg \max_{0 \leq \rho \leq 1} C_{\text{Tot}}(\rho) . \tag{2.41}$$

In hybrid channel scenario jointly choosing γ_c and ρ becomes important since different sum capacities and fairness levels could be achieved with these two values. If the macrocell users which have lower SINRs can be scheduled to the dedicated channel portion, there will be no victim users. Therefore, the number of users assigned to dedicated channel should be selected carefully since the amount of bandwidth corresponding to dedicated channel should be kept low in order to efficiently reuse the resources in both tiers. In this chapter we consider a scheduler similar to the one discussed in [70]. First the macrocell MSs are sorted with respect to their maximum achievable co-channel capacities, and then $N_{\mathrm{U,M}}^{(\rho)}$ MUEs with worse capacities are scheduled in the dedicated channel portion (i.e., $N_{\mathrm{U,M}}^{(1-\rho)}$ MUEs scheduled in co-channel portion). Note that, $N_{\mathrm{U,M}}^{(\rho)}$ and γ_c has a direct relation, that is, γ_c determines the number of users that will be assigned to dedicated channel portion $N_{\mathrm{U,M}}^{(\rho)}$. However it is also important to note that the value of SSR (ρ) determines the bandwidth to be assigned for each user depending on co-channel or dedicated channel spectrum. We investigate the optimum solution of this problem in our computer simulations in details. In our simulations, while selecting of $N_{\mathrm{U,M}}^{(\rho)}$, we consider max-min scheduler that maximizes the minimum capacity of macrocell users as follows:

$$N_{\mathrm{U,M}}^{(\rho)} = \arg \max_{N_{\mathrm{U,M}}^{(\rho)}} \left\{ \min_{k} \; C_{1,1,k} \right\} \quad . \tag{2.42}$$

$$\rho = \arg \max_{0 \le \rho \le 1} \left\{ C_{\mathrm{Tot}}(\rho, N_{\mathrm{U,M}}^{(\rho)}) \right\} \quad . \tag{2.43}$$

By using simple max-min capacity scheduling, the minimum capacity of mMSs are maximized by assigning them to dedicated channel portion while also maximizing the overall capacity of the macrocell-femtocell network. The fairness and QoS orientation constraint in the network can also be introduced by using fairness metric given in (2.10).

2.4 Numerical Results

In this section, the numerical results for both analytical derivations and simulations are presented. First, we investigate the behavior of the discussed fairness indices for a particular scenario. Then, we present the optimum spectrum splitting strategy based on computer simulations and analytical derivations for co-channel, dedicated channel, and hybrid scenarios. Mathematical modeling is shown to be aligned with simulation results when the basic simulation parameters shown in Table 2.3 are used. Finally, to investigate different approaches in further detail, a 3GPP compatible simulator using the parameters given in [71] is used together with a max-min fair scheduler for hybrid approach. Some of the critical parameters used for 3GPP aligned simulations are also summarized in Table 2.3. Both for simulation and theoretical results, round robin scheduling is considered for dedicated and cochannel approaches. For the hybrid approach theoretical analysis, $\gamma_c = 10^4$ bps is a capacity threshold that determines the number of users to be scheduled for co-channel and dedicated-channel portions in mBS, on the other hand for hybrid approach simulations, a max-min fair scheduler is considered for mBS and while a round robin scheduler is considered for fBS.

2.4.1 Comparison of Different Fairness Metrics

The effect of the number of networks and the number of users in each network with the bounds in Table 2.2 are investigated in a two-tier network case study ($T = 2$), where tier-1 has 1 network ($N_{\mathrm{N},1} = 1$) and tier-2 has 2 networks ($N_{\mathrm{N},2} = 2$). We consider two different scenarios to provide a better understanding for the metrics and their related bounds. In the first scenario, we assume that there are $N_{\mathrm{U},1,1} = 4$ users in tier-1, network-1, and $N_{\mathrm{U},2,1} = 3$, $N_{\mathrm{U},2,2} = 1$ users for tier-2, networks 1 and 2. Therefore, there are a total of 8 users in the network for the first scenario. In the second scenario, we do not change the total number of users; however, we consider $N_{\mathrm{U},1,1} = 6$ users in tier-1, network-1 and $N_{\mathrm{U},2,1} = 1$, $N_{\mathrm{U},2,2} = 1$ users for tier-2, networks 1 and 2.

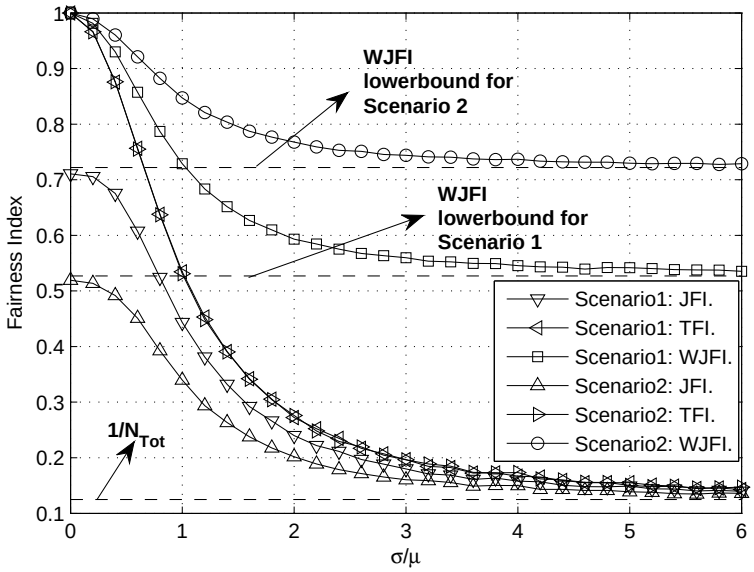

Figure 2.3 Fairness Index vs. Standard Deviation (σ) /Mean (μ) for Normally Distributed Resource Allocations for Each User

The allocated resources for each user are assumed to be partitioned in a round robin fashion within each network in all tiers and the capacity of each network is normally distributed with mean μ and variance σ^2 $\left(C_{i,j} \sim \mathcal{N}(\mu, \sigma^2)\right)$. Fig. 2.3 shows that proposed fairness index (TFI) is between $[1/N_{\text{Tot}}, 1]$ with controlled boundings, converging to WJFI at 1 for small standard deviation values. On the other hand TFI converges to JFI at 0.125 for increasing standard deviation. Moreover, upper bound of JFI is decreased and lower bound of WJFI is increased in scenario 2 compared to scenario 1. The non-even distribution of the users in networks increases the lower bound of the WJFI. For instance in scenario 2, the networks 1 and 2 in tier 2 have only 1 user. Calculating the lower bound of WJFI according to Table 2.2 for scenario 1 and scenario 2 provides 0.527 and 0.722, respectively, which could also be tracked from Fig. 2.3. Although an upper bound independent from allocated resource could not be achieved for JFI, Fig. 2.3 shows that while the number of users in a network (for instance the number of users in tier 1 network 1 is very high compared to tier 2 networks) increases, the upper bound decreases.

Table 2.3 Numerical Parameters for Analytical/Simulation Results

Parameter	**Description/Value**	
	Analytical Results and Basic Simulator	**3GPP Compatible Simulator**
Macrocellular	HPP for analytical and hexagonal layout with cell-center BSs for simulations.	Hexagonal layout with cell-center BSs.
Number of mBS	Infinite for analytical and 19 cell with wrap around for simulations.	19 cell with wrap around.
Inter-mBS distance	500 m in average. Therefore the density of macrocells (λ_{mBS}) is $\frac{1}{500\sqrt{3}/2} = 4.62 \times 10^{-}6$. Similarly density of femtocells $\lambda_{\text{fBS}} = 12 * \lambda_{\text{mBS}} = 5.54 \times 10^{-}5$.	500 m.
Number of fBS	12 per each macrocell.	12 per each macrocell.
fBs distribution	12 fBSs are randomly and uniformly distributed within each site.	4 fBSs are randomly and uniformly distributed within each sector.
Inter-fBS distance	Varies fBS locations and path loss model.	Varies fBS locations and path loss model.
mBS-mMS minimum distance constraint	35 m [71].	35 m [71].
fBS-fMS minimum distance constraint	5 m [71].	5 m [71].
Bandwidth	10 MHz.	10 MHz.
DL transmit power mBS	60 dBm Tx power at mBS.	46 dBm Tx power at mBS ,14 dBi Antenna gain [71]. 3 sectors with 3-D antenna pattern. Antenna height 32 meters.
DL transmit power fBS	20 dBm.	20 dBm with antenna gain of 5 dBm.
Thermal noise density	-174 dBm/Hz.	-174 dBm/Hz.
Path loss model (macrocell)	$128.1+40\log_{10}(R)$ (R in kilometers).	$128.1+37.6\log_{10}(R)$ (R in kilometers).
Path loss model (femtocell)	$127+40\log_{10}(R)$ (R in kilometers).	$127+30\log_{10}(R)$ (R in kilometers).
Wall attenuation loss	20 dB.	20 dB.

2.4.2 Numerical Results for Analytical Derivations

In this section, we present the numerical results for equations derived through (2.24) - (2.40) and verify them through computer simulations. The simulation scenario includes

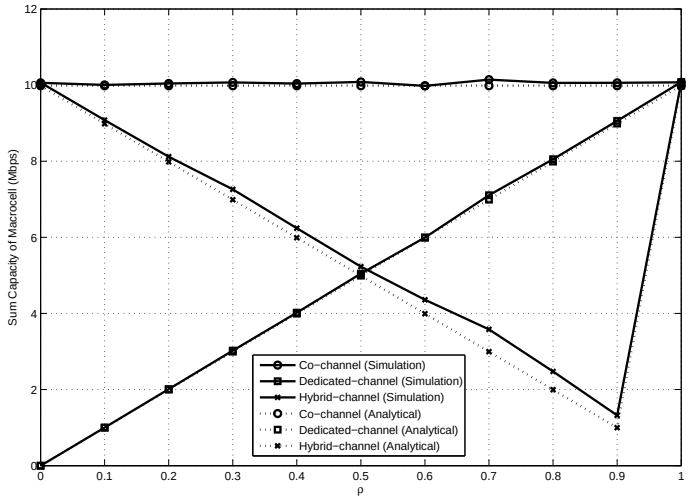

Figure 2.4 Sum Capacity of Macrocell Users vs. SSR ρ

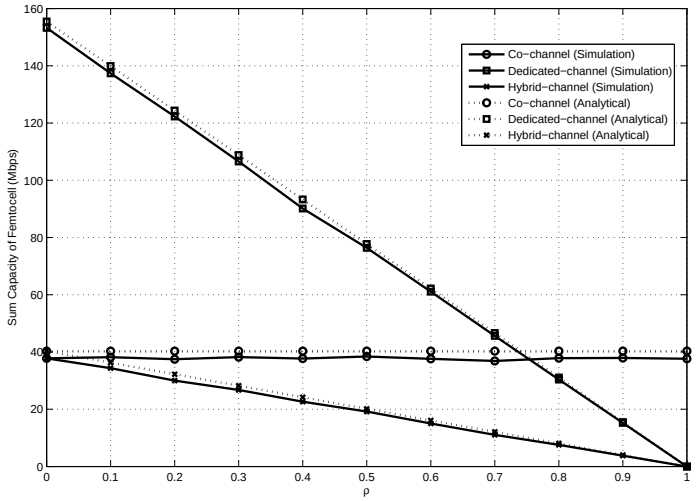

Figure 2.5 Sum Capacity of Femtocell Users vs. SSR ρ

analytical derivation assumptions and uses the parameters listed in Table 2.3. Note that path loss exponent (δ) for both macrocell and femtocell is selected as 4 in order to use the equations derived in section 2.3. 300 users are dropped randomly and uniformly within each site, with 2 users for each CSG femtocell [71]. Hence, there are $300 - 12 \times 2 = 276$ macrocell users within each cell.

Fig. 2.4 shows the sum capacity of a macrocell for different SSR values for co-channel, dedicated channel and hybrid approaches. Results show that co-channel scenario has better capacity when compared with dedicated and hybrid channel approaches. While ρ is increasing, the bandwidth assigned to macrocell users is increasing and at $\rho = 1$, the capacity of dedicated channel is almost same with the co-channel approach. This result shows that for the given scenario, CSG indoor femtocell BSs are not causing severe interference to macro MSs, and therefore co-channel scenario outperforms the dedicated channel scenario. On the other hand, for hybrid channel scenario, for the given $\gamma_c = 10^4$ bps, increasing SSR decreases the macrocell capacity. For a fixed γ_c value, the number of users assigned to dedicated channel portion is fixed and those users are the ones that has lowest capacity. Therefore, increasing the dedicated channel portion with increasing ρ decreases the capacity since the bandwidth assigned to a small number of users which has lower SINRs decreases the sum capacity in a macrocell. In the extreme cases $\rho = 0$, and $\rho = 1$, the hybrid approach converges to co-channel and dedicated channel approaches. It is also important to note that simulation results and analytical results are aligned.

Fig. 2.5 shows the sum capacity of a femtocell for different SSR values for co-channel, dedicated channel and hybrid approaches. The co-channel capacity of a femtocell is greater than dedicated-channel for larger values of SSR, where femtocell bandwidth is less. Note that similar capacities can be achieved with co-channel and dedicated channel approaches for $\rho \simeq 0.75$. On the other hand, increasing SSR for hybrid channel scenario also decreases the sum capacity of femtocells converging to cochannel at $\rho = 0$, and dedicated channel at $\rho = 1$. As a result, it can be concluded that for a fixed γ_c, and without fairness and QoS constraints, resource partitioning can not be done effectively since extreme points are maximizing the capacity for both macrocells and femtocells.

2.4.3 Detailed Computer Simulations with Max-Min Scheduling and Fairness Constraints

Section 2.4.2 shows that although computer simulations and analytical results are aligned, the sum capacity is maximized at extreme points for both macrocell and femtocell networks. Therefore in this section, we introduce the fairness criterion into the optimization, while also considering a more applicable scenario where parameters are selected from [71]. This study also considers the case where a portion of macrocell MSs are inside the CSG femtocell area which we called indoor ratio (IR). 100 users are randomly and uniformly distributed within each sector, and there are 2 users associated with each closed-access femtocell [71]. This yields $100 - 4 \times 2 = 92$ macrocell users within sector.

Fig. 2.6 and Fig. 2.7 show the SINR distributions for macrocell and femtocell scenarios, respectively. In Fig. 2.6, SINR CDFs for the co-channel scenario with IR=0, dedicated channel scenario, and hybrid channel scenarios SINRs are aligned with the 3GPP benchmarks in [71]. In co-channel scenario, for larger IR, SINRs of victim macrocell MSs get worse due to increasing interference. On the other hand, since dedicated channel approach uses separate bandwidths for macrocell and femtocell such a behavior is not observed. It is also important to note that if IR=0, the co-channel and dedicated channel SINRs are same, which validates the assumption in (2.39) for CSG scenario with wall loss. Moreover, hybrid approach with max-min fair scheduler also protects the victim macro MSs by assigning them to the dedicated portion of hybrid approach. In Fig. 2.7, dedicated channel SINRs of femtocell MSs are compared to co-channel approach. Since all femtocell users are co-channel with macrocell BSs, the SINRs of hybrid approach and co-channel approach are the same.

In Fig. 2.8 and Fig. 2.9, the sum capacity of a macrocell and 5-percentile capacity of macrocell MSs are provided for various IR and SSR, respectively. Note that in both figures the hybrid approach converges to co-channel at $\rho = 0$ and dedicated channel at $\rho = 1$. Co-channel macrocell sum-capacity decreases with increasing IR, and dedicated channel capacity does not change with IR since femtocells do not interfere with macrocells. Note that hybrid approach does not let sum capacity of macrocell decrease below a level

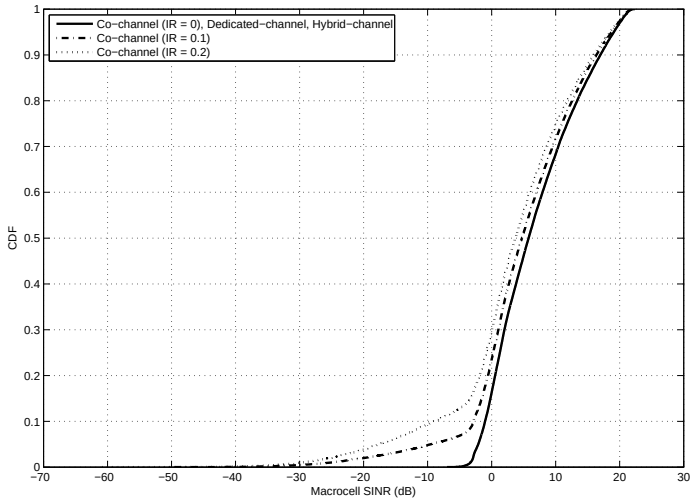

Figure 2.6 SINR of Macrocell Users vs. SSR ρ

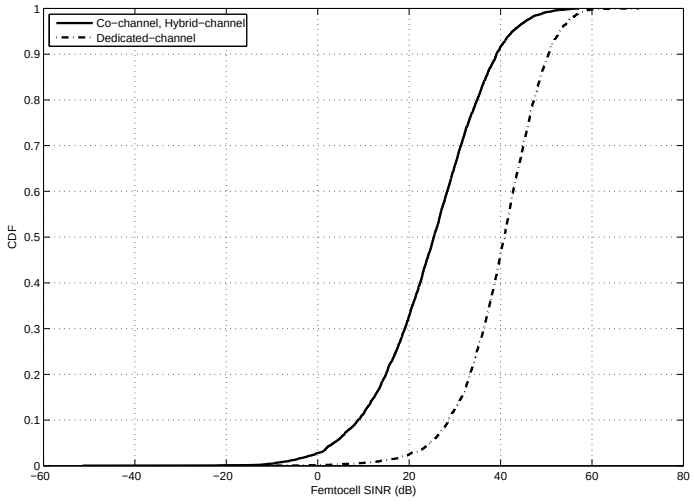

Figure 2.7 SINR of Femtocell Users vs. SSR ρ

in Fig. 2.8 and protects the victim users which are under increased interference in Fig. 2.9. Hybrid channel 5-percentile capacities are always better than both co-channel and dedicated-channel. While protecting the victim users by hybrid channel approach, max-min fair scheduler also tries to maximize the sum capacity of macrocell.

In Fig. 2.10, we present the femtocell sum capacities for various ρ values. Note that IR does not affect the femtocell capacities. Hybrid approach again converges to co-channel

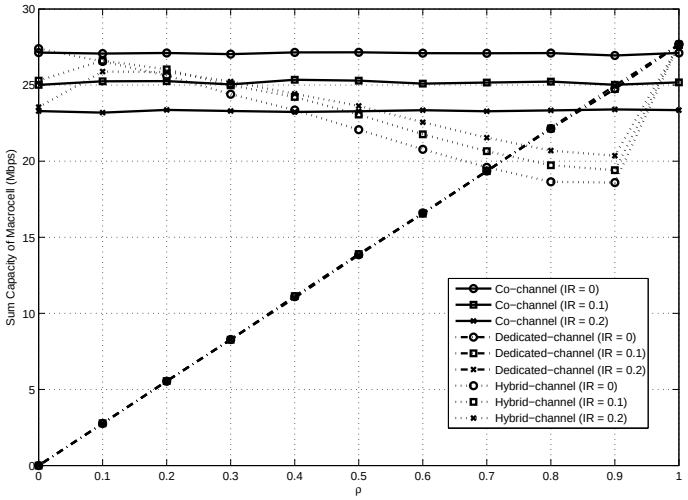

Figure 2.8 Sum Capacity of Macrocell vs. SSR ρ

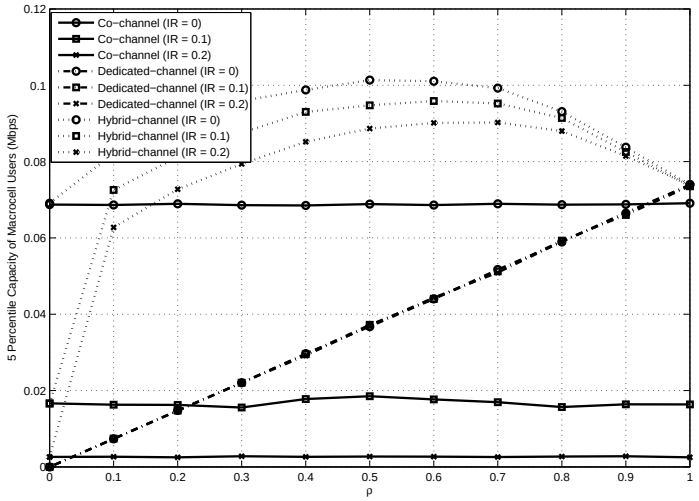

Figure 2.9 5-percentile Capacity of Macrocell vs. SSR ρ

case at $\rho = 0$ and dedicated channel at $\rho = 1$. Up to $\rho = 0.4$, dedicated channel outperforms co-channel scenario. Hybrid approach femtocell sum capacity is always lower than both co-channel and dedicated channel scenario for femtocells. However since femtocells have better SINRs (Fig. 2.7) compared to macrocells (Fig. 2.6), capacity of femtocells are still reasonable with this approach. One way to analyze this is to use the fairness metric defined in section 2.2 Fig. 2.11 presents the fairness level of tiered network for co-channel, dedicated-

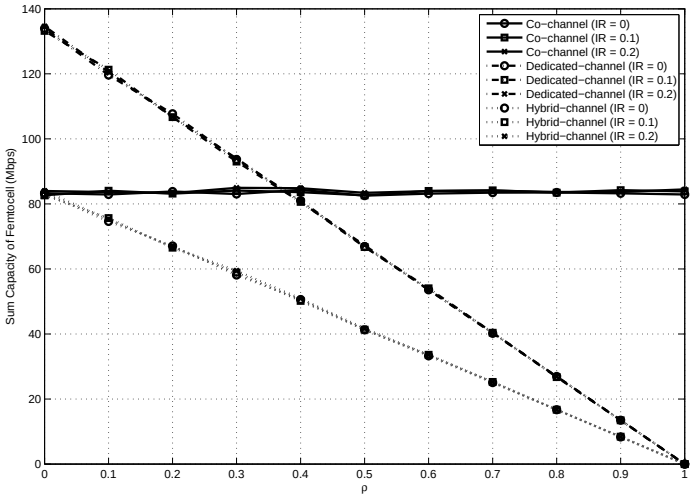

Figure 2.10 Sum Capacity of Femtocell vs. SSR ρ

channel and hybrid channel under various SSR and QoS parameters for IR=0. Note that hybrid approach $f_{\mathrm{QTFI}}(\rho)$ again converges to co-channel case at $\rho = 0$ and dedicated channel at $\rho = 1$.

In co-channel scenario femtocell user capacities are always larger than macrocell users, and therefore their fairness metric may only be moderately improved by changing β in Fig. 2.11. For example, for $\beta_2 = 1/3$, the expected femtocell user capacity is 3 times more than that of macrocell user, however the $f_{\mathrm{QTFI}}(\rho)$ is still as low as 0.5. On the other hand hybrid channel approaches fairness metric is always above the co-channel and hybrid channel approaches. Note that for hybrid channel approach the fairness maximization can be done for $\rho \approx 0.8$. This may also be traced by investigating Fig. 2.8 and Fig. 2.10, where since similar capacity values are achieved in both figures for $\rho \approx 0.8$. We also investigate the effect of IR on fairness metric for $\beta_2 = 1/2$ in Fig. 2.12. In dedicated channel scenario, IR does not change the fairness of the system. On the other hand, while IR increases, the fairness of the system decreases for hybrid and co-channel scenario. Observe that hybrid approach fairness is still greater than dedicated channel fairness for all ρ and IR values.

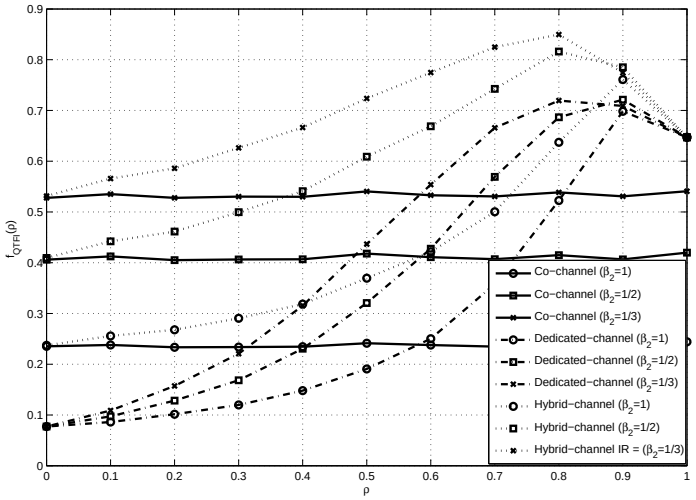

Figure 2.11 QoS-oriented Fairness Index ($f_{\mathrm{QTFI}}(\rho)$) vs. SSR ρ for Various β_2

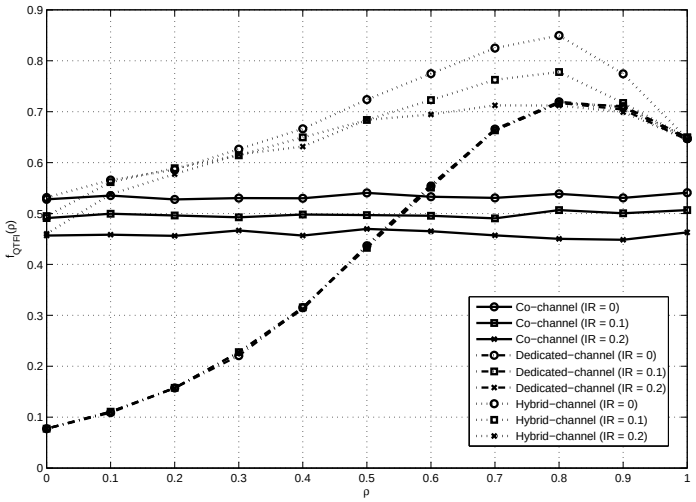

Figure 2.12 QoS-oriented Fairness Index ($f_{\mathrm{QTFI}}(\rho)$) vs. SSR ρ for Various IR ($\beta_2 = 1/3$)

2.5 Concluding Remarks and Discussion

In this chapter, using HPPs, we study the sum-capacities of co-channel, dedicated, channel, and hybrid spectrum allocation methods for two-tier macrocell-femtocell networks. For dedicated channel and hybrid approaches, optimum partitioning of the available spectrum resources between the macrocell and femtocell networks is derived analytically and

analyzed for various scenarios. The results show that without using fairness criteria, the capacity maximizing allocation is done by allocating the whole spectrum to femtocells due to their spectrum reuse capability. Since this approach leads to a very unfair spectrum allocation, we propose a QoS-oriented fairness metric. By using this metric as a constraint for the spectrum allocation, we present a capacity maximizing spectrum allocation method which guarantees a specific level of fairness and QoS. From a network provider point of view, partitioning of available resources with the hybrid approach yields the best trade-off from capacity maximization, fairness, and QoS perspectives. The findings in this chapter may also be easily extended to time-domain resource coordination among macrocells and femtocells as specified in 3GPP Release-10, where the duty cycle of ABSs may be optimized while jointly considering capacity maximization, fairness, and QoS constraints.

CHAPTER 3 :

NETWORK DENSIFICATION IN TIERED NETWORKS

Emerging solutions to handle the traffic explosion are pointing network densification and reusing the resources [1]- [2]. Although the traditional (regular, coordinated) macro-cellular network architectures has a successful history in wireless communications, it will be extremely challenging to meet the growth in the upcoming years as different capability networks will be required.

Benefits of building different capability networks in a multi-tiered manner can be summarized as increased data rates for users, reduced overall power transmission, enhanced network capacity, better load balancing, and extended coverage area. Therefore in the recent years, a mixture of different capability networks are started to built in a tiered manner to increase the capacity.

Increasing the number of nodes/BSs/links increases the capacity of the wireless communication systems for a well designed network. However, the uncoordinated increase in the number of cells may cause severe interference and failure in the system. Therefore the number of cells (links) and users in a certain area (the density of the network) should be selected carefully to not to cause a failure in the system [72]. The assignment of the users to these cells, in terms of call admission, cell selection, cell re-selection also should be handled carefully to decrease the burden of upper-layer control signals and ping-pong effects. Particularly, with the concepts of self organizing networks (SON), managing a dense network become important [73].

This chapter consist of two sections. In 3.1, we investigate the distributions of transmit power and SINR in Device-to-Device (D2D) Networks. For a given target SINR for links employing power control with set of network-assisted parameters (i.e., bandwidth,

noise power, path loss formula), what would be the density of the network is the focus of this study. In 3.2, we study gateway scheduling for dense heterogeneous networks. For a dense network, how should we do cell selection, cell re-selection, and scheduling to increase the capacity is the main focus of this section.

3.1 Distributions of Transmit Power and SINR in Device-to-Device Networks

In this section, we study the spatial distribution of transmit powers and signal to interference plus noise ratio (SINR) in device-to-device (D2D) networks. Using homogeneous Poisson Point Processes (PPP), cumulative distribution function (CDF) of the transmit power and SINR are analytically derived for a D2D network employing power control. Then, computer simulations are performed for the same network architecture and it is shown that device location modeling and analytical methods from stochastic geometry can enable us to obtain transmit power and SINR distributions of a D2D network. By using these distributions we identify the limitations on the density of the networks depending on the target SINRs.

3.1.1 Introduction

The explosion of wireless data has led to the emergence of a number of advanced wireless systems and networks whose common goal is to provide a very high data rate to a large number of users. One promising method for enhanced data rates is to employ one transmitter for each receiver (device-to-device (D2D) communication). When the number of such supported pairs increases, the spectrum reuse of a D2D network increases. The benefits of D2D networks include increased data rates, reduced power transmission, enhanced network capacity, better load balancing, and extended coverage [24].

In this work, we assume that the cellular and D2D network operate on different bands, so that there is no cross-tier interference. The capacity of a D2D network is directly related to the signal to interference plus noise ratio (SINR) at the receiver, and therefore, we

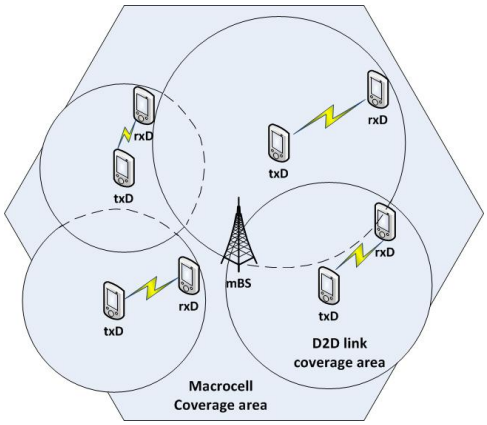

Figure 3.1 D2D Network Architecture within a Macrocell. Coverage Areas of D2D Links Differs due to Power Control

shall focus on the statistical properties of the SINR using Poisson Point Processes (PPP) [39, 40].

With increased densities of smaller cells, ideal (closed-loop) power control in the networks becomes important to manage uncoordinated interference scenarios. In most of the traditional macrocellular networks, fixed power is used for the downlink (DL) and path loss compensation-based (open-loop) power control is used for the uplink (UL). However as the number of the cells are increasing with an uncoordinated deployment manner, the overlapping regions and interference for the networks without power control becomes severe. Therefore most of the studies considers using power control for dense deployment for small cells. Power control is one of the key methods discussed in the literature of D2D to achieve a target SINR at the receiver [22, 23]. For a given target SINR for links employing power control with set of parameters (i.e., bandwidth, noise power, density of the links, path loss formula), how the transmitter power and SINR are distributed is the focus of this study.

The organization of this section is as follows. In subsection 3.1.2, we present the system model for D2D communications employing power control to provide target SINR at the receiver. In subsection 3.1.3, the distribution of transmit power and SINR are provided analytically. In subsection 3.1.4, we provide numerical results for both simulations and analytical derivations, followed by concluding remarks in the last subsection.

3.1.2 System Model

We consider a single tier D2D network [74] with transmitter devices (txD) and receiver devices (rxD). Fig. 3.1 shows an example of such devices deployed in a macrocell of the cellular network. We model the *active* txD locations in the plane by a homogeneous PPP Φ with (constant) intensity λ_{tx}:

1. The number of (active) txDs $N(\mathbb{B})$ in any finite region $\mathbb{B}$ is Poisson with mean $\lambda_{\text{tx}} \times \text{area}(\mathbb{B})$:

$$\mathbb{P}\{N(\mathbb{B}) = n\} = \mathrm{e}^{-\lambda_{\text{tx}} \times \text{area}(\mathbb{B})} \frac{[\lambda_{\text{tx}} \times \text{area}(\mathbb{B})]^n}{n!}, n \geq 0. \tag{3.1}$$

2. $\forall \mathbb{B}, \mathbb{B}' : \mathbb{B} \cap \mathbb{B}' = \emptyset \Rightarrow N(\mathbb{B}), N(\mathbb{B}')$ are independent.

3. $\forall \mathbb{B}$, given $N(\mathbb{B}) = n$, these n txD are independent and identically distributed (i.i.d.) uniformly over $\mathbb{B}$.

For tractability, our D2D model assumes the following: *Assumption 1*: I.i.d. transmit power distribution at all txDs.[1]

Assumption 2: Each rxD only receives from the nearest txD. Each txD transmits to exactly one rxD,[2] and no rxD receives from more than one txD.

Assumption 3: I.i.d. Rayleigh fading on all links (see [40]).

Assumption 4: Slope-intercept path loss model (see below). *Assumption 5*: The chosen target SINR γ depending on the quality of service (QoS) requirement is assumed to be fixed for all the links in the network, and the txDs employ ideal power control to achieve the target SINR at the receiver [75].

Consider an arbitrary such txD-rxD pair, and label them txD_0 and rxD_0. Thus txD_0 is the nearest txD to rxD_0. Let the distance between txD_0 and rxD_0 be R_0, and let

[1] This is not strictly true: if two txD-rxD links are very close to each other, each link's txD will cause severe interference at the other link's rxD, so power control creates a coupling between their transmit powers [75]. However, this is very unlikely for reasonable txD-rxD link distances given Assumption 2.

[2] This is ensured if rxDs outnumber txDs [74]; if not, some txDs will have no rxDs, and these txDs will be inactive, equivalent to a decrease in λ_{tx}.

the transmit power of txD_0 be P_0. Then the received power at rxD_0 is

$$P_0 H_0 / R_0^{\delta}, \quad H_0 \sim \text{Exp}(\mu), \tag{3.2}$$

where δ is the path loss exponent, and from the Rayleigh fading assumption, H_0 is Exponential. The total interference power at rxD_0 from all other transmitters except txD_0 is

$$J(R_0) = \sum_{t \in \Phi : R_t > R_0} \frac{P_t H_t}{R_t^{\delta}}, \tag{3.3}$$

where $\{P_t\}$ are the i.i.d. transmit powers, $\{H_t\}$ are i.i.d. $\text{Exp}(\mu)$, and R_t is the distance between the rxD and txD t. Therefore the SINR at rxD_0 is

$$\Gamma_0 = \frac{P_0 H_0 / R_0^{\delta}}{J(R_0) + N_0}, \tag{3.4}$$

where N_0 is the thermal noise power at rxD_0.

3.1.3 Transmit Power Allocation Strategies and Maximum/Minimum Power Constraints

In this subsection, we formulate the problem depending on the transmit power allocation strategy, and maximum/minimum power constraints in two cases as follows.

1. There exists no transmit power allocation $\{P_t\}_{t \in \Phi}$ such that the target SINR is satisfied on all links simultaneously. Links try to maximize the probability that they achieve (or exceed) the target SINR γ, i.e., each txD $t \in \Phi$ tries to find P_t that maximizes $\mathbb{P}\{\Gamma_t \geq \gamma\}$. This problem is investigated in [76] and the following results are obtained: a) A Nash Equilibrium exists, and the corresponding policy is for all links to transmit at constant power. b) With no maximum power constraint, this constant power is $P_t = \infty$ for all t, so there is breakdown in the

system. c) $P_0 \in [P_{\min}, P_{\max}]$: Given a minimum/maximum power constraint, this constant power is $P_t = P_{\max}$ for all t.

2. A transmit power allocation $\{P_t\}_{t\in\Phi}$ exists such that if there is no maximum power constraint, the target SINR is achieved on all active links simultaneously.

The present work focuses on Case 2. Note that in contrast to [76], the target SINR can be achieved (at least in the absence of a maximum power constraint) on all links (with probability 1), so our goal is not to maximize the probability of achieving or exceeding the SINR target. Instead, we seek the transmit power allocation on each link that achieves the SINR target with minimum transmit power. It is known that in the absence of minimum/maximum power constraints, this allocation can be obtained by a distributed algorithm [77]. However, our interest in this work is in the distribution of allocated transmit power under minimum/maximum power constraints.

3.1.3.1 Distribution of Link Transmit Power with Constraints

Before studying the transmit power distribution under minimum/maximum power constraints, let us consider the unconstrained case. Then the above assumptions yield $\Gamma_0 = \gamma$:

$$\frac{P_0 H_0 / R_0^\delta}{J(R_0) + N_0} = \gamma \Rightarrow P_0 H_0 = \gamma R_0^\delta [J(R_0) + N_0]. \tag{3.5}$$

Thus the cumulative distribution function (CDF) of P_0 without power constraints, denoted P_0^{uc}, is

$$\begin{aligned}
\mathbb{P}\left\{P_0^{\text{uc}} \le p_0\right\} &= \mathbb{P}\left\{H_0 \ge \frac{\gamma R_0^\delta [J(R_0) + N_0]}{p_0}\right\} \\
&= \mathbb{E}_{R_0}\left\{ \exp\left(-\frac{\gamma R_0^\delta N_0}{p_0 \mu}\right) \mathbb{E}\left[\exp\left(-\frac{\gamma R_0^\delta}{\mu p_0} J(R_0)\right) \mid R_0\right] \right\} \\
&= \int_0^\infty f_{R_0}(r_0) \exp\left(-\frac{\gamma r_0^\delta N_0}{p_0 \mu}\right) \mathbb{L}_{J(r_0)}\left(\frac{\gamma r_0^\delta}{\mu p_0}\right) \mathrm{d}r_0,
\end{aligned} \tag{3.6}$$

where $f_{R_0}(\cdot)$ is the probability density function (PDF) of R_0, and $\mathbb{L}_{J(r_0)}(s) = \mathbb{E}[\mathrm{e}^{-sJ(R_0)}|R_0 = r_0]$ is the Laplace transform of (the PDF of) $J(R_0)$ given $R_0 = r_0$. Since R_0 is the distance of the nearest txD to the given rxD, the PPP model for txD locations yields [78, eqn. (31)]

$$f_{R_0}(r_0) = 2\pi\lambda_{\mathrm{tx}} r_0 \, \mathrm{e}^{-\pi\lambda_{\mathrm{tx}} r_0^2}, \quad r_0 \geq 0. \tag{3.7}$$

From (3.3) and following the same steps as in the derivation of [78, eqns. (23), (24)], we obtain

$$\mathbb{L}_{J(r_0)}(s) \geq \exp\left\{-\pi\lambda_{\mathrm{tx}} (s\,\mathbb{E}[P_0^{\mathrm{uc}}])^{\frac{2}{\delta}} G_\delta\left(\frac{r_0^2}{(s\,\mathbb{E}[P_0^{\mathrm{uc}}])^{\frac{2}{\delta}}}\right)\right\}, \tag{3.8}$$

where the inequality arises from Jensen's Inequality, and

$$G_\delta(d) = \begin{cases} 1/\mathrm{sinc}(2/\delta), & d = 0; \\ \frac{2d/(\delta-2)}{(1+d^{\delta/2})} {}_2\mathrm{F}_1(1,1;2-\frac{2}{\delta};\frac{1}{1+d^{\delta/2}}), & d > 0, \end{cases} \tag{3.9}$$

where ${}_2\mathrm{F}_1(a,b;c;z) = 1 + \sum_{n=1}^{\infty} \frac{z^n}{n!} \prod_{m=0}^{n-1} \frac{(a+m)(b+m)}{c+m}$ is the *hypergeometric function*. When $\delta = 4$, $G_4(d) = \cot^{-1}(d)$, $d \geq 0$. Therefore, when $\delta = 4$, (3.8) and (3.6) respectively become

$$\begin{aligned} \mathbb{L}_{J(r_0)}\left(\frac{\gamma r_0^4}{\mu p_0}\right) &\geq \exp\left[-r_0^2 \frac{ab}{\sqrt{p_0}} \cot^{-1}\left(\frac{\sqrt{p_0}}{a}\right)\right], \\ \mathbb{P}\left\{P_0^{\mathrm{uc}} \leq p_0\right\} &\geq \mathrm{erfc}\left\{\frac{b}{2}\sqrt{\frac{p_0}{c}}\left[\frac{a}{\sqrt{p_0}} \cot^{-1}\left(\frac{\sqrt{p_0}}{a}\right) + 1\right]\right\} \\ &\quad \times \frac{b}{2}\sqrt{\frac{\pi p_0}{c}} \exp\left\{\frac{b^2 p_0}{4c}\left[\frac{a}{\sqrt{p_0}} \cot^{-1}\left(\frac{\sqrt{p_0}}{a}\right) + 1\right]^2\right\}, \end{aligned} \tag{3.10}$$

where $a = \sqrt{\gamma\,\mathbb{E}[P_0^{\mathrm{uc}}]/\mu}$, $b = \pi\lambda_{\mathrm{tx}}$, $c = \gamma N_0/\mu$, and $\mathrm{erfc}(x) = 2/\sqrt{\pi}\int_x^\infty \mathrm{e}^{-u^2}\,\mathrm{d}u$ is the *complementary error function*.

If we have minimum/maximum power constraints, the unconstrained transmit power allocation P_0^{uc} that, by hypothesis, achieves the SINR target on all links may not necessarily satisfy these constraints on every link.

1. $\mathbb{P}\{P_0^{\text{uc}} < P_{\min}\}$ is the fraction of the links that require less power than $P_{\min}$ to achieve the link SINR requirement. Since these rxDs will always have greater SINRs than γ, they are not of interest, and we may set $P_{\min} = 0$ without loss of generality.

2. $\mathbb{P}\{P_0^{\text{uc}} > P_{\max}\}$ is the fraction of links that require more transmit power than $P_{\max}$ to achieve the target SINR γ. Such links set their transmit power to $P_{\max}$.[3]

Thus in general, the transmit power of an arbitrary link with these constraints is

$$P_0^{\text{c}} = \min\{P_0^{\text{uc}}, P_{\max}\}. \tag{3.11}$$

The CDF of the link transmit power with these constraints is

$$\mathbb{P}\{P_0^{\text{c}} \leq p_0\} = \begin{cases} \mathbb{P}\{P_0^{\text{uc}} \leq p_0\}, & p_0 < P_{\max}, \\ 1, & p_0 \geq P_{\max}. \end{cases} \tag{3.12}$$

3.1.3.2 Distribution of Link SINR under Power Constraints

When the txDs transmit with i.i.d. powers $\{P_t^{\text{c}}\}_{t\in\Phi}$, denote the total received interference power at rxD_0 by

$$J^{\text{c}}(R_0) = \sum_{t\in\Phi: R_t > R_0} \frac{P_t^{\text{c}} H_t}{R_t^{\delta}}. \tag{3.13}$$

Conditioned on $P_0^{\text{uc}} > P_{\max}$ for the link between txD_0 and rxD_0, we have $P_0^{\text{c}} = P_{\max}$ and the SINR at rxD_0 is then

$$\Gamma_0 \mid (P_0^{\text{uc}} > P_{\max}) = \frac{P_{\max} H_0 / R_0^{\delta}}{J^{\text{c}}(R_0) + N_0}, \tag{3.14}$$

[3] In [76], different fixed powers are investigated for such txDs. Although not shown in the present study for the sake of brevity, the same derivation also holds with slight modification in (3.9). It is also important to note that these links can be switched off by controlling the admission in a D2D network. The relationship between density, target SINR and the $P_{\max}$ is discussed in numerical examples in Sec. 3.1.4.

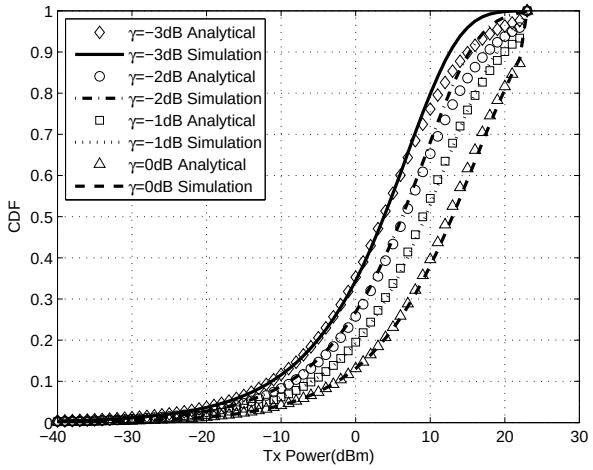

Figure 3.2 Transmit Power CDF for 12 D2D Links per Macrocell Coverage Area with ISD=500 m

and the corresponding conditional complementary CDF is then

$$\begin{aligned}\mathbb{P}\{I_0 > \tilde{\gamma} \mid P_0^{\mathrm{uc}} > P_{\max}\} &= \mathbb{P}\left\{H_0 \geq \frac{\tilde{\gamma} R_0^{\delta}[J^{\mathrm{c}}(R_0) + N_0]}{P_{\max}}\right\} \\ &= \int_0^{\infty} f_{R_0}(r_0) \exp\left(-\frac{\gamma r_0^{\delta} N_0}{\mu P_{\max}}\right) \mathbb{L}_{J^{\mathrm{c}}(r_0)}\left(\frac{\gamma r_0^{\delta}}{\mu P_{\max}}\right) \mathrm{d}r_0, \end{aligned} \tag{3.15}$$

where $\mathbb{L}_{J^{\mathrm{c}}(r_0)}(s)$ is bounded by the right hand side (RHS) of (3.8) with $\mathbb{E}[P_0^{\mathrm{uc}}]$ replaced by $\mathbb{E}[P_0^{\mathrm{c}}]$. Then for $\delta = 4$, $\mathbb{P}\{I_0 > \tilde{\gamma} \mid P_0^{\mathrm{uc}} > P_{\max}\}$ is bounded by the RHS of (3.10) with p_0 replaced by $P_{\max}$ and $\mathbb{E}[P_0^{\mathrm{uc}}]$ replaced by $\mathbb{E}[P_0^{\mathrm{c}}]$. From (3.11), we have

$$\mathbb{E}[P_0^{\mathrm{c}}] = \int_0^{P_{\max}} \mathbb{P}\{P_0^{\mathrm{uc}} > x\} \, \mathrm{d}x. \tag{3.16}$$

Finally,

$$\mathbb{P}\{I_0 \leq \tilde{\gamma}\} = \begin{cases} \mathbb{P}\{P_0^{\mathrm{uc}} > P_{\max}\} & \\ \times \mathbb{P}\{I_0 \leq \tilde{\gamma} \mid P_0^{\mathrm{uc}} > P_{\max}\}, & \tilde{\gamma} < \gamma, \\ 1, & \tilde{\gamma} \geq \gamma. \end{cases} \tag{3.17}$$

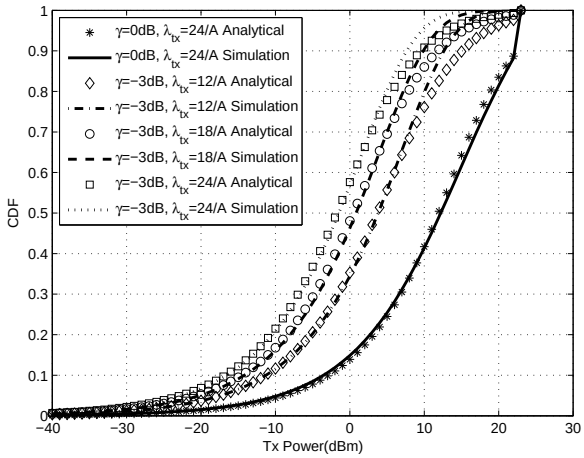

Figure 3.3 Transmit Power CDF for 12, 18, 24 D2D Links per Macrocell Coverage Area with ISD=500 m, and $\gamma = 0, -3$ dB

3.1.4 Numerical Results

We provide simulation results for a D2D network deployed in a 19-macrocell area with wraparound and inter-site-distance (ISD) of 500 m. (Owing to power control employed in each link, wraparound is important, as it affects the distributions of transmit powers and SINRs.) The txDs and rxDs are independently and uniformly distributed in the area. The area A of a hexagonal macrocell as defined in [71] is used in simulations and 12, 18, or 24 D2D links are chosen per macrocell. The path loss between a txD and rxD is $\mathrm{PL(dB)} = 30.6 + 40\log_{10}(d)$, where d is the distance between the txD and rxD in meters, and the minimum and maximum transmit powers are -40 dBm and 23 dBm, respectively [71]. Other details of the simulation are given in Table 3.1. Power allocation is performed using the Foschini-Miljanic algorithm [77].

From the simulation parameters, it follows that the corresponding parameters of the analytical model are $\delta = 4$ and $\lambda_{\mathrm{tx}} = 12/A$, $18/A$, or $24/A$, depending on the number of active links chosen per macrocell. From the path loss model, we should choose $10\log_{10}\mu = -30.6$. However, we note that the CDF of P_0^{uc}, which is also required to calculate the CDF (3.17) of SINR, is not known exactly, but only upper-bounded by the RHS of (3.6) and (3.10). For $\delta = 4$, instead of using this value for μ in the upper-bound (3.10), we *set*

Table 3.1 D2D Simulation Parameters

Parameter	Value	Description
γ	$-3, -2, -1, 0$ dB	Target SINR
ISD	500 m	Inter macro site distance
A	$A = \sqrt{3}(\text{ISD})^2/2$	Area of a macro-cell
B	9×10^6 Hz	Bandwidth
$\tilde{N_0}$	-174 dBm/Hz	Thermal noise power spectral density
NF	5 dB	Noise figure
N_0	$\tilde{N_0} + 10\log_{10}(B) + NF$	Thermal noise power
PL	$30.6 + 40\log_{10}(d)$	Path loss in dB, d in m
$P_{\min}, P_{\max}$	-40, 23 dBm	Minimum and maximum power constraints [71]

the value of μ such that the RHS of (3.10) is the *closest match* to the empirical CDF of transmit power P_0^{uc} as obtained via simulation.[4] In other words, we use the RHS of (3.10) with the appropriate μ as the model for the exact CDF of P_0^{uc}, instead of an upper bound to it. Further, the value of $\mathbb{E}[P_0^{\text{uc}}]$ in (3.10) is simply set to be the empirical mean obtained from simulation.

In Fig. 3.2, we plot both the empirical CDF of transmit power P_0^{c} (from simulation), and the analytical result (3.12), for the target SINR $\gamma = -3, -2, 1, 0$ dB with 12 active D2D links per macrocell coverage area. Fig. 3.3 includes the CDF curves with 18 and 24 active D2D links per macrocell for $\gamma = -3$ dB, and for $\gamma = 0$ dB with 24 active D2D links per macrocell.[5]

For a given set of parameters (bandwidth, noise power, density of the links, path loss formula), while the target SINR is increasing, the transmit powers are increasing, as

[4] As seen from Fig. 3.2 and Fig. 3.3, the transmit power constraints do not apply when $\gamma = -3$ dB, so $P_0 = P_0^{\text{uc}}$ for these cases.

[5] Compare Fig. 3.2 for $\gamma = 0$ dB with Fig. 3.3 $\gamma = 0$ dB for $\lambda_{\text{tx}} = \frac{24}{A}$. Since similar results are obtained for various densities, for the sake of brevity, we only plot the CDF with $\lambda_{\text{tx}} = \frac{24}{A}$ for $\gamma = 0$ dB in Fig. 3.3.

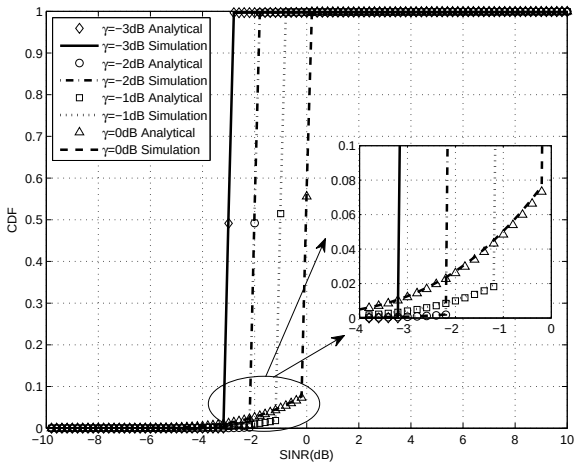

Figure 3.4 SINR CDF for 12 D2D Links per Macrocell Coverage Area with ISD=500 m

seen in Fig. 3.2. However, increasing target SINR to a certain level can cause some of the transmit powers to be at the maximum value (23 dBm in Fig. 3.2 and Fig. 3.3). This occurs due to severe interference between links with overlapping coverage areas as depicted in Fig. 3.1. As discussed earlier, the target SINR can not be satisfied on such links. This is seen from the CDF of SINR plotted in Fig. 3.4 for the same parameters as in Fig. 3.2. The analytical CDF of SINR is given by (3.17), with the analytical CDF of P_0^{uc} as used in Fig. 3.2, but with $\mathbb{E}[P_0^{\text{c}}]$ set to be the empirical value obtained from simulation instead of being calculated from (3.16).

In Fig. 3.3, we investigate the effect of D2D link density for different target SINRs. For $\gamma = -3$ dB, while the density of the links is increasing, the transmit powers are decreasing. This shows that power control can carefully take advantage of the increase in the density and decrease the overall transmit powers in the network. However, similar behavior is not observed for $\gamma = 0$ dB. For $\gamma = 0$ dB, even though we increase the density of the links, we still see very similar transmit powers. This behavior is due to power control and for a given γ, increasing density does not let the power control algorithm find a valid set of transmit powers which satisfies the boundary conditions while ensuring the target SINR requirement of the links.

It is also important to note that in all figures (for CDF of transmit power and SINR) our analytical findings and the simulation results match well when a nonzero fraction of links cannot satisfy the target SINR requirement even at full transmit power. When nearly all links can satisfy the target SINR without hitting the power constraint, our analytical results for transmit power CDF are accurate upto about 10 dBm for 12 D2D links per macrocell, and about 8 dBm for 18 and 24 D2D links per macrocell.

3.1.5 Conclusions

In this section, we investigate the transmit power distributions for D2D links with ideal power control. We characterize a D2D network with a group of parameters and show the feasibility of a D2D network in terms of transmit power distributions and SINR. We investigate the problem both with analytical derivations and numerical results, and find a good match between simulations and theory. The findings in this study may easily be extended to find transmit power and SINR distributions for devices which have different QoS requirements in each link therefore different target SINRs.

3.2 Gateway Scheduling for Dense Heterogeneous Networks

In this section, we analyze various user assignment and scheduling policies for neighboring femtocell networks. The trade-off between capacity maximization and fairness is investigated and a combined user assignment and proportional fair (PF) scheduling procedure for a femtocell gateway is proposed. The flexibility of the proposed architecture in terms of capacity and fairness is studied via various simulation scenarios. It is shown that by changing parameters in the proposed method one can play-out between fairness and capacity in a femtocell network. In order to decrease the number of the handovers between femtocells, we propose that a femtocell user should be scheduled with the same femtocell base station for a duration of superframe, i.e, cell re-selection should be done in every superframe. The performance of the combined user assignment and PF scheduling scheme is investigated under different superframe considerations and it is shown that a wide range of performance results (capacity, fairness, handover) could be achieved.

3.2.1 Introduction and Motivation

Femtocells have a strong potential to improve the capacity of next generation wireless systems since they offer better link qualities and wider spectrum resources for connected users. Scheduling of the users carries critical importance for minimizing the interference, maximizing the system capacity, and achieving fairness in femtocell networks [21]. Achieving high-capacity with fair scheduling techniques have been investigated extensively in the past for conventional cellular architectures. For example, [79] aims to maximize the sum-rate of all the users within a cellular network; however, fairness issues have not been considered. A maximum fairness technique has been discussed in [80], which essentially tries to maximize the capacity of the user that has the lowest data rate and achieve similar data rates for all users. Finally, proportional fair scheduling [81] can be considered as a compromise between the maximum capacity and maximum fairness approaches.

Scheduling in femtocell networks, on the other hand, involves more complications due to involvement of multiple (typically co-channel) small-size cells, as well as the macrocell. In addition to scheduling the users to appropriate frequency bands for achieving high capacity and fairness, intelligent assignment of users to different cells is also required. In co-channel femtocell deployments, femtocells and macrocells are assigned the same spectrum, yielding co-channel interference to each other. Moreover, there may be load imbalances in neighboring femtocells, where a certain femtocell may have significantly larger number of users compared to other femtocells in the vicinity (e.g., popular stores in shopping malls). These unique problems in femtocell networks necessitate intelligent scheduling algorithms that can have a good compromise between maximization of the fairness and the sum-rate.

There are some limited contributions in the literature on the scheduling of the users in femtocell networks. In [82], a capacity-maximizing power control and scheduling approach has been considered for neighboring femtocell networks. A centralized radio resource management (RRM) approach has been considered where a femtocell gateway handles the resource assignments of the femtocells connected to it. However, fairness perspectives have not been considered in [82]; even when the capacity gets maximized, the individual users on

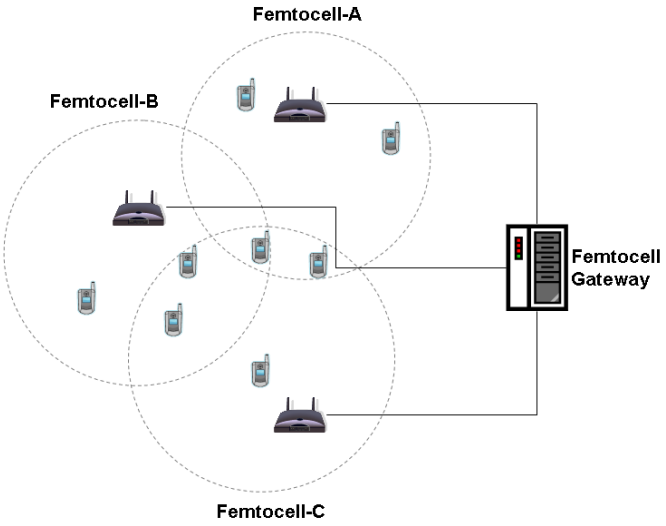

Figure 3.5 Dense Femtocell Scenario in Consideration, where Femtocell Gateway Handles the Resource Management

the cell edge may suffer significant interference and therefore may have poor channel capacities. In [83], a distributed femtocell resource allocation has been proposed, which does not require any coordination among femtocells, and utilizes distributed hash tables. A cognitive femtocell framework has been introduced in [84], where femtocells cognitively recognize the interference signature, and implement an opportunistic channel scheduler in order to avoid interference to/from neighboring femtocells and the macrocell users. Finally, [69] proposes a decentralized spectrum allocation policy which is shown to be optimal in terms of area spectral efficiency, and guarantees a prescribed data rate for both the macrocell and femtocell networks.

Since it has a strong potential for mitigating interference between neighboring femtocells, a centralized resource allocation as in [82] results in higher channel capacities compared to distributed resource allocation. This has also been recognized in 3GPP, where a recent contribution emphasizes the importance of a centralized coordinator that schedules femtocell transmissions, so that neighboring femtocells will transmit in non-overlapping sub-frames [85].

In this section, we introduce different scheduling approaches in neighboring femtocell networks with centralized coordination as in Fig. 3.5, and investigate techniques for improving the capacity and fairness of the users. It is important to note that unlike traditional architectures composed of a single macrocell, the scheduling problem in femtocell networks involves both the assignment of users to femtocells and the bandwidth allocation within each femtocell. Moreover, interference between the users in densely deployed femtocells is another criterion that impacts the scheduling decisions and performance.

We first consider assignment of the users to neighboring femtocells through different approaches, and investigate the fairness versus capacity trade-offs. Then, once an initial assignment has been achieved, we investigate how the proportional fairness scheduling (PFS) method can be used to find a good compromise between maximizing the capacity and maximizing the fairness.

The organization of this section is as follows. Subsection 3.2.2 presents the assignment of users to the femtocells under different constraints. The round robin and proportional fair scheduling schemes are investigated for the proposed femtocell scenario in subsection 3.2.3. Subsection 3.2.4 combines the femtocell scheduling problem, both in terms of femtocell assignment of users and scheduling of users within each femtocells considering the capacity, fairness and number of handovers to optimize the resource allocation. Finally in subsection 3.2.5, we conclude and provide a roadmap for future research.

3.2.2 Assignment of Users to Femtocells

Let $B_{i,j}$ and $N_{i,j}$ denote the bandwidth of the i^{th} user with j^{th} femtocell and number of users in the j^{th} femtocell, respectively. Then, the downlink capacity of user-i with the j^{th} femtocell can be written as;

$$C_{i,j} = B_{i,j} \log_2 \left(1 + \text{SINR}_{i,j}\right) \tag{3.18}$$

where $\text{SINR}_{i,j}$ denotes the signal to interference plus noise ratio (SINR) of the i^{th} user with the j^{th} femtocell.

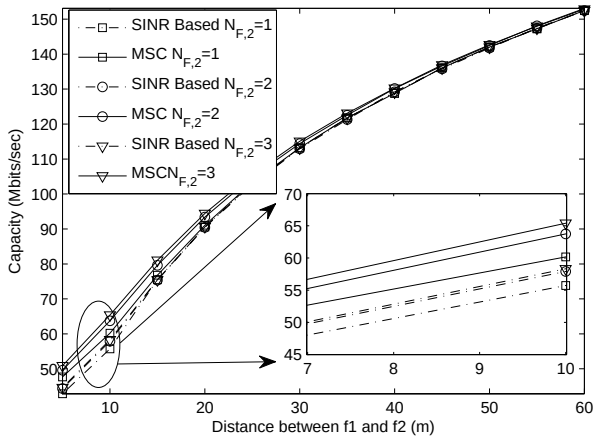

Figure 3.6 Capacity vs. Inter-femtocell Distance for 2 Femtocell Scenario

Then, given the SINRs of all the users with different femtocells (which is assumed available at the femtocell gateway in Fig. 3.5), a sum-capacity maximizing assignment of the users to different femtocells can be written as

$$\left\{\tilde{F}_1, ..., \tilde{F}_{N_\mathrm{F}}\right\} = \arg \max_{\tilde{F}_1,...,\tilde{F}_{N_\mathrm{F}}} \sum_{j=1}^{\mathrm{N_F}} \sum_{i \in \tilde{F}_j} C_{i,j}, \tag{3.19}$$

where $\tilde{F}_j$ denotes a hypothesized set of indices for users connected to femtocell-j, and N_F denotes the total number of femtocells in consideration. Once the assignment of all users are done for femtocells, the number of users in j^{th} femtocell could be given as $N_{\mathrm{F},j}$. In this study, we refer (3.19) as the maximum sum capacity (MSC) based assignment. Note that (3.19) requires a search over all possible combinations of user assignments to different neighboring femtocells, which results in various interference settings. Even though (3.19) maximizes the sum capacity, the complexity of the scheme increases exponentially with the number of users. Moreover it may result in unfair capacity distributions among different users, since it typically tends to allocate more bandwidth to users with better SINRs.

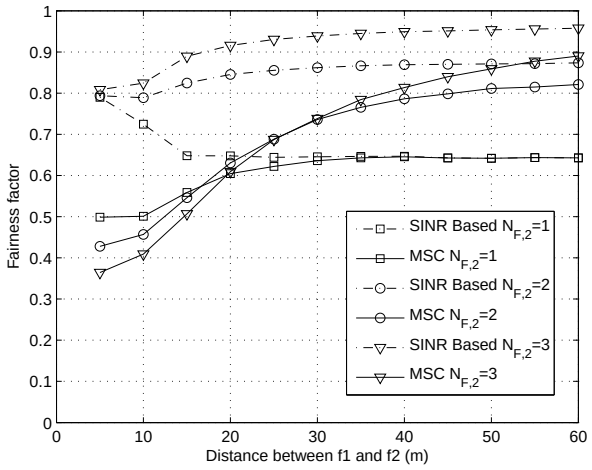

Figure 3.7 Fairness Index vs. Inter-femtocell Distance for 2 Femtocell Scenario

Alternatively, in an SINR based user assignment, users may simply choose the cells that have the best SINR, where the serving femtocell index j for user-i can be simply written as[6]

$$\tilde{j}_i = \arg\max_j \text{SINR}_{i,j}. \tag{3.20}$$

The fairness of the user capacities in the entire system for both approaches can be captured by using the Jain's fairness index [37]:

$$FI = \frac{\left(\sum_{j=1}^{N_\text{F}} \sum_{i=1}^{N_{\text{F},j}} C_{i,j}\right)^2}{N_\text{T} \sum_{j=1}^{N_\text{F}} \sum_{i=1}^{N_{\text{F},j}} C_{i,j}^2}, \tag{3.21}$$

where N_T denotes the total number of users in all the femtocells, i.e, $N_\text{T} = \sum_{j=1}^{N_\text{F}} N_{\text{F},j}$.

In order to evaluate the capacity and fairness of the users within neighboring cells with different assignment methods, we consider a simulation scenario similar to the one described in Fig. 3.5. For simplicity, we present two neighboring femtocells with a bandwidth of 10 MHz in each femtocell base station. To have different interference configurations, the

[6]Note that (3.20) treats all the femtocells equally likely without biasing any of the femtocells. Recent contributions on 3GPP (e.g., [86]) assign an additive bias term to SINR of hot-spot femtocells in order a hot-spot cell to be favored to be selected. This technique is commonly referred as range expansion and left as a future study.

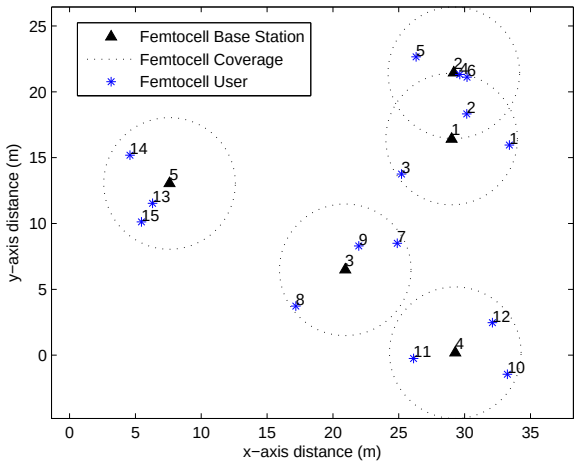

Figure 3.8 Example Femtocell and User Distribution for a 5-femtocell Scenario

distance between the two femtocells is changed between 5 m to 60 m, and realistic path-loss models are considered which are defined in [87]. There are $N_{\mathrm{F},1}$=4 users randomly distributed within Femtocell-1, while the number of users within Femtocell-2 $N_{\mathrm{F},2}$ is varied. The results in Fig. 3.6 show that the sum capacity improves considerably in all cases with increasing femtocell separation, which is due to the decreasing inter-femtocell interference. On the other hand, especially at very small femtocell separations, MSC yields at least 5 Mbps better sum-capacity compared to SINR based assignment for all cases, and gains degrade as the separation between the two femtocells increases.

Fairness index plots in Fig. 3.7 show that MSC typically results in very unfair distribution of the capacity to the users compared to SINR based assignment, and the fairness index values of the two assignment schemes become similar for larger femtocell separations. For smaller number of users at Femtocell-2, the SINR based assignment always results in less fair assignments for increasing $N_{\mathrm{F},2}$. On the other hand, with MSC, smaller $N_{\mathrm{F},2}$ yields better fairness at smaller femtocell separations, which becomes less fair at larger femtocell separations. Fairness is seen to improve with larger femtocell separation in general, except for SINR based allocation with $N_{\mathrm{F},2} = 1$.

3.2.3 Proportional Fair Scheduling in Femtocells

The assignment of the users to different femtocells is investigated in the previous subsection. Once the users are assigned to different femtocells, their channel qualities may fluctuate over time, and the scheduler should consider both capacity and fairness issues while assigning resources to the users. We consider frame by frame scheduling of users using proportional fairness (PF) criteria for duration of a superframe (which may contain more than one frame duration) in which the users will be assumed to be served within the same femtocell. On the other hand, with the granularity of each superframe, the users may be re-assigned to different femtocells[7] depending on one of the methods presented in subsection 3.2.2. This architecture allows to play out between throughput and fairness within each femtocell while decreasing the handovers between femtocells. In this subsection we present how we model PF scheduling within each superframe.

With the described frame structure, the capacity of the i^{th} user with the j^{th} femtocell in the k^{th} frame can be written as

$$C_{i,j}(k) = B_{i,j}(k) \log_2 \left(1 + \text{SINR}_{i,j}(k)\right) \tag{3.22}$$

where $\text{SINR}_{i,j}(k)$ and $B_{i,j}(k)$ are the SINR level and assigned bandwidth, respectively, of the i^{th} user with the j^{th} femtocell in the k^{th} frame.

The fairness index can also be calculated for each femtocell by using a modified version of (3.21). The fairness index could be calculated either by using capacity of each user or assigned bandwidth of each user. However, it is important to note that fully fair bandwidth assignment does not ensure that the capacity of each user is equal since the SINR levels affect the capacity. Moreover, the fairness between users in the entire system and within each femtocell BS reveals different fairness indices. Fairness index of each femtocell

[7]For example, in 3GPP, cell-reselection may be performed at every few seconds [88].

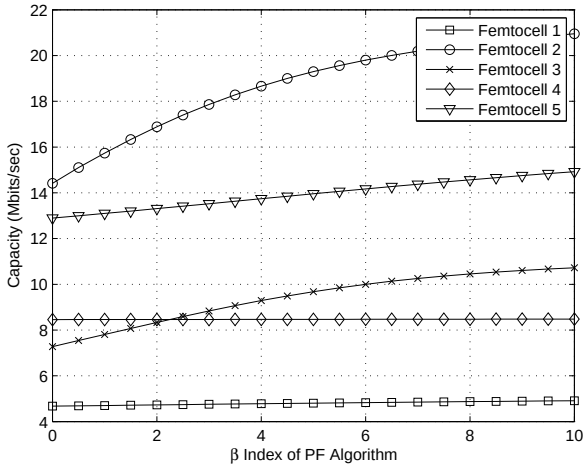

Figure 3.9 Capacity vs. β for a 5-femtocell Scenario

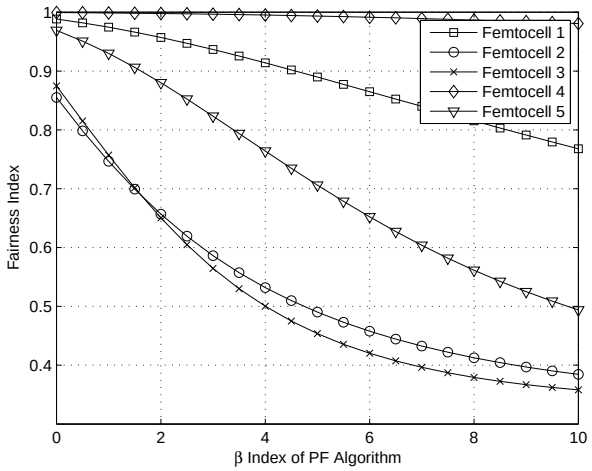

Figure 3.10 Fairness vs. β for a 5-femtocell Scenario

is calculated with the following equation

$$FI_j = \frac{\left(\sum_{i=1}^{N_{\mathrm{F},j}} \tilde{C}_{i,j}\right)^2}{N_{\mathrm{F},j} \sum_{i=1}^{N_{\mathrm{F},j}} \tilde{C}_{i,j}^2}, \tag{3.23}$$

where $\tilde{C}_{i,j}$ is the long term average of the capacity of the i^{th} user with the j^{th} femtocell in the superframe.

We implement the PF scheduling within each superframe as follows. We consider that the PF indicies of each user is calculated at the beginning of each frame within each femtocell as

$$\mathrm{PF}_{i,j}(k) = \frac{C_{i,j}^{\beta}(k)}{W_{i,j}(k)}, \tag{3.24}$$

where $\mathrm{PF}_{i,j}(k)$ is proportional fairness index of the i^{th} user with the j^{th} femtocell and $W_{i,j}(k)$ is the long term average rate of the i^{th} user with the j^{th} femtocell, all observed at the beginning of the k^{th} frame. The parameter β is used to tune the fairness properties of the proposed scheduler. On the other hand, updating of $W_{i,j}(k)$ within each frame is done as follows:

$$W_{i,j}(k+1) = (1-\alpha)W_{i,j}(k) + \alpha C_{i,j}(k), \tag{3.25}$$

where α is a memory index which adjusts the memory of the $W_{i,j}(k)$. In order to evaluate the performance of the PFS, a scenario where femtocells and users are randomly distributed is realized. In particular, three users for each femtocell are generated and a simulation is done for a duration of superframe with various β values. During each superframe, the users do not change their cell associations, and it is assumed their SINRs are not varying (i.e., interference conditions do not change). An illustration of the proposed scheme in a particular scenario is given in Fig. 3.8

For $\alpha = 0.1$, the sum-capacities within each femtocell with respect to β are illustrated in Fig. 3.9, while corresponding fairness index values are shown in Fig. 3.10. Results show that using larger values of β improves the capacity, while it results in worse fairness. In the limiting case when $\beta = 0$, the PF algorithm converges to round robin algorithm, which implies that the fairness index of users in each femtocell is converging to 1 depending on the SINR values of each user. As discussed before, equally partitioning the bandwidth does not mean that capacity is fairly distributed, the convergence of fairness indicies of different femtocells show variations.

Note that the sum-capacity of some femtocells are greater than the others which has more users closer to the femtocell base station. For instance in femtocell 2, the users closer to the femtocell base station are relatively more (see Fig. 3.8) and proportional fair algorithm take advantage of it in order to maximize the capacity with the increase of β. On the other hand the fairness of the users in that femtocell decrease dramatically with β. Femtocell 4 users are almost in same distance from femtocell 4 base station and therefore their SINRs are similar. Proportional fair algorithm cannot take advantage it, and acts like round robin algorithm. Increasing β does not increase the capacity, yet do not decrease the fairness. The increase in the capacity and decrease in the fairness are highly correlated which shows the trade-off between Fig. 3.9 and Fig. 3.10.

3.2.4 Femtocell Gateway Scheduling

In this subsection we combine the femtocell scheduling problems which are individually analyzed in the previous subsections and provide a complete solution for the scheduling in femtocell gateway architecture illustrated in Fig. 3.5. Fig. 3.11 summarizes the proposed assignment procedure referring to the equations given in previous subsections. In order to provide both femtocell user assignment and scheduling within each femtocell, we propose a two-step scheduling method. This model provides a solution for capacity-fairness trade-off and also considers the number of cell re-selections by each user through adjusting the superframe length.

Scheduling of the current frame starts with assigning users to the femtocells which is assumed to be done in each superframe. Therefore in step-1, depending on the length of a superframe, a new femtocell assignment for each user is done or current assignment is preserved. As it is analyzed in subsection 3.2.2, either MSC or SINR based assignment is realized depending on the capacity-fairness trade-off. In step-2, for a duration of superframe assignment of bandwidth to each user is performed in each frame for the corresponding cell-selection. Proportional fair algorithm is used for scheduling the users for various combinations of β. Note that $\beta = 0$ corresponds to round robin scheduling, and while for

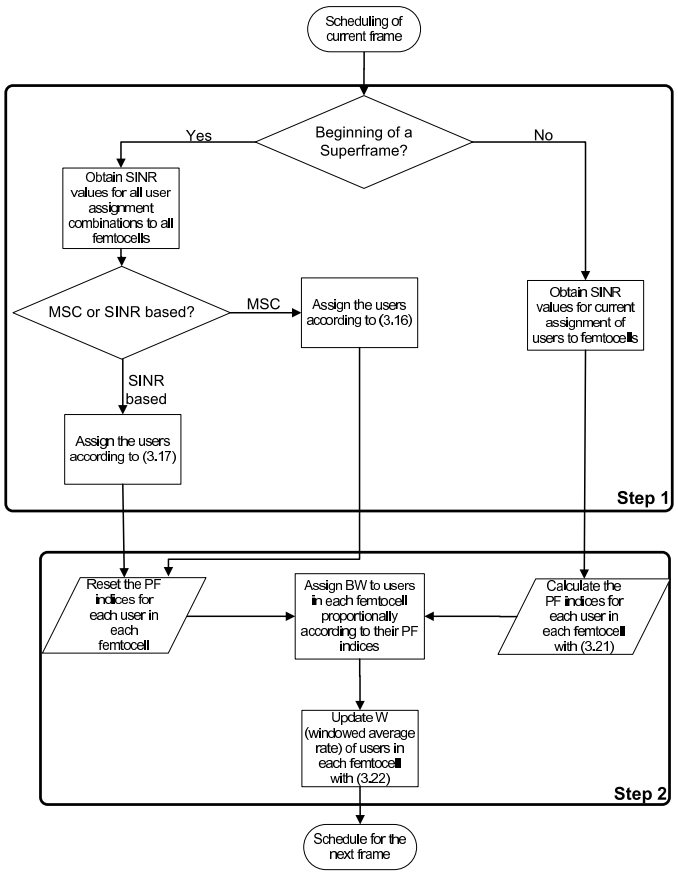

Figure 3.11 Scheduling Architecture in a Femtocell Gateway

increasing β, the bandwidth is aggressively assigned to the users which can achieve higher data rates.

In order to evaluate the performance of the above scheduling architecture we consider a scenario with 5 femtocells and 15 users as described in subsection 3.2.2. However to provide more realistic scenario, we assume independent SINR values are observed in each frame which corresponds to the independent block fading as defined in [89]. We simulate a densely deployed neighboring femtocell scenario therefore SINR values of users are changing in each frame with a Rayleigh distribution with parameter $\sigma = 10$ dB. Simulation results for the total capacity for 5 femtocells vs. superframe duration is presented in Fig. 3.12.

The capacity decreases with increase in the superframe length. However the decrease in the capacity could be compensated with increasing β. Note that the gap between different

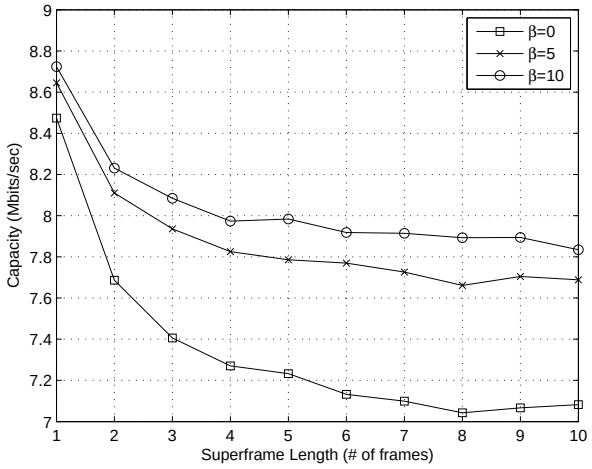

Figure 3.12 Capacity vs. Superframe Length for a 5-femtocell Scenario

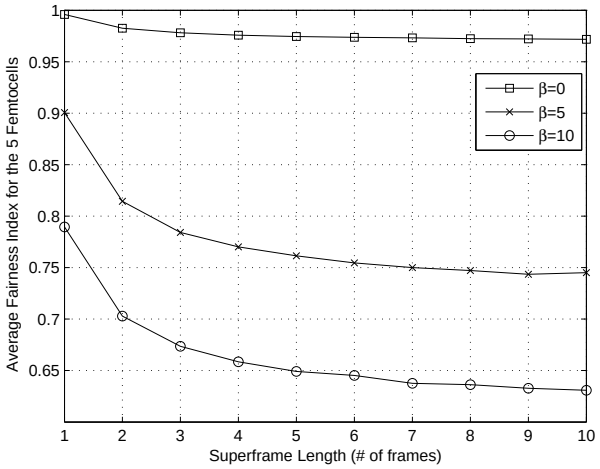

Figure 3.13 Average Fairness Index of 5 Femtocells vs. Superframe Length

β curves is increasing with the increase in the superframe length which could be explained as follows. With the increase in the superframe length, the proportional fair algorithm starts to take more and more advantage of users which have higher SINR value, and therefore limits the decrease in the capacity (see Fig. 3.12). On the other hand, Fig. 3.13 shows that the PF algorithm takes advantage of the above described situation with a trade-off in the

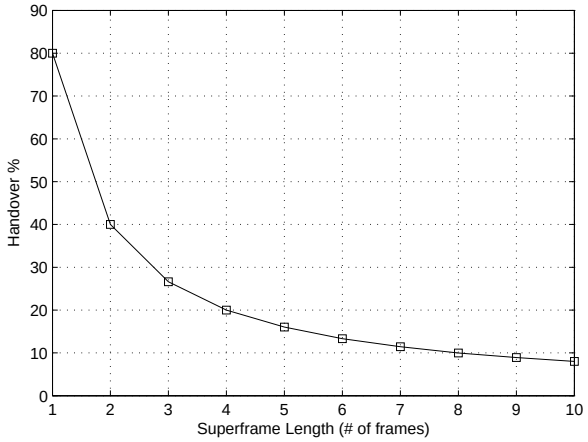

Figure 3.14 Handover Percentage of a User vs. Superframe Length

average fairness factor for the 5 femtocells which can be defined as

$$AFI = \frac{1}{N_{\mathrm{F}}} \sum_{j=1}^{N_{\mathrm{F}}} FI_j. \tag{3.26}$$

Finally, Fig. 3.14 presents the percentage of handovers versus superframe length. As the superframe length increases the percentage of the handovers decreases. As described in Fig. 3.11, increasing the superframe length decreases the cell re-selection for the users. Therefore, superframe structure forces users to be connected to the same femtocell and therefore decreases the handovers. Note that the handovers might increase in a densely deployed femtocell scenario and users might experience higher accessing costs and complexity, similar to ping-pong effect in cellular structures [90]. With the increase in superframe length the users are generally serviced by the same femtocells that they have been serviced in the previous frames. It is important to note that the channel re-selection policy adds another dimension to be considered within the femtocell gateway scheduling since larger number of handovers increase the complexity of the system.

3.2.5 Conclusions

This section proposes a two-step femtocell gateway scheduling algorithm i.e., assigning users to femtocells and scheduling frequency resources to the users within each femtocell. MSC and SINR based schemes are proposed for the cell-selection procedure. Comparison shows that although MSC based procedure maximizes capacity, it might lead very unfair cell assignment comparing to SINR based scheme.

In parallel to the contributions in 3GPP, we propose that cell re-selection should be optimized considering capacity, fairness, and number of handovers. Therefore we propose a superframe structure for cell re-selection. In a superframe duration, in which users do not change their assigned femtocells, femtocell base station assigns bandwidth according to the PF algorithm. We show that various capacity-fairness performance could be achieved by changing the β parameter defined by PF scheduling algorithm.

The effectiveness of PF scheduling is presented under different superframe lengths. The results show that increasing the superframe duration decreases the fairness and capacity. On the other hand, the PF algorithm is shown to take advantage of longer superframe durations, and therefore it does not let capacity to decrease dramatically while β is increasing. Moreover, number of handovers of users between femtocells is also decreasing, and hence, the complexity of the system decreases. It is shown that with the provided 2-step scheduling architecture, various capacity-fairness-handover performance targets may be achieved depending on different system requirements.

CHAPTER 4 :

MOBILITY IN TIERED NETWORKS

Mobility causes Doppler effect and therefore is an important issue that limits the performance of wireless communication networks. In mobile terrestrial wireless communication systems, the channel model is generally based on the assumption that directions of arrival (DOA) of the signal at the receiver are uniformly distributed which yields to a Doppler spectrum of the classical Jakes model. As opposed to the Jakes Doppler spectrum in mobile terrestrial communications, aeronautical communication network (ACN) channels are modeled with dual Doppler shift. Therefore, it is possible to estimate and mitigate the effect of Doppler in ACN. In this chapter, we study the mobility issues in a two-tiered ACN to increase the throughput.

Doppler spectrum in aeronautical channels is modeled with dual Doppler shift instead of classical Jakes model. Orthogonal frequency division multiplexing (OFDM) based systems are sensitive to Doppler shifts/spread since the time variation of the channel causes inter-carrier interference (ICI). In this study, ICI analysis is provided for OFDM-based systems in aeronautical channels; the effect of ICI on the received signal is presented and its power is derived. As opposed to terrestrial channels, where ICI is generally overcome by increasing the subcarrier spacing and bounding the normalized Doppler frequency (NDF), we propose to mitigate the effect of Doppler shifts in aeronautical channels. First, we use parametric spectrum estimation methods to extract the Doppler shifts by exploiting the predictable number of paths. Then, a beamforming-based method is introduced to resolve the incoming rays for compensating the effect of Doppler shifts separately in each branch. Finally, computer simulations are performed to provide numerical results. It is shown that a mean square error (MSE) performance of **1%** is achieved with the parametric estima-

tion methods, and bit error rate (BER) performance approaching to no-Doppler scenario is obtained with the beamforming-based mitigation method.

4.1 Introduction

Aeronautical communications (AC) is an emerging concept in which aeronautical platforms are considered as a part of the multi-tier network for future wireless communication systems. Programs led by the National Aeronautics and Space Administration (NASA), the Federal Aviation Administration (FAA), and EUROCONTROL all include the aeronautical platforms as part of the multi-tier network [15, 26]. The driving reasons for development of high data rate AC systems are: 1) The increase in data demand for Air Traffic Control and Air Traffic Management due to the growth in air transportation [28], 2) The need for low latency and low cost services to provide in-flight multimedia access [18], and 3) The potential to use AC systems as a backbone for terrestrial communication networks [19]. AC systems can provide service for ground networks, public safety, military communications, and improved cockpit data communications. To date, most ground/aircraft cockpit communications are done through voice only, and they are prone to language differences, accents, stress, and cultural barriers [29]. High data rate AC systems can augment the cockpit verbal communication with video and text to reduce cockpit errors. Furthermore, there is a growing demand for high speed data to meet commercial in-flight Internet activities [30].

Orthogonal frequency division multiplexing (OFDM) based schemes have been adopted for several current communication systems all over the world [31]. In OFDM-based systems, a serial symbol stream is converted into parallel streams and each symbol is modulated with different orthogonal subcarriers. Orthogonal subcarriers and cyclic prefix (CP) usage provide robustness to OFDM-based systems against the frequency selectivity of wireless channel. However, OFDM-based systems have relatively longer symbol durations compared to single carrier systems. Longer symbol duration leads to weakness against the time variation of the channel, i.e., Doppler spread, which causes loss of orthogonality between subcarri-

ers. If the orthogonality is not preserved within an OFDM symbol duration, there will be inter-carrier interference (ICI).

ICI degrades channel estimation and symbol detection performances of OFDM-based systems [41], [42]. If not compensated, ICI will cause an error floor for the symbol detection. For example, in the terrestrial OFDM systems, the channel model is generally based on the assumption that directions of arrival (DOA) of the signal at the receiver are uniformly distributed which yields to a Doppler spectrum of the classical Jakes model. The estimation of the channel and the compensation of the channel effect on the received signal are computationally complex in the Jakes Doppler spectrum scenario. Therefore, ICI is generally overcome by increasing the subcarrier spacing (decreasing the length of the OFDM symbol) and bounding the normalized Doppler frequency (NDF)[1] which causes an error floor for symbol detection in terrestrial communications [43].

As opposed to the Jakes Doppler spectrum in terrestrial communications, aeronautical channels are modeled with dual Doppler shift [25]. The result of the dual Doppler shift is also ICI in OFDM-based AC system. However, in aeronautical channels, as the received signal has a dual path with corresponding Doppler shifts, the Doppler spectrum can be interpreted as a combination of two frequency offset with corresponding gains. Therefore, it is possible to estimate and mitigate the effect of Doppler shifts by separating and compensating the shifts individually.

In the literature, OFDM channel estimation and ICI compensation for the dual Doppler shift are investigated in [44–47]. In [44], a Kalman filter-based estimation method with zero-forcing equalization is provided to cancel the effect of ICI. In [45], a digital phase lock loop is proposed to be used in order to track parameters of LOS path, and a maximum-likelihood estimator is suggested to resolve the reflected path. Then, the authors propose a Kalman-based approach to provide more accurate estimation, and to utilize an iterative cancellation method for the ICI compensation. In [46], Doppler shift compensation is suggested only for the line of sight (LOS) path, and demodulation is performed in the presence

[1]Note that this method also decreases the efficiency of OFDM-based systems and will be discussed in section 4.2.2.

of ICI. A different version of OFDM, Non-Contiguous Orthogonal Signal Division Multiplex (NCOSDM), is considered in [47] where the number of subcarriers are decreased depending on the channel to decrease the ICI and maintain the system performance.

In this study, an OFDM-based system[2] is considered in aeronautical environment. For dual Doppler shift scenario, the effect of ICI on the received signal is provided and its power is derived. We use parametric spectrum estimation methods to extract Doppler shifts by exploiting the predictable number of paths, i.e., two [25] or three [91]. We investigate the channel modeling order error and its impact on the estimation performance. Then, a beamforming-based approach is proposed to separate the paths based on DOA. Once the signals are separated then conventional methods are used to compensate the Doppler shift's individually [92]. Estimation performance for different modeling order errors, types of parametric spectrum estimation methods, and Rice factors are investigated through simulations. It is shown that an average mean square error (MSE) performance of 1% is achieved with the parametric estimation methods. Based on various estimation errors and diversity combining techniques, the impact of using different number of antenna elements on bit error rate (BER) performance is investigated. We show that the proposed method can achieve BER performance approaching to no-Doppler scenario.

The remainder of this chapter is organized as follows. In section 4.2, aeronautical channel is introduced and ICI analysis for OFDM-based system is provided. Then, parametric spectrum estimation techniques are introduced for the estimation of Doppler shifts in section 4.3. In section 4.4, the beamforming-based signal separation methodology is used to compensate the Doppler shifts. Numerical results for both estimation and compensation are presented in section 4.5, followed by concluding remarks in section 4.6.

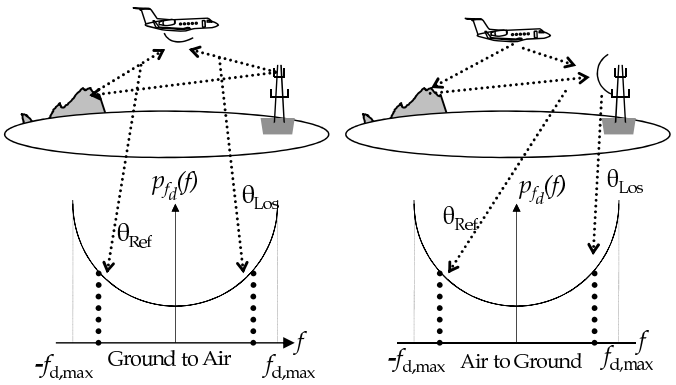

Figure 4.1 Doppler Power Spectrum in Aeronautical Channel

4.2 Two-tier Aeronautical Communication Network Channels

Aeronautical environment posses numerous challenges for developing a high data rate AC system, one of which is the channel [93]. Aeronautical channel can be broken into

[2]We focus on multi-carrier system, i.e., OFDM in this study. However, the methods investigated in this chapter to estimate and resolve the aeronautical channel effect on received signal can also be applied to single-carrier systems. Reader is referred to [48] for investigation of interference mitigation schemes in single-carrier systems.

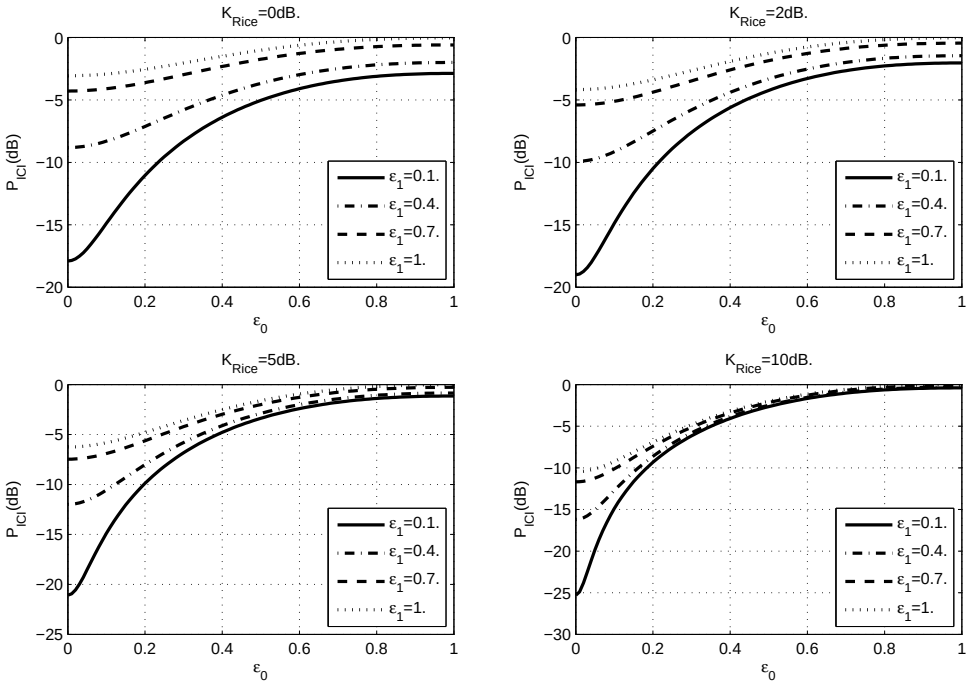

Figure 4.2 ICI Power for Various ϵ_0 and ϵ_1 Values

three segments: Takeoff/landing, en route, and taxing/parked. In this chapter, we will focus on the en route channel, which is generally modeled as a two-ray channel model [25]. The remaining two cases fall under the non-line of sight (NLOS) dispersive Jakes models.

4.2.1 Doppler Spectrum in Aeronautical Channels

The en route channel depicts different conditions between air to ground and ground to air wireless link. For each channel condition, a progressive increase and decrease of multipath and received Doppler spread of arriving signal need to be evaluated, as the aeronautical platform moves from a flat surface area to mountainous area. In an extremely rough environment, the en route channel might experience an intermittent loss of LOS signal with increasing Doppler spread which will cause channel Doppler spectrum of classical Jakes model [94]. However, aeronautical channel is generally modeled with a two-ray model, which consists of narrow sparsely populated Doppler shifts [95]- [97].

Fig. 4.1 presents the two-ray Doppler spectrum in an aeronautical channel. Both the direct and the reflected paths have a narrow spread and random Doppler frequencies. Therefore it can be assumed that two Doppler shifts can uniformly span anywhere between $-f_{\mathrm{d,max}}$ to $f_{\mathrm{d,max}}$ [25]. Thus, Doppler spectral density for aeronautical channel can be given as

$$p_{f_d}(f_d) = \sum_{l=0}^{L-1} (h_l)^2 \delta(f_d - f_{\mathrm{D}_l}) \ , \tag{4.1}$$

where h_l, f_{D_l} are the path gains, and Doppler frequencies, respectively ($L = 2$).

4.2.2 ICI Analysis in Aeronautical Channels

The ICI analysis is one of the key issues that has to be done to evaluate the performance of an OFDM system. The analysis will follow a general sample-spaced multipath fading channel model for analytical traceability. $x(n)$ are the discrete time samples of the transmitted OFDM signal, which can be given as: $x(n) = \sum_{k=0}^{N-1} X(k) e^{\frac{j2\pi kn}{N}}$, $0 \leq n \leq N-1$, where $X(k)$ is the symbol transmitted on the k^{th} subcarrier and N is the number of subcarriers. Let ϵ_0 and ϵ_1 be the NDF for the first and the second ray respectively, i.e., $\epsilon_0 = \frac{f_{\mathrm{D}_0}}{\Delta f}$

and $\epsilon_1 = \frac{f_{D_1}}{\Delta f}$, where, f_{D_0} and f_{D_1} are the Doppler shifts due to two paths, and Δf is the OFDM subcarrier spacing. Then, the general equation for L path channel can be given as

$$h(n) = \sum_{l=0}^{L-1} h_l e^{\frac{j2\pi\epsilon_l(n-\tau_l)}{N}} \delta(n-\tau_l), \tag{4.2}$$

where h_l's are the path gains with normalized overall power, i.e., $\mathbb{E}[h_l] = 0$, and $\sum_{l=0}^{L-1} \mathbb{E}\left[|h_l|^2\right] = 1$, and τ_l is the delay corresponding to l^{th} path as given in the model of Doppler shifts with exponentials in [41]. Therefore, assuming that receiver is synchronized to the first path $\tau_0 = 0$, and $\tau_1 = \tau$, i.e., τ being an integer, the received signal is

$$y(n) = h_0 e^{\frac{j2\pi\epsilon_0 n}{N}} x(n) + h_1 e^{\frac{j2\pi\epsilon_1(n-\tau)}{N}} x(n-\tau) + w(n)\ , \tag{4.3}$$

where $0 \le n \le N-1$, and $w(n)$ is additive white Gaussian noise (AWGN) with one-sided spectral density of N_0. Taking the discrete Fourier transform (DFT) of (4.3)

$$Y(k) = X(k)S(k,k) + \underbrace{\sum_{m=0,\ m\neq k}^{N-1} X(m)S(m,k)}_{\text{ICI}} + \underbrace{W(k)}_{\text{Noise}}\ , \tag{4.4}$$

where the received symbol is related to the transmitted symbol in interested subcarrier with coefficient $S(k,k)$ and also related to the other subcarrier's symbols with $S(m,k)$ (see [98]):

$$S(m,k) = \underbrace{\frac{h_0 \sin(\pi(m-k+\epsilon_0))}{N\sin(\pi(m-k+\epsilon_0)/N)}\ e^{j\pi(1-1/N)(m-k+\epsilon_0)}}_{\text{First Ray}} + \underbrace{\frac{h_1 \sin(\pi(m-k+\epsilon_1))}{N\sin(\pi(m-k+\epsilon_1)/N)}\ e^{j\pi(1-1/N)(m-k+\epsilon_1)}\ e^{\frac{-j2\pi\tau(m+\epsilon_1)}{N}}}_{\text{Second Ray}}. \tag{4.5}$$

The exact ICI power (P_{ICI}) as a function of the Doppler spectral density is given as [43]

$$P_{\text{ICI}} = 1 - \int_{-f_{\text{d,max}}}^{f_{\text{d,max}}} p_{f_d}(f_d)\text{sinc}^2(\frac{f_d}{\Delta f})df_d. \tag{4.6}$$

Therefore using (4.1) in (4.6), the ICI power in two-ray aeronautical channel can be given as

$$P_{\text{ICI}} = 1 - \left[|h_0|^2 \operatorname{sinc}^2(\epsilon_0) + |h_1|^2 \operatorname{sinc}^2(\epsilon_1) \right]. \tag{4.7}$$

Assuming $|h_0| \in \mathcal{R}$ is the amplitude of the LOS path and the $|h_1| \in \mathcal{R}$ is the amplitude of the reflected path then the power ratio, the so-called Rice factor can be given as [25]

$$K_{\text{Rice}}(\text{dB}) = 10 \times \log_{10} \left(\frac{|h_0|^2}{|h_1|^2} \right). \tag{4.8}$$

Therefore the following normalization as a function of the Rice factor can be obtained: $|h_0| = \sqrt{\frac{K_{\text{Rice}}}{1+K_{\text{Rice}}}}$, $|h_1| = \sqrt{\frac{1}{1+K_{\text{Rice}}}}$.

The ICI power caused by aeronautical channel is illustrated in Fig. 4.2 for various ϵ_0, ϵ_1, and K_{Rice} values span through best to the worst case scenarios. Note that ICI power can be high even for very small NDFs in dual Doppler shift aeronautical channel scenario comparing to terrestrial two-ray channel model given in [43].

ICI power in aeronautical channel will effect the detection of the symbols since it can be seen as a near-Gaussian noise [41]. In the terrestrial OFDM systems, ICI is overcome by increasing the subcarrier spacing (decreasing the length of the OFDM symbol) and bounding the NDF [31], [43]. However, this method has a twofold drawback: first, the system must be dynamic to change the system parameters depending on the level of Doppler, and second, more importantly it reduces the efficiency (therefore data rate) of the system:

$$\eta_{\text{OFDM}} = \frac{\frac{N \log_2(M_{\text{sub}})}{T_s + CP}}{N\Delta_f} = \frac{\log_2(M_{\text{sub}})}{1 + CP\Delta_f}, \tag{4.9}$$

where N, T_s, CP, and Δ_f are the number of subcarriers, symbol duration, cyclic prefix size, and subcarrier spacing of OFDM system, respectively, and M_{sub} is the modulation order of each subcarrier, i.e., $M_{\text{sub}} = 2^4$ for 16-QAM. Note that for a given CP size, increasing Δ_f decreases the efficiency of OFDM system. However, comparing to the method of decreasing OFDM symbol duration to bound the effect of Doppler in terrestrial networks, since the

shape of the Doppler has the particular characteristics defined in 4.2, it is possible to estimate the Doppler shifts with parametric estimation techniques (4.3) and remove the effect of aeronautical channel on the received signal by beamforming techniques (4.4).

4.3 Parametric Doppler Estimation for Aeronautical OFDM

As it is discussed in the previous section, in order to mitigate the effect of ICI, the Doppler shifts need to be estimated. For spectrum estimation, if the signal process (i.e., modeling order) is known as in AC, the parametric methods outperform the non-parametric methods, since the parametric methods try to understand the process [99]. Parametric methods are categorized as autoregressive (AR), moving average (MA), autoregressive moving average (ARMA), and harmonic. In this study, harmonic process is chosen, since we use a pilot (single tone) as a training symbol. In parametric methods, the frequencies of interest are extracted through a method known as eigendecomposition of the autocorrelation matrix. Autocorrelation matrix is decomposed into two subspaces, the signal subspace and the noise subspace, which can be shown for aeronautical channel as follows. Let us assume a training tone is generated by encoding only one subcarrier of an OFDM symbol, i.e., $X(k) = 1$ for $k = \rho$ and $X(k) = 0$ for all other k, i.e., $x(n) = e^{\frac{j2\pi\rho n}{N}}$. Then the received signal can be given using (4.3) as

$$y(n) = h_0 e^{jn\omega_0} + h_1 e^{j(n-\tau)\omega_1} + w(n) \quad , \tag{4.10}$$

where, ω_i's are the Doppler shifted pilot tone frequencies in radians for $i = 0, 1$ where, $\omega_i = \frac{2\pi(\epsilon_i+\rho)}{N}$, h_l's are the path gains with normalized overall power, i.e., $\mathbb{E}[h_l] = 0$, and $w(n)$ is AWGN with one-sided spectral density of N_0. Assuming the variance of $w(n)$ as σ_w^2, the autocorrelation matrix (size of $M_\mathrm{A} \times M_\mathrm{A}$) can be presented similar to the example given in [99, pp. 455-458]:

$$\mathbf{R}_y = \mathbf{D}_s \mathbf{V}_s \mathbf{V}_s^H + \mathbf{D}_v \mathbf{V}_n \mathbf{V}_n^H \ , \tag{4.11}$$

which is projecting a vector into signal and noise subspaces, respectively. Note that $\mathbf{D}_s$ and $\mathbf{D}_v$ are diagonal matrices that contain the eigenvalues of autocorrelation matrix due to signal $\lambda_i = \lambda_i^s + \sigma_w^2$ and noise $\lambda_i = \sigma_w^2$, respectively. $\mathbf{V}_s = [\mathbf{v}_1, \mathbf{v}_2, \dots \mathbf{v}_p]$ are the eigenvectors of $\mathbf{R}_y$ with their respective eigenvalues greater than σ_w^2 (p is the modeling order), and $\mathbf{V}_n = [\mathbf{v}_{p+1}, \mathbf{v}_{p+2} \dots \mathbf{v}_{M_\mathrm{A}}]$ is the group of eigenvectors of $\mathbf{R}_y$ that spans the noise subspace and consists of eigenvalues equal to σ_w^2.

4.3.1 Multiple Signal Classification (MUSIC) Method

Let $\mathbf{R}_y$ be $M_\mathrm{A} \times M_\mathrm{A}$ autocorrelation matrix of $x(n)$ with $M_\mathrm{A} > p+1$, and assume the eigenvalues are arranged in decreasing order with their corresponding eigenvectors. The eigenvectors are divided into two groups, the p signal eigenvectors with the largest eigenvalue, and the $M_\mathrm{A} - p$ noise vectors that mostly have eigenvalue equal to σ_w^2. The eigenvectors of $\mathbf{R}_y$ will have a length of M_A, and each of the noise subspace eigenfilters will have $M_\mathrm{A} - 1$ roots (zeros). p of the roots will lie on the unit circle at the frequencies of the complex exponentials and therefore eigenspectrum will exhibit sharp peaks at the frequencies of interest. The remaining $(M_\mathrm{A} - p - 1)$ zeros may lie anywhere, and some may cause spurious peaks in the eigenspectrum. However, the MUSIC algorithm takes care of these spurious peaks by means of averaging, as follows

$$P_{\mathrm{MU}}(e^{jw}) = \frac{1}{\sum_{i=p+1}^{M_\mathrm{A}} |\mathbf{e}^H \mathbf{v}_i|^2} \quad , \tag{4.12}$$

where $\mathbf{e} = [1,\ e^{j\omega},\ e^{j2\omega}, \cdots,\ e^{j(M_\mathrm{A}-1)\omega}]^T$. Thus, finding the angles of the roots of P_{MU}, i.e., $\hat{\omega}_i$, allows to estimate the Doppler shift due to each ray. Finally, subtracting the known transmitted tone, the $\hat{\epsilon}_i$ can be extracted as:

$$\hat{\epsilon}_i = \frac{N\hat{\omega}_i}{2\pi} - \rho \ , \quad i = 0, 1. \tag{4.13}$$

4.3.2 Eigenvector Method

The eigenvector method is slightly different from the MUSIC algorithm, since a compensation of each eigenvector is performed with its associated eigenvalue and therefore this method produces less spurious peaks:

$$P_{\mathrm{EV}}(e^{jw}) = \frac{1}{\sum_{i=p+1}^{M_{\mathrm{A}}} \frac{1}{\lambda_i} \left|\mathbf{e}^H \mathbf{v}_i\right|^2} \ , \tag{4.14}$$

where λ_i is the eigenvalue associated with each eigenvector $\mathbf{v}_i$. The angles of the roots of P_{EV} also consist the Doppler frequencies and the estimation can be done as in (4.13).

4.3.3 Minimum Norm Algorithm Method

The minimum norm algorithm uses a single vector $\mathbf{a}$ that is constrained to lie in the noise subspace, instead of forming an eigenspectrum that uses all of the noise eigenvectors, that is,

$$P_{\mathrm{MN}}(e^{jw}) = \frac{1}{\left|\mathbf{e}^H \mathbf{a}\right|^2} \ , \tag{4.15}$$

where $\mathbf{a} = \mathbf{V}_{\mathrm{n}}\mathbf{V}_{\mathrm{n}}\mathbf{v}$ is the projection matrix that projects an arbitrary vector $\mathbf{v}$ on to the subspace. The z-transform of $\mathbf{a}$ will be: $A(z) = \sum_{k=0}^{M-1} a(k) z^{-k}$. where, z_k for $k = p+1, ..., M_{\mathrm{A}} - 1$ are the spurious roots. The minimum norm algorithm constrains the selection of roots to minimize the effect of spurious roots. Determining the roots of P_{MN} allows to estimate $\hat{\epsilon}_i$ as in (4.13).

4.3.4 Parametric Modeling Sensitivity

The parametric Doppler estimation techniques are driven by the prior knowledge of the signal process. Depending on the modeling technique, each of the AR, MA, and ARMA incur a different modeling error. Splitting of a single spectral peak into two or more peaks occurs when the incoming signal is over modeled, i.e., when modeling order (p) is larger. If the signal process is known, and an appropriate model with a known modeling order is selected, a higher resolution spectrum estimation can be achieved within a short signal

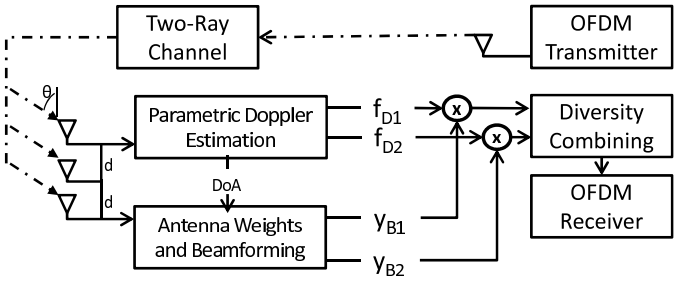

Figure 4.3 Aeronautical Receiver Block Diagram

duration. Since the aeronautical channel is based on a two-ray model, for the nominal case based on [25], we are assuming two Doppler shifts. However, as it is discussed in [91], the number of paths might be greater than two. This issue lies within the scope of this study and is investigated with various modeling errors via simulations in section 4.5.

4.4 Beamforming-based Signal Separation for Aeronautical Doppler Correction

The ICI due to dual or multiple Doppler shifts can be compensated by a simple use of beamforming with separating the arriving paths. Once the paths are separated, the Doppler shift's can be compensated individually with the conventional methods [92]. By taking advantage of estimated individual shifts in the previous section, we find the DOA and the weights of the antennas to separate the paths for individual processing. The signals are then further combined to improve the receiver performance using diversity combining schemes. See Fig. 4.3 for the proposed aeronautical receiver block diagram [100, 101].

The spatial filtering, also known as beamforming, describes how an array of antenna elements combined with signal processing can either block or direct the radiation or reception of signals in the desired signal [102]. In an aeronautical channel, the Doppler shifts due to wide range of DOAs can be taken as an advantage for first separating the paths with beamforming, and then compensating and combining them with diversity techniques.

In an array of antenna sensors, if the angle of the signal arriving at the sensor is θ and each of the M sensors is d distance apart, the received signal in the adjacent sensor travels

a difference of $\frac{f_c}{c} d \cos(\theta)$, where f_c is the signal carrier frequency and c is the propagation speed. Therefore, the phase difference between two elements is $-m\frac{f_c}{c} d \cos(\theta)$, where md is the distance between the two sensor elements [103]. Then, the received signal $y(n)$ at m^{th} sensor elements will be

$$y_m(n) = y(n) e^{jm\frac{f_c}{c} d \cos(\theta)} \ , \tag{4.16}$$

since the signal $y(n)$ will experience the antenna array factor due to the geometry of the sensor at reception. Let us assume that we multiply the m^{th} sensor element by a weighting factor. Then, the beamform to receive the signal for l^{th} path will be

$$y_{\text{B},l}(n) = \sum_{m=0}^{M-1} y_m(n) w_{m,l} \ , \ l = 0, 1, ..., L-1 \ , \tag{4.17}$$

where $y_{\text{B},l}(n)$ is the outcome of the signal spatially processed through $w_{m,l}$ weights of M sensor elements for L arriving paths. Therefore, L rays of signal each associated with angle of arrivals θ_l will be received at the array of sensors. If the angles were to be known, the respective array weights can be calculated as

$$w_{m,l} = e^{jm\frac{f_c}{c} d \cos(\theta_l)} \ . \tag{4.18}$$

Each of the l paths will have its associated array of weighting factors, $w_{m,l}$, $l = 0, ..., L-1$, based on DOA. Therefore, given that we have estimated the Doppler frequencies with (4.13), and know the speed of the mobile platform (v), the arriving angle of different paths can be calculated as[3]

$$\theta_l = \cos^{-1}\left(\frac{f_{\text{D}_l} c}{f_c v}\right) \ . \tag{4.19}$$

For multi-beamforming to separate signals, each arriving angle will be used to generate a different array of weights using (4.18). For aeronautical two-ray channel there will be two, i.e., $L = 2$, arriving signals with different DOA [25]. For one particular case of

[3]In the current model, θ_l, $l = 0, 1$, is assumed to be the projection of velocity vector on the direction of propagation. Therefore the direction of arrival of the signal cannot be from upper 180^0s for the aeronautical node and lower 180^0s for the ground node since there will be no propagation from those directions.

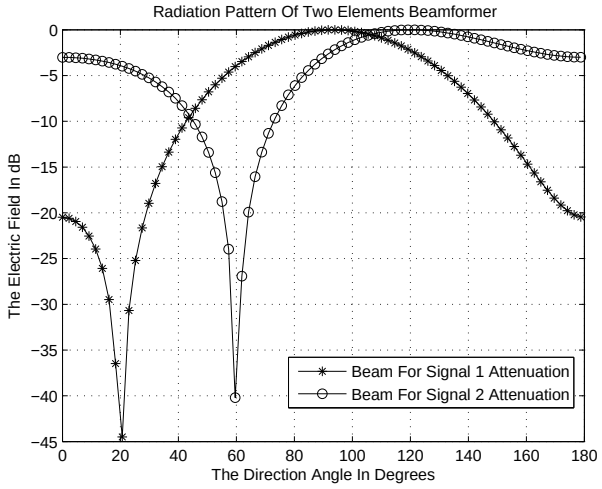

Figure 4.4 Beamforming Radiation Patterns

paths arriving from angle 20° and 60°, two beamforming weights are generated. Fig. 4.4 shows the radiation pattern for the respective DOA with two antenna elements. Note that the beam for first signal will attenuate the signal with angle of arrival 20°, and allows the second signal with angle of arrival 60° to pass through. Similarly, the second beam will attenuate the signal with angle of arrival 60°. Thus for the aeronautical two-ray channel, there will be two such spatially processed signals, $y_{\mathrm{B},0}(n)$ and $y_{\mathrm{B},1}(n)$[4]. The signals are then combined to improve the performance of the receiver. In this study, we selected selective combining (SC) and maximal ratio combining (MRC) for investigation.

1. Selection Combining: In SC the signal with highest signal power is selected for further processing [104]:

$$\beta_l = \begin{cases} 1 & l = l_0 \\ 0 & \text{o/w} \end{cases}, \tag{4.20}$$

where β_l's are weights for each branch, and l_0 is the branch with the highest received signal power.

[4]Note that two processing chains are assumed to be available for processing each path separately as the weights of two paths are different.

Table 4.1 ACN Simulation Parameters

Simulation Parameters	
Carrier (f_c)	1000 Mhz (L-band)
Aeronautical node speed (v)	800 km/hr
Bandwidth (B)	800 kHz
Subcarrier number (N)	128
Subcarrier spacing (Δ_f)	6.25 kHz
OFDM symbol duration (T_s)	160 μs
OFDM CP size (T_{CP})	1/4 T_s , 40 μs
Modulation	QPSK (uncoded)
Channel	Rician two-ray Model
1st and 2nd Ray Angles	Uniform distr. $\{0, 2\pi\}$
Maximum delay $\tau_{\max}$	33 μs [25]
Antenna separation	0.3m
Antenna number (M)	2,4,6
Autocorrelation matrix length (M_A)	50, 75, 100, 125

Thus for the aeronautical channel the SC equation will be:

$$y_{\text{SC}}(n) = y_{\text{B},0}(n)\beta_0 e^{\frac{j2\pi\epsilon_0 n}{N}} + y_{\text{B},1}(n)\beta_1 e^{\frac{j2\pi\epsilon_1 n}{N}} \ . \tag{4.21}$$

where β_l's are defined in (4.20).

2. Maximum Ratio Combining: In MRC, the beamformed aeronautical signals are co-phased. The diversity combining branch weights for this method can be given as [105]

$$\beta_l = a_l e^{j\theta_l}, l = 0, 1, ..., L-1 \ . \tag{4.22}$$

where $a_l = \frac{\mathbb{E}[y_{\text{B},l}(n)]}{N_0}$, $\mathbb{E}[y_{\text{B},l}(n)]$ and N_0 denote the mean signal amplitude in the l^{th} branch and noise power. Note that the gain on each branch becomes proportional to the signal amplitude in this method. The MRC output can also be given as in (4.21) with using weights as in (4.22).

4.5 Numerical Results

Computer simulations are performed based on an OFDM system with uncoded QPSK modulation in a two-ray channel model as it is defined in section 4.2. Some of the

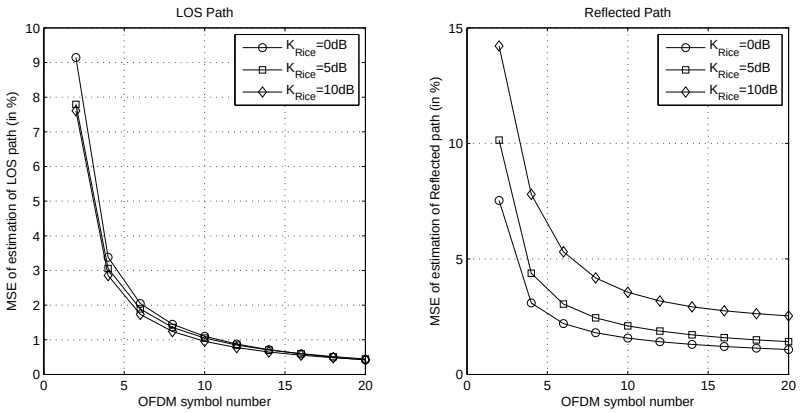

Figure 4.5 MSE Performance of Individual Paths for Various Rice Factors

parameters used in simulations are summarized in Table 4.1. Doppler estimation simulation with a Signal to Noise Ratio (SNR) of 20 dB[5], and a randomly and uniformly distributed dual Doppler shift ranging from $-\Delta f$ to $+\Delta f$ (i.e., $\epsilon_i \sim \mathcal{U}(-1,1), i = 0,1$) is performed for the aeronautical channel[6].

Fig. 4.5 presents the MSE performance for the first and second paths separately for various Rice factors (K_{Rice}) and OFDM symbol numbers[7] with an autocorrelation matrix length of $M_{\text{A}} = 100$. As the K_{Rice} increases, MSE of LOS path decreases; on the other hand, MSE of reflected path increases since the reflected path's power becomes smaller. Although the MSE of the reflected path increases with the K_{Rice}, since its power decreases, the effect of it also decreases on the ICI power. This can also be tracked from (4.7) and Fig 4.2. Therefore, we will investigate the rest of our results with an average MSE with

[5]We studied different SNR levels; however, there is no significant performance improvement for range of SNR $\in \{0\text{dB}, 20\text{dB}\}$. Therefore, we only provide SNR= 20 dB. Note that this behavior is due to generating the training tone only for one subcarrier for the estimation, i.e., if the number of the subcarriers in a training OFDM symbol is increased, the MSE will be affected with noise level significantly. Therefore in the current simulation scenario, the cross effect of individual paths on the estimation is dominant compared to noise. The scope of this study is to investigate the effect of two Doppler shifts, and the optimization of the number of training subcarriers depending on the noise level to provide better estimation is left as a future work.

[6]We also investigated the MSE with various constant Doppler scenarios. As the two Doppler shifts become closer, their separability becomes harder – the complexity and latency for the estimation is increasing, thus MSE performance becomes worse. For the sake of brevity, we provide the results only with randomly and uniformly distributed Doppler frequencies to find the average value for MSE (given in (4.23)) as it is discussed in [25].

[7]The derivations for estimations of Doppler shifts are provided for only one OFDM symbol for analytical tractability. However, to provide better estimation, multiple OFDM symbols and increasing autocorrelation matrix length (M_{A}) is investigated in simulations.

weighting factors as follows

$$\text{Average MSE} \triangleq \mathbb{E}\left\{\frac{1}{L}\sum_{i=0}^{L-1}|h_i|^2\,\frac{|\epsilon_i-\hat{\epsilon}_i|^2}{|\epsilon_i|^2}\right\}. \tag{4.23}$$

In our simulations, K_{Rice} is randomly changed with a uniform distribution between $2-20$ dB to simulate an en-route scenario [25][8]. Fig. 4.6 shows the MSE performance of the MUSIC algorithm for various number of OFDM symbols and lengths of autocorrelation matrix M_{A}. Note that at around $12-14$ OFDM symbols, the MSE is below 1%. The increase of M_{A} and OFDM symbols shows a trade-off between increase in the number of computations and increase in the latency. Simulations show that various MSE performances can be achieved depending on OFDM symbols and M_{A}. In Fig. 4.7 MUSIC, EV, and minimum norm algorithms are studied for a given autocorrelation matrix length, i.e., $M_{\text{A}} = 100$. Although the performance curve of the three algorithms is relatively close, the EV method shows a slightly better performance of estimating the dual Doppler shift for less training OFDM symbols.

Fig. 4.8 shows the performance of the MUSIC algorithm when the modeling order is chosen incorrectly. The incorrect model order, i.e., $p = 3$ causes an average of 5% MSE difference while two-ray model is used, which will impact the overall system BER performance (see Fig. 4.10 for the effect of estimation error on BER performance.). Therefore, techniques to estimate modeling parameters, i.e., order, need to be considered [106]. Channel estimation techniques that have the capability to estimate channel multipaths or echos can be used for better estimation of modeling order [107, 108].

The paths are separated using beamforming for M sensor elements as it is described in section 4.4. Fig. 4.9 shows BER performance for different sensor numbers and combining techniques together with no Doppler channel ($M = 6$) scenario as a benchmark. As the number of antenna elements increases, narrower beams are formed for the incoming paths; therefore BER performance increases significantly. In addition, when the separated two

[8]The reader is referred to [45, 46] for an in depth discussion on path gains and Rice factor for aeronautical channel for particular scenarios i.e., en-route, take-off/arrival, taxiing, and parking.

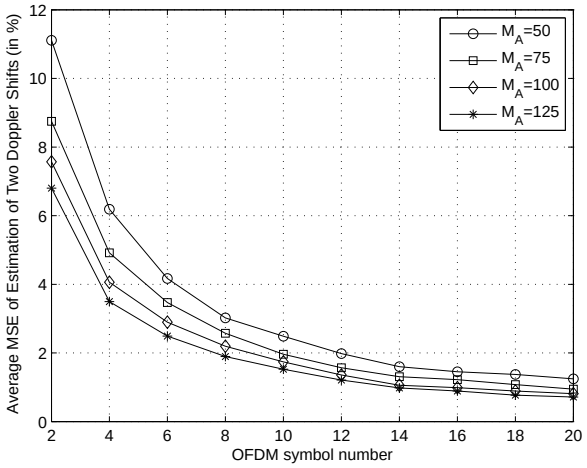

Figure 4.6 MSE Performance for Various Autocorrelation Matrix Lengths and OFDM Symbols for MUSIC

signals are combined using MRC, there is 4 dB increase in performance compared to SC. Another simulation is run to estimate the BER performance with respect to estimation error. Fig. 4.10 shows the respective performance for 1% to 5% MSE for MRC with $M = 6$. It can be concluded that the impact of Doppler shifts in aeronautical channel on OFDM-based system can be mitigated with the parametric spectrum estimation and beamforming. Moreover, the performance loss due to frequency estimation error can easily be compensated by beamforming and diversity combining the multiple paths.

4.6 Conclusions

In this study, an OFDM-based system is analyzed particularly for aeronautical environment and it is shown that ICI can be mitigated by exploiting the dual Doppler shift characteristics of the aeronautical channels. As the number of paths is predictable, parametric spectrum estimation algorithms are used to estimate the Doppler shifts. Simulations using the MUSIC, EV, and minimum norm algorithms show that the estimation can be done efficiently with an MSE performance less than 1%. It is shown that increasing the autocorrelation matrix size or number of OFDM symbols for estimation increases the MSE performance. However, they also cause an increase in the number of computations, and

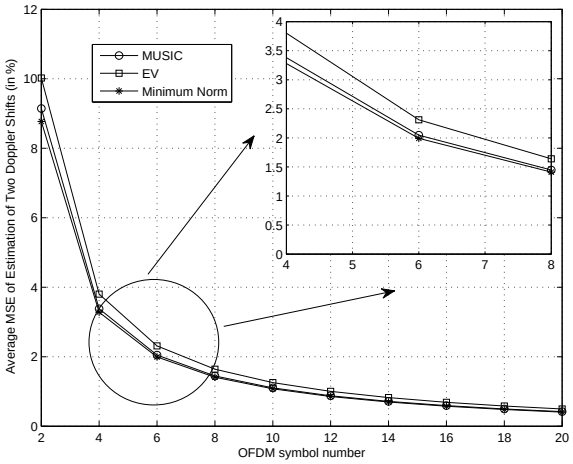

Figure 4.7 MSE Performance for Various Methods and OFDM Symbols with Autocorrelation Matrix Length $M_{\mathrm{A}} = 100$

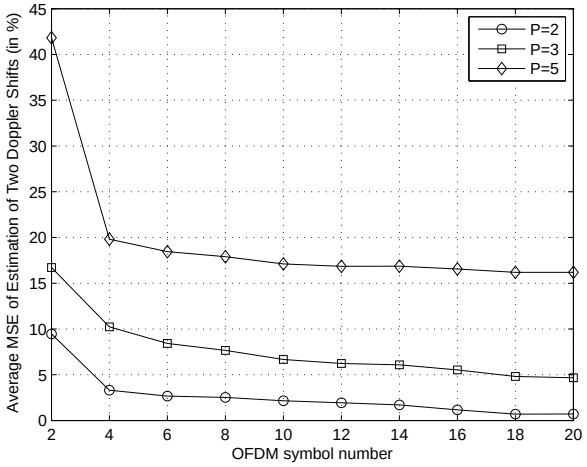

Figure 4.8 MUSIC Method Modeling Sensitivity with Autocorrelation Matrix Length $M_{\mathrm{A}} = 100$

the latency of the estimation, respectively. We show that if the modeling order is not selected correctly, the estimation performance degrades dramatically. For the compensation of ICI using the estimated Doppler shifts, we first find the DOAs of the paths. Based on DOA and estimation errors, we show that beamforming with different number of antenna elements can create beams with resolutions that are capable of separating these Doppler affected paths. The separated signals are first compensated for single Doppler shift and

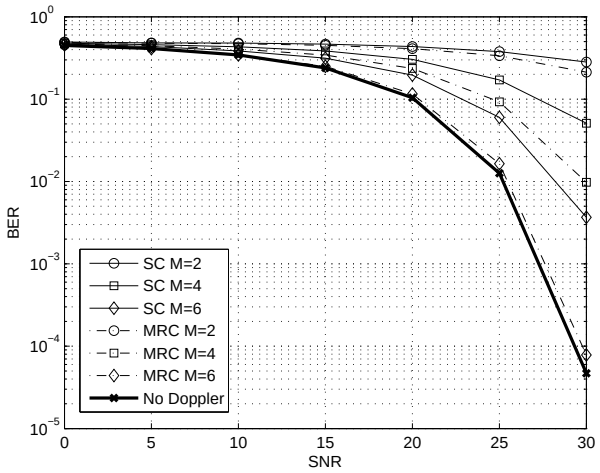

Figure 4.9 BER Performance of Beamforming-based Signal Separation and Diversity Combining

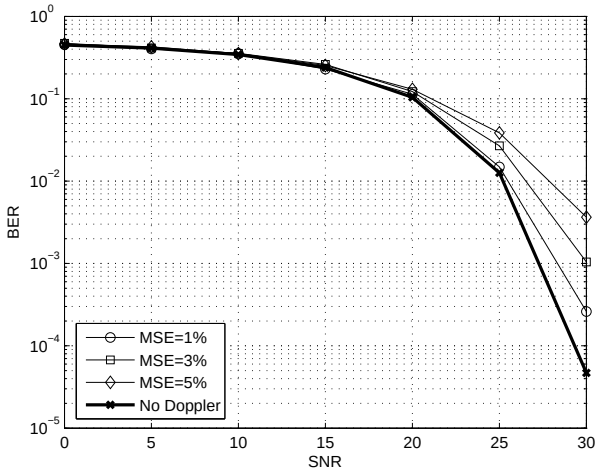

Figure 4.10 BER Performance with Various Estimation Errors for MRC with $M = 6$ Antennas

then diversity combining techniques are used to improve the system BER performance. Numerical results show that BER performance approaches to no-Doppler scenario with the beamforming-based mitigation method. The estimation and compensation methods proposed in this chapter can easily be applied to single-carrier systems. The future direction of this study includes recursive estimation of the dual Doppler frequency shift using fewer OFDM symbols and lower autocorrelation matrix.

CHAPTER 5 :

CONCLUSIONS, DISCUSSIONS AND FUTURE WORK

In this dissertation, throughput performance of tiered network structures are improved with novel resource/interference management methods, node densification schemes, and transceiver designs; with their applications to advanced tiered network structures such as heterogeneous networks (i.e., picocells, femtocells, relay nodes, and distributed antenna systems), device-to-device (D2D) networks, and aeronautical communication networks (ACN).

As it is discussed before, three approaches are considered to enhance the capacity of wireless networks to satisfy this exponential growth in data traffic (i.e., increasing the spectrum, increasing the spectrum efficiency, and increasing the density of the network (spectrum reuse)) for the future radio access schemes. We particularly focus on the network densification. Although the traditional (regular, coordinated) macrocellular network architectures have a successful history in wireless communications, it will be extremely challenging to meet the growth in the data traffic in the upcoming years therefore different capability networks will be required. The benefits of using different capability networks in a tiered manner include increased data rates, reduced power transmission, enhanced total network capacity, better load balancing, extended coverage (less deadzones), and enhanced mobility. Increasing the reuse by adding different capability nodes into the network in an uncoordinated (irregular in terms of power, spectrum, hardware, coverage, mobility, complexity, technology) manner include heterogeneity to the traditional wireless networks which will lead to multi-tier resource management problems in uncoordinated interference environments. In this dissertation, we present novel resource/interference management methods to maximize the capacity, fairness under QoS constraints, node densification schemes to

understand the limitations of the dense networks, and transceiver designs to handle the mobility and improve the performance of tiered networks. We apply our methodologies to heterogeneous networks, D2D networks, and ACN.

5.1 Resource Management in Tiered Networks

In the chapter, using HPPs, we study the sum-capacities of co-channel, dedicated, channel, and hybrid spectrum allocation methods for two-tier macrocell-femtocell networks. For dedicated channel and hybrid approaches, optimum partitioning of the available spectrum resources between the macrocell and femtocell networks is derived analytically and analyzed for various scenarios. The results show that without using fairness criteria, the capacity maximizing allocation is done by allocating the whole spectrum to femtocells due to their spectrum reuse capability. Since this approach leads to a very unfair spectrum allocation, we propose a QoS-oriented fairness metric. By using this metric as a constraint for the spectrum allocation, we present a capacity maximizing spectrum allocation method which guarantees a specific level of fairness and QoS. From a network provider point of view, partitioning of available resources with the hybrid approach yields the best trade-off from capacity maximization, fairness, and QoS perspectives. The findings in this chapter may also be easily extended to time-domain resource coordination among macrocells and femtocells as specified in 3GPP Release-10, where the duty cycle of ABSs may be optimized while jointly considering capacity maximization, fairness, and QoS constraints.

5.2 Network Densification in Tiered Networks

In this chapter, we investigate the transmit power distributions for D2D links with ideal power control. We characterize a D2D network with a group of parameters and show the feasibility of a D2D network in terms of transmit power distributions and SINR. As the dense network simulations are time consuming, slow, expensive, and in some cases impractical, we propose a set of analytical derivations as a tool for investigation of dense

network structures using power control. We investigate the problem both with analytical derivations and numerical results, and find a good match between simulations and theory.

We study the relationship between the network density, transmit power distribution, and target SINR together with scheduling strategies for dense networks. The contribution of this study is to find the limits of network densification in a power controlled D2D network scenario.

5.3 Mobility in Tiered Networks

Mobility causes Doppler effect and therefore is an important issue that limits the performance of wireless communication networks. In mobile terrestrial wireless communication systems, the channel model is generally based on the assumption that directions of arrival (DOA) of the signal at the receiver are uniformly distributed which yields to a Doppler spectrum of the classical Jakes model. As opposed to the Jakes Doppler spectrum in mobile terrestrial communications, ACN channels are modeled with dual Doppler shift. Therefore, it is possible to estimate and mitigate the effect of Doppler in ACN. The contribution of this chapter is to present novel transceiver schemes that addresses the mobility issues in a two-tiered ACN to increase the throughput.

In this study, an OFDM-based system is analyzed particularly for aeronautical environment and it is shown that ICI can be mitigated by exploiting the dual Doppler shift characteristics of the aeronautical channels. As the number of paths is predictable, parametric spectrum estimation algorithms are used to estimate the Doppler shifts. Simulations using the MUSIC, EV, and minimum norm algorithms show that the estimation can be done efficiently with an MSE performance of less than 1%. It is shown that increasing the autocorrelation matrix size or number of OFDM symbols for estimation, increases the MSE performance. However, they also cause an increase in the number of computations, and the latency of the estimation, respectively. We show that if the modeling order is not selected correctly, the estimation performance degrades dramatically. For the compensation of ICI using the estimated Doppler shifts, we first find the DOAs of the paths. Based on

DOA and estimation errors, we show that beamforming with a different number of antenna elements can create beams with resolutions that are capable of separating these Doppler affected paths. The separated signals are first compensated for single Doppler shift and then diversity combining techniques are used to improve the system BER performance. Numerical results show that BER performance approaches to no-Doppler scenario with the beamforming-based mitigation method. The estimation and compensation methods proposed in this chapter can easily be applied to single-carrier systems. The future direction of this study includes recursive estimation of the dual Doppler frequency shift using fewer OFDM symbols and lower autocorrelation matrix.

5.4 Discussions and Future Work on Tiered Networks for Future Radio Communications

Increasing the number and/or capabilities of nodes/BSs/links increases the capacity of the wireless communication systems for a well-designed network. However, the uncoordinated increase in the number of cells may cause severe interference and failure in the system. Therefore, the number of cells (links) in a certain area (the density of the network) should be selected carefully to not to cause a failure in the system. While the density of the networks increase, handover between both same tier networks (horizontal handover), and different tier networks (vertical handover) will become an important issue. In conventional homogeneous networks, mobile users use the same set of handover parameters (i.e., hysteresis margin, time-to-trigger (TTT)). However, in tiered networks, using the same set of handover parameters for all cells and/or for all tiers may degrade mobility performance. Moreover, usage of hard handover schemes become questionable in terms of capacity as the cell sizes decrease. Therefore the requirement of coordination between links and multipoint transmission techniques utilizing multiple input multiple output (MIMO) techniques to provide soft handover or coordinated multipoint processing (CoMP) become important for the tiered network structures. In this context, the findings in this dissertation may also

be extended to mobility enhancement techniques to manage and model tiered networks in order to provide a stable network operation point.

In this dissertation, the relationship between network density, resource management in dense networks, and the mobility in these networks are investigated to present a stable tiered network architecture: Theoretically, while there is no mobility, if each user is assigned to a BS (link) and reuse the resource intelligently, the capacity of the network will be directly proportional with the number of such links. In the limiting case, if the number of BSs is infinity for a given area, the capacity will be infinity for the ideal case. However, the overheads due to cell re-selections will limit the capacity, even for very small mobilities. While the density of the network increases, the multi-dimensional resource management schemes and network densification and mobility methods presented in this dissertation will provide a roadmap for increased capacities.

To meet the requirements in the growth of wireless communications, tiered networks have to satisfy extreme densification of small-cells deployed both by cellular/internet service providers and users. Adding different capability cells with different backhaul options (which might use part of their capacity for backhaul), while utilizing higher dedicated spectrum bands such as 3.6 GHz (which are more suitable for small cells in terms of propagation characteristics) will be important. The densification of cellular networks also include a significant importance from energy perspective since smaller cells will have low power consumptions.

The findings in this dissertation may also be extended easily to other network entities present in a tiered network structure. The future direction of this study and dissertation include to take advantage of the resource/interference management techniques presented in this dissertation to provide an overall capacity improvement of the network, which would be scaled with the increasing penetration of small cells.

REFERENCES

[1] Keith Mallinson, "2020 vision for LTE," June 2012. [Online]. Available: http://www.3gpp.org/Industry-White-Papers

[2] Qualcomm Inc., "The 1000x data challenge," Oct. 2012. [Online]. Available: www.qualcomm.com/1000x

[3] NTT DOCOMO, "LTE enhancements and future radio access," Nov. 2010. [Online]. Available: www.nttdocomo.com

[4] Nokia Siemens Networks, "2020: Beyond 4G radio evolution for the gigabit experience," April 2012. [Online]. Available: http://www.nokiasiemensnetworks.com/news-events/e-unite/beyond-4g-creating-the-gigabit-experience

[5] Real Wireless, Ltd., "Strategies for mobile network capacity expansion," White Paper, West Sussex, UK, 2010.

[6] R. J. Matheson", "The Electrospace Model as a Frequency Management Tool," in *ISART Conference*, 2003.

[7] J. G. Andrews, A. Ghosh, and R. Muhamed, *Fundamentals of WiMAX: Understanding Broadband Wireless Networking*. Prentice-Hall, Feb. 2007.

[8] J. Andersen, T. Rappaport, and S. Yoshida, "Propagation measurements and models for wireless communications channels," *IEEE Commun. Mag.*, vol. 33, no. 1, pp. 42–49, Jan. 1995.

[9] G. Yuan, X. Zhang, W. Wang, and Y. Yang, "Carrier aggregation for LTE-Advanced mobile communication systems," *IEEE Commun. Mag.*, vol. 48, no. 2, pp. 88–93, Feb. 2010.

[10] P. Mogensen, W. Na, I. Kovacs, F. Frederiksen, A. Pokhariyal, K. Pedersen, T. Kolding, K. Hugl, and M. Kuusela, "LTE capacity compared to the shannon bound," in *Proc. IEEE Veh. Tech. Conf. (VTC)"*, April 2007, pp. 1234–1238.

[11] I. ChihLin, L. Greenstein, and R. Gitlin, "A microcell/macrocell cellular architecture for low- and high-mobility wireless users," *IEEE J. on Sel. Areas in Commun.*, vol. 11, no. 6, pp. 885–891, Aug. 1993.

[12] M. Erturk, S. Mukherje, I. Guvenc, and H. Arslan, *Femtocell Networks: Deployment, PHY Techniques and Resource Management*. Cambridge University Press, 2012, Chapter 4: Spectrum Assignment and Fairness in Femtocell Networks.

[13] H. Dhillon, R. Ganti, F. Baccelli, and J. Andrews, "Modeling and analysis of K-tier downlink heterogeneous cellular networks," *IEEE J. on Sel. Areas in Commun.*, vol. 30, no. 3, pp. 550–560, April 2012.

[14] A. Damnjanovic, J. Montojo, Y. Wei, T. Ji, T. Luo, M. Vajapeyam, T. Yoo, O. Song, and D. Malladi, "A survey on 3GPP heterogeneous networks," *IEEE Wireless Commun.*, vol. 18, no. 3, pp. 10–21, June 2011.

[15] NASA-ACAST, "Future aeronautical communication infrastructure technology investigation," http://acast.grc.nasa.gov/main/projects/, 2008, 215144.

[16] T. S. Rappaport, *Wireless Communications: Principles and Practice*, 2nd ed. NJ: Prentice Hall, 2003.

[17] H. Arslan, *Cognitive Radio, Software Defined Radio, and Adaptive Wireless Systems*. Springer, 2007.

[18] E. Sakhaee and A. Jamalipour, "The global in-flight internet," *IEEE J. on Sel. Areas in Commun.*, vol. 24, pp. 1748–1757, Sept. 2006.

[19] J. Lai, "Broadband wireless communication systems provided by commercial airplanes," *US. Patents 6 285 878*, Sept. 4, 2001.

[20] R. Madan, J. Borran, A. Sampath, N. Bhushan, A. Khandekar, and T. Ji, "Cell association and interference coordination in heterogeneous LTE-A cellular networks," *to appear in IEEE J. on Sel. Areas in Commun. (JSAC)*, 2010.

[21] V. Chandrasekhar, J. G. Andrews, and A. Gatherer, "Femtocell networks: a survey," *IEEE Commun. Mag.*, vol. 46, no. 9, pp. 59–67, Sep. 2008.

[22] C. Yu, O. Tirkkonen, K. Doppler, and C. Ribeiro, "On the performance of device-to-device underlay communication with simple power control," in *Proc. IEEE Veh. Tech. Conf. (VTC)*, Barcelona, Spain, April 2009, pp. 1–5.

[23] C. Yu, K. Doppler, O. Tirkkonen, and C. Ribeiro, "Power optimization of device-to-device communication underlaying cellular communication," in *Proc. IEEE Int. Conf. on Commun. (ICC)*, Dresden, Germany, June 2009, pp. 1–5.

[24] K. Doppler, M. Rinne, C. Wijting, C. Ribeiro, and K. Hugl, "Device-to-device communication as an underlay to LTE-advanced networks," *IEEE Commun. Mag.*, vol. 47, no. 12, pp. 42–49, Dec. 2009.

[25] E. Haas, "Aeronautical channel modeling," *IEEE Trans. on Veh. Tech.*, vol. 51, no. 2, pp. 254–264, March 2002.

[26] M. Schnell and S. Scalise, "NEWSKY - concept for NEtWorking the SKY for civil aeronautical communications," *IEEE Aero. and Elect. Sys. Mag.*, vol. 22, no. 5, pp. 25–29, May 2007.

[27] M. Erturk, J. Haque, W. Moreno, and H. Arslan, *Aeronautics*. InTech Press, 2011, Chapter 3: Aeronautical Data Networks.

[28] R. Kerczewski, "Aeronautical communications research and development needs for future air traffic management applications," in *Proc. IEEE Aero. Conf. (AEROCONF)*, Mar. 2002, pp. 1169–1176.

[29] L. Connell, "Pilot and controller communications issues," in *Proc. of the Methods and Metrics of Voice Commun. Workshops.*, 1995, NASA-Ames Research Center.

[30] A. Jahn and M. Holzbock, "Evolution of aeronautical communications for personal and multimedia services," *IEEE Commun. Mag.*, pp. 104–112, July, 2003.

[31] R. Prasad, *OFDM for Wireless Communication Systems.* Artech House, 2004.

[32] H. A. Mahmoud and I. Guvenc, "A comparative study of different deployment modes for femtocell networks," in *Proc. IEEE Indoor Outdoor Femtocells (IOFC) Workshop (co-located with PIMRC 2009)*, Tokyo, Japan, Sep. 2009, pp. 1–5.

[33] D. Lopez-Perez, A. Valcarce, A. Ladanyi, G. de la Roche, and J. Zhang, "Intracell handover for interference and handover mitigation in OFDMA two-tier macrocell-femtocell networks," *EURASIP Journal on Wireless Communications and Networking, Article ID 142629*, vol. 2010, no. 4, pp. 1–15, 2010.

[34] I. Demirdogen, I. Guvenc, and H. Arslan, "A simulation study of performance trade-offs in open access femtocell networks," in *Proc. IEEE Indoor Outdoor Femtocells (IOFC) Workshop (co-located with PIMRC 2010)*, Istanbul, Turkey, Sep. 2010, pp. 1–5.

[35] Z. Bharucha, A. Saul, G. Auer, and H. Haas, "Dynamic resource partitioning for downlink femto-to-macro-cell interference avoidance," *EURASIP Journal on Wireless Communications and Networking, Article ID 143413*, vol. 2010, no. 4, pp. 1–12, 2010.

[36] M. Dianati, X. Shen, and S. Naik, "A new fairness index for radio resource allocation in wireless networks," in *Proc. IEEE Wireless Comm. and Net. Conf.*, vol. 2, New Orleans, LA, Mar. 2005, pp. 712–717.

[37] D. C. R. Jain and W. Hawe, "A quantitative measure of fairness and discrimination for resource allocation in shared computer system," *DEC Technical Report 301*, 1984.

[38] X. Gao, T. Nandagopal, and V. Bharghavan, "Achieving application level fairness through utility-based wireless fair scheduling," in *Proc. IEEE Global Telecommun. Conf. (GLOBECOM)*, vol. 6, San Antonio, TX, 2001, pp. 3257–3261.

[39] M. Win, P. Pinto, and L. Shepp, "A mathematical theory of network interference and its applications," *Proc. of the IEEE*, vol. 97, no. 2, pp. 205–230, Feb. 2009.

[40] J. Andrews, F. Baccelli, and R. Ganti, "A new tractable model for cellular coverage," in *Proc. 2010 Allerton Conference*, Monticello, Il, Oct. 2010, pp. 1204–1211.

[41] P. Robertson and S. Kaiser, "Analysis of the loss of orthogonality through Doppler spread in OFDM systems," in *Proc. IEEE Global Telecommun. Conf. (GLOBECOM)*, Dec. 1999, pp. 701–706.

[42] H. Cheon and D. Hong, "Effect of channel estimation error in OFDM-based WLAN," *IEEE Commun. Lett.*, vol. 6, no. 5, pp. 190 –192, May 2002.

[43] Y. Li and J. Cimini, L.J., "Bounds on the interchannel interference of OFDM in time-varying impairments," *IEEE Trans. on Commun.*, vol. 49, no. 3, pp. 401–404, Mar. 2001.

[44] J. An, Y. Wu, and G. Liu, "Delay and Doppler shift joint tracking method for OFDM based aeronautical communication systems," in *Proc. Int. Conf. on Wireless Commun., Net. and Mobile Comput.*, Oct. 2008, pp. 1–4.

[45] B. Xiangyuan, X. Wei, and Z. Ronghua, "A novel channel estimation scheme for wideband OFDM aeronautical communication," in *Proc. Int. Conf. on Wireless Commun., Net. and Mobile Comput.*, Sept. 2009, pp. 1–4.

[46] X. Wu, J. Zhang, and Z. Liu, "Performance analysis of ICI elimination by information aid for aviation mobile broadband communication," in *Proc. IEEE Veh. Tech. Conf. (VTC)*, Sept. 2008, pp. 1–5.

[47] C. Zhang, H. Han, and H. Yu, "NC-OSDM transmission for ICI cancelation in high speed mobile systems," in *Proc. Second Int. Workshop on Cog. Radio and Adv. Spect. Man. (CogART)*, May. 2009, pp. 50–53.

[48] O. Popescu, M. Saquib, D. Popescu, and M. Rice, "Interference mitigation in aeronautical telemetry systems using Kalman filter," *IEEE Trans. on Aero. and Elect. Sys.*, vol. 43, no. 4, pp. 1624–1630, Oct. 2007.

[49] S. Ramanath, E. Altman, V. Kumar, and M. Debbah, "Optimizing cell size in picocell networks," in *Proc. IEEE Int. Symp. on Modeling and Optimization in Mobile, Ad Hoc, and Wireless Networks (WiOPT)*, Seoul, Korea, June 2009, pp. 1–9.

[50] K. Loa, C. C. Wu, S. T. Sheu, Y. Yuan, M. Chion, D. Huo, and L. Xu, "IMT-advanced relay standards," *IEEE Commun. Mag.*, vol. 48, no. 8, pp. 40–48, Aug. 2010.

[51] A. Morimoto, M. Tanno, Y. Kishiyama, K. Higuchi, and M. Sawahashi, "Investigation on optimum radio link connection using remote radio equipment in heterogeneous network for LTE-Advanced," in *Proc. IEEE Veh. Tech. Conf. (VTC)*, Barcelona, Spain, Apr. 2009, pp. 1–5.

[52] M. Erturk, S. Mukherjee, I. Guvenc, and H. Arslan, "Fairness and resource assignment in heterogeneous networks," *submitted to EURASIP Journal on Wireless Communications and Networking*, July. 2012.

[53] Nokia Siemens Networks, "Macro+HeNB performance with escape carrier," 3GPP Standard Contribution (R1-101453), Feb. 2010.

[54] Samsung, "CSI measurement issue for macro-femto scenarios," 3GPP Standard Contribution (R1-106051), Jacksonville, FL, Nov. 2010.

[55] InterDigital Communications, LLC, "eICIC macro-femto: Time-domain muting and ABS," 3GPP Standard Contribution (R1-105951), Jacksonville, FL, Nov. 2010.

[56] Ericsson, ST-Ericsson, "Details of almost blank subframes," 3GPP Standard Contribution (R1-105335), Xian, China, Oct. 2010.

[57] A. Damnjanovic, J. Montojo, Y. Wei, T. Ji, T. Luo, M. Vajapeyam, T. Yoo, O. Song, and D. Malladi, "A survey on 3GPP heterogeneous networks," *IEEE Wireless Commun.*, vol. 18, no. 3, pp. 10–21, June 2011.

[58] Samsung, "CSI measurement issue for macro-femto scenarios," 3GPP Standard Contribution (R1-106051), Nov. 2010.

[59] D. Choi, P. Monajemi, S. Kang, and J. Villasenor, "Dealing with loud neighbors: The benefits and tradeoffs of adaptive femtocell access," in *Proc. IEEE Global Telecommun. Conf. (GLOBECOM)*, New Orleans, LA, Dec. 2008, pp. 1–5.

[60] I. Guvenc, M. R. Jeong, F. Watanabe, and H. Inamura, "A hybrid frequency assignment for femtocells and coverage area analysis for co-channel operation," *IEEE Commun. Lett.*, vol. 12, no. 12, pp. 880–882, Dec. 2008.

[61] V. Chandrasekhar, J. Andrews, T. Muharemovic, Z. Shen, and A. Gatherer, "Power control in two-tier femtocell networks," *IEEE Trans. on Wireless Commun.*, vol. 8, no. 8, pp. 4316–4328, Aug. 2009.

[62] J. P. M. Torregoza, R. Enkhbat, and W.-J. Hwang, "Joint power control, base station assignment, and channel assignment in cognitive femtocell networks," *EURASIP Journal on Wireless Communications and Networking, Article ID 285714*, vol. 2010, no. 4, pp. 1–14, 2010.

[63] K. Huang, V. Lau, and Y. Chen, "Spectrum sharing between cellular and mobile ad hoc networks: transmission-capacity trade-off," *IEEE J. on Sel. Areas in Commun.*, vol. 27, no. 7, pp. 1256–1267, Sept. 2009.

[64] D. Bertsekas and R. Gallager, *Data Networks*. Prentice-Hall, 1987.

[65] A. Kumar and J. Kleinberg, "Fairness measures for resource allocation," in *Proc. 41st Annual Symp. on Found. of Comp. Sci.*, Redondo Beach, CA, 2000, pp. 75–85.

[66] S. Sesia, T. Issam, and B. Matthew, *LTE, The UMTS Long Term Evolution : From theory to practice*. Wiley, 2009.

[67] M. Erturk, H. Aki, I. Guvenc, and H. Arslan, "Fair and QoS-oriented spectrum splitting in macrocell-femtocell networks," in *Proc. IEEE Global Telecommun. Conf. (GLOBECOM 2010)*, Dec. 2010, pp. 1–6.

[68] S. Mukherjee, "UE coverage in LTE macro network with mixed CSG and open access femto overlay," in *Proc. IEEE Int. Conf. on Commun. Workshops (ICC), 2011*, June 2011, pp. 1–6.

[69] V. Chandrasekhar and J. Andrews, "Spectrum allocation in tiered cellular networks," *IEEE Trans. Commun.*, vol. 57, no. 10, pp. 3059–3068, Oct. 2009.

[70] I. Guvenc, "Capacity and fairness analysis of heterogeneous networks with range expansion and interference coordination," *IEEE Commun. Lett.*, vol. 15, no. 10, pp. 1084–1087, Oct. 2011.

[71] 3GPP TR 36.814 Release 9 2 V9.0.0 (2010-03), "Technical specification group radio access network; evolved universal terrestrial radio access (E-UTRA); further advancements for E-UTRA physical layer aspects (release 9)," March 2010.

[72] M. Erturk, S. Mukherjee, I. H., and H. Arslan, "Distributions of transmit power and sinr in device-to-device networks," *revisions submitted to IEEE Commun. Lett.*, Oct. 2012.

[73] M. Erturk, I. Guvenc, and H. Arslan, "Femtocell gateway scheduling for capacity and fairness improvement in neighboring femtocell networks," in *Proc. IEEE Per., Indoor and Mob. Rad. Commun. (PIMRC)*, Sept. 2010, pp. 54–59.

[74] M. Corson, R. Laroia, J. Li, V. Park, T. Richardson, and G. Tsirtsis, "Toward proximity-aware internetworking," *IEEE Wireless Commun.*, vol. 17, no. 6, pp. 26–33, Dec. 2010.

[75] N. Bambos, "Toward power-sensitive network architectures in wireless communications: concepts, issues, and design aspects," *IEEE Personal Commun.*, vol. 5, no. 3, pp. 50–59, June 1998.

[76] X. Zhang and M. Haenggi, "Random Power Control in Poisson Networks," *IEEE Transactions on Communications*, 2012, accepted. Available at http://www.nd.edu/~mhaenggi/pubs/tcom12b.pdf.

[77] G. Foschini and Z. Miljanic, "A simple distributed autonomous power control algorithm and its convergence," *IEEE Trans. on Veh. Tech.*, vol. 42, no. 4, pp. 641–646, Nov. 1993.

[78] S. Mukherjee, "Downlink SINR Distribution in a Heterogeneous Cellular Wireless Network," *IEEE J. on Sel. Areas in Commun. (JSAC)*, vol. 30, no. 3, pp. 575–585, April 2012.

[79] Y. J. Zhang and K. B. Letaief, "Multiuser adaptive subcarrier and bit allocation with adaptive cell selection for OFDM systems," *IEEE Trans. on Wireless Commun.*, vol. 3, no. 4, pp. 1566–1575, Sep. 2004.

[80] W. Rhee and J. M. Cioffi, "Increase in capacity of multiuser OFDM system using dynamic subchannel allocation," in *Proc. IEEE Veh. Tech. Conf. (VTC)*, Tokyo, Japan, May 2000, pp. 1085–1089.

[81] H. Kim and Y. Han, "A proportional fair scheduling for multicarrier transmission systems," *IEEE Commun. Lett.*, vol. 9, no. 3, pp. 210–212, Mar. 2005.

[82] J. Y. Kim and D. H. Cho, "A joint power and subchannel allocation scheme maximizing system capacity in dense femtocell downlink systems," in *Proc. IEEE Int. Symp. Personal, Indoor, Mobile Radio Commun. (PIMRC)*, Tokyo, Japan, Sep. 2009.

[83] K. Sundaresan and S. Rangarajan, "Efficient resource management in OFDMA femto cells," in *Proc. MobiHoc*, New Orleans, LA, May 2009, pp. 33–42.

[84] Y. Y. Li, M. Macuha, E. S. Sousa, T. Sato, and M. Nanri, "Cognitive interference management in 3G femtocells," in *Proc. IEEE Int. Symp. Personal, Indoor, Mobile Radio Commun. (PIMRC)*, Tokyo, Japan, Sep. 2009.

[85] Motorola, "Using a centralized coordinator to mitigate interference between neighboring HeNBs," 3GPP TSG-RAN Working Group 4 (Radio) Meeting, Miyazaki, Japan, Oct. 2009. [Online]. Available: http://www.3gpp.org/ftp/tsg_ran/WG4_Radio/TSGR4_52bis/Documents/R4-093932.zip

[86] A.-L. S. Bell and Alcatel-Lucent, "DL Pico/Macro HetNet Performance: Cell Selection ," 3GPP TSG RAN WG1 Meeting-60 R1-100945, Feb. 2010.

[87] Alcatel-Lucent and Vodafone, "Simulation assumptions and parameters for FDD HeNB RF requirements," 3GPP TSG RAN WG4 (Radio) Meeting-51 R4-092042, May 2009.

[88] "3rd Generation Partnership Project (3GPP); Technical Specification Group Radio Access Network; User Equipment (UE) procedures in idle mode and procedures for cell reselection in connected mode (Release 9)," 3GPP, TS 25.304 v9.0.0, Dec. 2009.

[89] E. Biglieri, J. Proakis, and S. Shamai, "Fading channels: information-theoretic and communications aspects," *IEEE Trans. on Inf. Theory*, vol. 44, no. 6, pp. 2619 –2692, oct 1998.

[90] G. Fan, I. Stojmenovic, and J. Zhang, "A triple layer location management strategy for wireless cellular networks," in *Proc. IEEE Int. Conf. Computer Comm. and Networks (ICCCN)*, Miami, FL, 2002, pp. 489–492.

[91] M. Rice, A. Davis, and C. Bettweiser, "Wideband channel model for aeronautical telemetry," *IEEE Trans. on Aero. and Elect. Sys.*, vol. 40, no. 1, pp. 57–69, Jan. 2004.

[92] M. J.J. Van De Beek and P. Borjesson, "Ml estimation of the time and frequency offset in OFDM system," *IEEE Trans. on Sig. Process.*, vol. 45, pp. 1800–1805, July. 1997.

[93] M. C. Erturk, J. Haque, and H. Arslan, "Challenges in Aeronautical Data Networks," in *Proc. IEEE Aerospace Conf. (AEROCONF)*, Mar. 2010, pp. 1–4.

[94] I. Sen and D. Matolak, "The 5-ghz airport surface area channel: Part II, Measurement and modeling results for small airports," *IEEE Trans. on Veh. Tech.*, vol. 57, no. 4, pp. 2027–2035, July 2008.

[95] A. Bello, P, "Aeronautical channel characterization," *IEEE Trans. on Commun.*, vol. T3, no. 11, pp. 548–563, May 1973.

[96] S. "Elnoubi, "A simplified stochastic model for the aeronautical mobile radio channel," in *Proc. Vehicular Techn. Conf. (VTC)*, vol. 2, 1992, pp. 960–963.

[97] P. Hoeher and E. Haas", "Aeronautical channel modeling at VHF-band," in *Proc. IEEE Veh. Tech. Conf. (VTC)*, vol. 4, 1999, pp. 1961–1966.

[98] J. Haque, M. Erturk, and H. Arslan, "Aeronautical ICI analysis and doppler estimation," *IEEE Commun. Lett.*, vol. 15, no. 9, pp. 906–909, Sept. 2011.

[99] M. H. Hayes, *Statistical Digital Signal Processing and Modeling.* John Wiley and Sons, Feb. 2006, pages 115-116.

[100] M. Erturk, J. Haque, W. Moreno, and H. Arslan, "Doppler mitigation in aeronautical communications," *revisions submitted to IEEE Trans. on Aero. and Elect. Sys.*, Aug. 2012.

[101] J. Haque, *An OFDM Based Aeronautical Communication System.* Ph.D. dissertation, University of South Florida, Sept. 2011.

[102] B. D. V. Veen and K. M. Buckley., "Beamforming: A versatile approach to spatial filtering," *IEEE ASSP Mag.*, April 1998.

[103] L. Godara, "Application of antenna arrays to mobile communications: Part II, Beamforming and direction-of-arrival considerations," *Proc. of the IEEE*, vol. 85, no. 8, pp. 1195–1245, Aug. 1997.

[104] N. Kong and L. Milstein, "Average SNR of a generalized diversity selection combining scheme," *IEEE Commun. Lett.*, vol. 3, no. 3, pp. 57–59, Mar. 1999.

[105] A. Shah and A. Haimovich, "Performance analysis of maximum ratio combining and comparison with optimum combining for mobile radio communications with cochannel interference," *IEEE Trans. on Veh. Tech.*, vol. 49, pp. 1454–1463, Mar. 2000.

[106] S. Rezek, I.A.; Roberts, "Parametric model order estimation: a brief review," *Model Based Digital Signal Processing Techniques in the Analysis of Biomedical Signals (Digest No. 1997/009), IEE Colloquium on the Use of Biomedical Signals (Ref. No.1997/009)*, pp. 3/1– 3/6, 1997.

[107] M. Vanderveen, A.-J. Van der Veen, and A. Paulraj, "Estimation of multipath parameters in wireless communications," *IEEE Trans. on Sig. Proc.*, vol. 46, no. 3, pp. 682–690, Mar. 1998.

[108] M. Vanderveen, C. Papadias, and A. Paulraj, "Joint angle and delay estimation (JADE) for multipath signals arriving at an antenna array," *IEEE Commun. Lett.*, vol. 1, no. 1, pp. 12–14, Jan. 1997.

APPENDICES

Appendix A : Acronyms

Acronym	Description
3G	3rd generation
3GPP	3rd Generation Partnership Project
4G	4th generation
AOA	angle of arrival
AR	auto-regressive
AWGN	additive white Gaussian noise
BER	bit error rate
BWA	broadband wireless access
BS	base station
CDF	cumulative distribution function
CP	cyclic prefix
CSG	closed-subscriber-group
DFT	discrete Fourier transform
DL	downlink
EGC	equal gain-combining
FAA	Federal Aviation Administration
fBS	femtocell base station
FCC	Federal Communications Commission
FDD	frequency division duplexing
FFT	fast Fourier transform
fMS	femtocell mobile station
GPS	global positioning system
GSM	global system for mobile communications
ICI	inter-carrier interference
IDFT	inverse discrete Fourier transform

Appendix A (Continued)

Acronym	Description
IEEE	Institute of Electrical and Electronics Engineers
IFFT	inverse fast Fourier transform
i.i.d.	independent and identically distributed
IP	Internet protocol
ISI	inter-symbol interference
ITU	International Telecommunication Union
LHS	left-hand side
LOS	line-of-sight
LTE	long term evolution
mBS	macrocell base station
MIMO	multiple-input multiple-Output
mMS	macrocell mobile station
MMSE	minimum mean-square error
MRC	maximum ratio combining
MSE	mean-squared-error
MUSIC	multiple signal classification
NASA	National Aeronautics and Space Administraion
NLOS	non-line-of-sight
OFDMA	orthogonal frequency division multiple access
OFDM	orthogonal frequency division multiplexing
PDF	probability density function
PHY	physical layer
QoS	quality of service
QPSK	quadrature phase shift keying
RAT	radio access technology

Appendix A (Continued)

Acronym	Description
RF	radio frequency
RHS	right-hand side
SC	selection combining
SNR	signal-to-noise ratio
SIR	signal-to-interference ratio
SINR	signal-to-interference-plus-noise ratio
TDD	time division duplexing
TPC	transmit power control
UL	uplink
UE	User Equipment
WCSP	wireless communications and signal processing
WiFi	wireless fidelity
WiMAX	worldwide interoperability for microwave access

Appendix B : Bibliographical Notes

This dissertation is based on research that I have performed between 2008 and 2012 with a number of outstanding colleagues in University of South Florida, Tampa Fl, and DOCOMO USA Communication Laboratories, Palo Alto California. Part of the material presented in Chapter 2 appear in [67], [52] co-authored with Hazar Aki, Ismail Guvenc, Sayandev Mukherjee, and Huseyin Arslan and also appears in book chapter in [12], co-authored with Ismail Guvenc, Sayandev Mukherjee, and Huseyin Arslan. Some of the material in Chapter 3 is also published in [73], [72] co-authored with Ismail Guvenc, Sayandev Mukherjee, Hiroyuki Ishii, and Huseyin Arslan. Some part of the work on Chapter 4, appears in three papers [93] [98], [100] co-authored with Jamal Haque, Wilfrido Moreno, and Huseyin Arslan and also appears in the dissertation of Jamal Haque [101], and book chapter in [27] co-authored with Jamal Haque, Wilfrido Moreno, and Huseyin Arslan.

ABOUT THE AUTHOR

M. Cenk Ertürk received the B.Sc. (summa cum laude) and M.Sc. degrees in electrical engineering from Nigde and Bilkent Universities, Turkey in 2005 and 2008, respectively. From 2006 to 2009, he was with the Defense and Security Research Group in the Scientific and Technological Research Council of Turkey (Ankara, Turkey) where he involved several communication projects servicing to the improvement of Turkey's defense technologies and from 2011 to 2012, he was with the Docomo USA Communications Laboratories (Palo Alto, CA) where he involved system level designs of future radio access systems. He is currently working towards the Ph.D. degree with the Department of Electrical Engineering, University of South Florida, Tampa, FL. His research interests include system level design of heterogeneous networks, aeronautical communication networks, and baseband signal processing in wireless communication networks.